BOLU ABANT IZZET BAYSAL UNIVERSITY

THE GRADUATE SCHOOL OF NATURAL AND APPLIED SCIENCES

SYNTHESIS, STRUCTURAL CHARACTERIZATION AND OPTICAL PROPERTIES OF Dy, Ho AND Er DOPED MAGNESIUM PYROBORATE NANOPARTICLES

MASTER OF SCIENCE

CEREN ŞAHİN

BOLU, SEPTEMBER 2019

BOLU ABANT IZZET BAYSAL UNIVERSITY

THE GRADUATE SCHOOL OF NATURAL AND APPLIED SCIENCES

DEPARTMENT OF CHEMISTRY

SYNTHESIS, STRUCTURAL CHARACTERIZATION AND OPTICAL PROPERTIES OF Dy, Ho AND Er DOPED MAGNESIUM PYROBORATE NANOPARTICLES

MASTER OF SCIENCE

CEREN ŞAHİN

BOLU, SEPTEMBER 2019

APPROVAL OF THE THESIS

SYNTHESIS, STRUCTURAL CHARACTERIZATION AND OPTICAL PROPERTIES OF Dy, Ho AND Er DOPED MAGNESIUM PYROBORATE NANOPARTICLES submitted by **Ceren ŞAHİN** and defended before the below named jury in partial fulfillment of the requirements for the degree of **Master of Science** in **Department of Chemistry, The Graduate School of Natural and Applied Sciences of Bolu Abant Izzet Baysal University in 9.09.2019** by
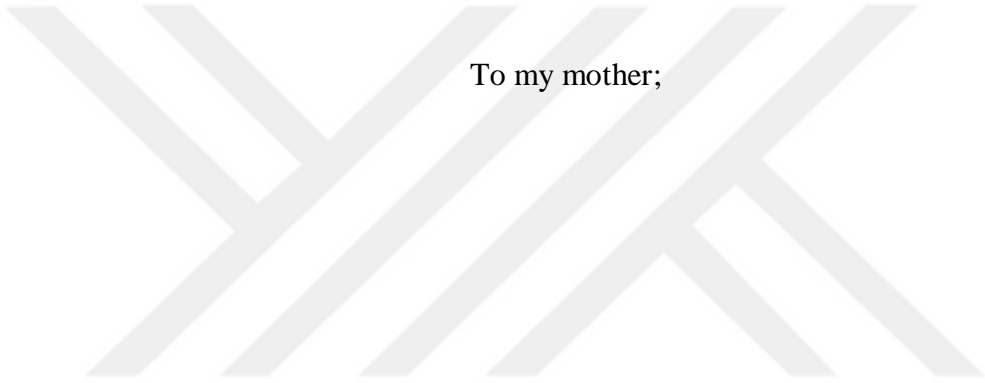
Examining Committee Members	Signature
Supervisor Prof. Dr. Ayşe MORKAN Bolu Abant İzzet Baysal University	....
Member Prof. Dr. F. Devrim ÖZDEMİRHAN Bolu Abant İzzet Baysal University	....
Member Assoc. Prof. Dr. Mecit AKSU Düzce University	....

Prof. Dr. Ömer ÖZYURT ....

Director of Graduate School of Natural and Applied Sciences V.
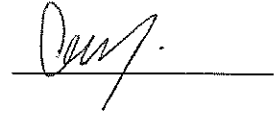
To my mother;

DECLARATION

I hereby declare that all information in this document has been obtained and presented in accordance with academic rules and ethical conduct. I also declare that, as required by these rules and conduct, I have fully cited and referenced all material and results that are not original to this work.

Ceren ŞAHİN

ABSTRACT

**SYNTHESIS, STRUCTURAL CHARACTERIZATION AND OPTICAL
PROPERTIES OF Dy, Ho AND Er DOPED MAGNESIUM PYROBORATE
NANOPARTICLES
MSC THESIS
CEREN ŞAHİN
BOLU ABANT IZZET BAYSAL UNIVERSITY GRADUATE SCHOOL OF
NATURAL AND APPLIED SCIENCES
DEPARTMENT OF CHEMISTRY
(SUPERVISOR: PROF. DR. AYŞE MORKAN)**

BOLU, SEPTEMBER 2019

In this study, Dy^{3+}, Ho^{3+}, Er^{3+} doped magnesium pyroborates were synthesized with various concentrations at different temperatures by solution combustion synthesis method. The final products were well characterized by X-ray Diffraction (XRD), Fourier Transform Infrared Spectroscopy (FTIR) and Ultraviolet Visible Spectroscopy (UV-VIS).

In the first part of this work, 0.005, 0.010, 0.020, 0.050 mole amount of RE (Dy^{3+}, Ho^{3+}, Er^{3+}) metal ion doped $Mg_2B_2O_5$ were synthesized using five different fuels; glycine, tartaric acid, citric acid, urea and hexamethylenetetramine (HMTA) with magnesium nitrate ($Mg(NO_3)_2.6H_2O$) and boric acid (H_3BO_3) sources via solution combustion technique. The synthesized materials were furtherly subjected to the heating processes at 400^oC with 10 min. in which the combustion reaction was completed and followed at 700^oC with 2h, 800^oC with 1h and 900^oC with 1h. to remove organic residues and to obtain pure, crystalline RE doped $Mg_2B_2O_5$ nanoparticles.

In the FTIR study, the strong vibrational bands assigned at 1450-1550 cm^{-1} and 600-750 cm^{-1} indicated the characteristic vibrations of $Mg_2B_2O_5$. Additionally, the crystallite size of the products were calculated using Debye Scherrer equation and founed between 10-19 nm which proved the products were nanoparticles.

In the UV-VIS analysis, the effect of temperature and the doping concentration of Dy^{3+}, Ho^{3+}, Er^{3+} ion on the optical properties of the products was examined due to the changed in wavelengths as red shift and/or blue shift.

KEYWORDS: Solution Combustion Synthesis (SCS), $Mg_2B_2O_5$, RE doped $Mg_2B_2O_5$ nanoparticles, FTIR, XRD, UV-VIS.

ÖZET

**Dy, Ho VE Er KATKILI MAGNEZYUM PİROBORAT
NANOPARTİKÜLLERİN SENTEZİ, YAPISAL KARAKTERİZASYONU VE
OPTİK ÖZELLİKLERİ
YÜKSEK LISANS TEZI
CEREN ŞAHİN
BOLU ABANT İZZET BAYSAL ÜNİVERSİTESİ
FEN BİLİMLERİ ENSTİTÜSÜ
KIMYA ANABILIM DALI
(TEZ DANIŞMANI: PROF. DR. AYŞE MORKAN)**

BOLU, EYLÜL - 2019

Bu çalışmada Dy^{3+}, Ho^{3+}, Er^{3+} katkılı magnezyum diborat yanma yöntemi ile sentezlenmiş ve bu ürünlerin karakterizasyonu FTIR, XRD ve UV-VIS yöntemlerle karşılaştırmalı olarak incelenmiştir.

Çalışmanın ilk aşamasında 0.005, 0.010, 0.020, 0.050 mol miktarda nadir geçiş metalleri (Dy^{3+}, Ho^{3+}, Er^{3+}), 5 farklı yakıt (glisin, tartarik asit, sitrik asit, üre ve heksametilentetramin) ile katkı yapılmıştır. Magnezyum nitrat ve borik asit kullanılarak yanma yöntemi ile sentezlenmiştir. Saf madde elde etmek amacıyla sentezlenen maddeler 400ºC, 700ºC, 800ºC ve 900ºC olarak ısıtılmıştır. 400ºC 10dk'lık ısıtma işleminde yanma reaksiyonu gerçekleşmiştir. 700ºC'de 2 saat, 800ºC'de 1 saat ve 900ºC'de 1 saat işlemleri organik safsızlıkları uzaklaştırmak ve saf $Mg_2B_2O_5$ nanopartiküllerini elde etmek amacıyla yapılmıştır. Ürünlerin her bir sıcaklık ve konsantrasyonda FTIR, XRD ve UV-VIS aracılığıyla karakterizasyonu yapılmıştır.

FTIR çalışmasında, 1450-1550 cm^{-1} ve 600-750 cm^{-1} dalga sayıları arasında $Mg_2B_2O_5$'in karekteristik titreşimleri güçlü bağ olarak gözlemlenmiştir. Ek olarak, Bu maddenin tane büyüklüğü Scherrer denklemi kullanılarak 10-19 nm arasında bulunup nanopartikül yapıda elde edildiği ispatlanmıştır. UV-VIS analizinde, sıcaklık ve Dy^{3+}, Ho^{3+}, Er^{3+} iyonlarının doping konsantrasyonunun ürünlerin optik özellikleri üzerindeki etkisi, dalga boylarındaki kırmızı kayma ve /veya mavi kayma olarak değiştiği için incelenmiştir.

ANAHTAR KELİMELER: Yanma Yöntemi, $Mg_2B_2O_5$, Dy^{3+}, Ho^{3+} Er^{3+} katkılı $Mg_2B_2O_5$ nanopartikülleri, FTIR, XRD, UV-VIS

TABLE OF CONTENTS

LIST OF FIGURES

LIST OF TABLES

LIST OF ABBREVIATIONS AND SYMBOLS

SCS   **:** Solution Combustion Synthesis

CS   **:** Combustion Synthesis

XRD   **:** X-ray Diffraction Spectroscopy

FTIR   **:** Fourier-Transform Infrared Spectroscopy

UV-VIS   **:** Ultraviolet-Visible Spectrometer

ICDD   **:** International Centre for Diffraction Data

Gly   **:** Glycine

CA   **:** Citric Acid

TA   **:** Tartaric Acid

U   **:** Urea

HMTA   **:** Hexamethylenetetramine

RE   **:** Rare Earth

ACKNOWLEDGEMENTS

1. INTRODUCTION

1.1 Borates

Borates are known in which the basic unit is mononuclear (1 B molecule), bi-, tri- , tetra- or penta atomic. In structures of crystalline borates, BO_3 triangles and BO_4 tetrahedra can be attached with each other over common corners to form B_xO_y groups. The several crystal structures of borates are derived from the large variety in the bonding of boron with oxygen (Ma et al., 2018). In crystalline metal borates, the basis of bonding are follows:

1- Boron can bond three oxygens to form a triangle (BO_3) or four oxygens to form a tetrahedron (BO_4).

2- Polynuclear anions are composed by corner sharing only of boron-oxygen triangles and tetrahedra in the manner that a compact insular group results.

Examples of minerals and compounds containing monomeric triangular, BO_3 units, shown in Figure 1.1.a, these are rare-earths orthoborates written as $M^{III}BO_3$ and the minerals examples as $CaSn^{IV}(BO_3)_2$ and $Mg_3(BO_3)_2$. Binuclear trigonal planar units are found in the pyroborates, shown in Figure 1.1.b, written as $M^{II}B_2O_5$; $Mg_2B_2O_5$, $Co^{II}_2B_2O_5$ and $Fe^{II}_2B_2O_5$. Trinuclear cyclic units occur in the metaborates $NaBO_2$ and KBO_2 written as $M_3B_3O_6$, shown in Figure 1.1.c (Grenwood N (1998) Chemistry of The Elements, Second Edition, Butterworth Heinemann Pub., Great Britain).
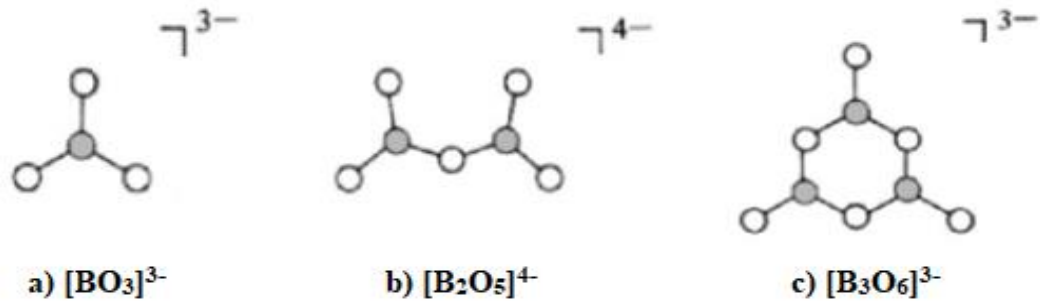
Figure 1.1. Types of borates a) orthoborates, b) pyroborates, c) metaborates

Borates are typically found at low concentrations in the sea, aqueous rocks, coal, clayey schist, and some soils. Most important commercial borate products and minerals are borax, sodium perborate, borax pentahydrate, boric acid, colemanite, and ulexite. The inorganic borate compounds, remarkably boric acid and borax (sodium tetraborates), are used in the industrial and medical application, for example, in textiles, adhesives, insulation materials, fiberglass, fire retardants, borosilicate glass, detergents, soaps, bleaches, cosmetics, pesticides, soldering and welding fluxes, fertilizers, wood preservatives, boron neutron capture therapy, and pharmaceutical preparations (Ince et al., 2017).

1.2   Magnesium Borates

Magnesium borates which different chemical compositions such as $Mg_2B_2O_5$, MgB_4O_7 and $Mg_3B_2O_6$, are significant functional materials. Among them, $Mg_2B_2O_5$ has good mechanical properties related with good heat and corrosion resistance, supermechanical strength, superinsulation and high coefficient of elasticity: in recent years, it has been widely used as an antiwear material to reduce the friction coefficient. Various types of borates with different chemical compositions such as $Mg_2B_2O_5$, MgB_4O_7, and $Mg_3B_2O_6$ established in nature as well as synthesizing in the laboratory. Magnesium borates might be used as antiwear composites, thermoluminescent phosphors materials, antifriction additives, , and flame retardant because these borates have attracted much attention. Various high temperature methods such as hydrothermal and solvothermal which used to expand magnesium

borate applications as MgB_4O_7 nanowires, $Mg_2B_2O_5$ nanorods, $Mg_3B_2O_6$ nanobelts and nanotubes, $MgBO_2(OH)$ nanowhiskers (Dosler et al., 2010; Dou et al., 2010).

Magnesium borates can be used in ceramic industry, in superconducting material production, in detergent composition, in friction reducing additive manufacture, in fluorescent discharge lamps as luminescent material, in ferroelastic material production, in cathode ray tube screens, in X-ray screens, as thermoluminescent phosphor, and as catalysts for the conversion of hydrocarbons. Additionally, magnesium borates have great potential in areas of electronic ceramics reinforcement, semiconductor material synthesis, and plastics or aluminum/magnesiummatrix alloy production, high degree of thermal shock resistance (Kipcak et al., 2014; Elssfah et al., 2007).

1.3   Magnesium Pyroborates

In pyroborate groups, each boron atom is in triangular coordination with three oxygen atoms. This group consists of two such triangles with one shared oxygen shown in Figure 1.2. Boron should form sp^2 hybridization with three coplanar bonds as interbond angles of 120° in this coordination type. The two triangles are not identical in $Mg_2B_2O_5$ structure. Each has a different circle and nonsymmetric bond lengths. The O_{II} - O_{IV} distance is shorter than all other sides of the triangles. This is, however, the only edge of a triangle within the pyroborate group, which is shared with an edge of a magnesium octahedron. Within each triangle there are two B-O distances averaging l.39 A and one somewhat shorter at about 1.36 A. The mean value of all six B-O bonds is l.38. Within the $B_2O_5{}^{4-}$ group, the B_I- O_{IV}- B_{II} angle is 134.5° and the angle between the planes of the triangles is 16 °. B_I and B_{II} are within 0.03 and 0.02 A, respectively, of the planes determined by the three coordinated oxygens. The two outer oxygens in the triangle surrounding B_{II} are coordinated as expected to six magnesium atoms while the two peripheral oxygen atoms in the triangle surrounding B_I are coordinated to only five magnesium atoms. The center O_{IV} is bound to both borons as well as one Mg. O_V is only bonded to two magnesium atoms, as well as the central boron. All other oxygens are linked to one boron and three magnesiums (Block et al., 1959).
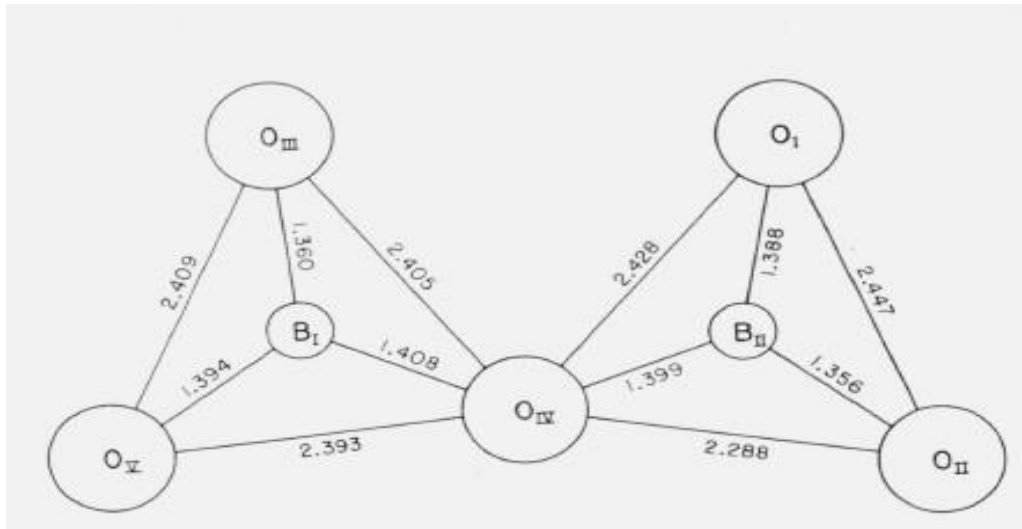
Figure 1.2. Protection of the pyroborate group showing all interatomic distances in angstrom units. (Block et al., 1959).

The pyroborates are compounds with chemical formula M or $M^I B_2 O_5$ where M or M^I stands for Mg, Ca, or a divalent 3d transition metal. Their crystalline structure is triclinic with space group P-1 (number 2). The metals M and M^I are found inside oxygen octahedra that shares edges and form substructures like ribbons, four rows wide, shown in Figure 1.3. These ribbons are parallel to the crystallographic a axis and contain two different sites for the metal ions. The boron ions have trigonal coordination forming borate groups $B_2 O_5^{-4}$, shown in Figure 1.4. The five oxygen ions of each borate group belong to three distinct ribbons shown in Figure 1.3 (Freitas et al., 2003).
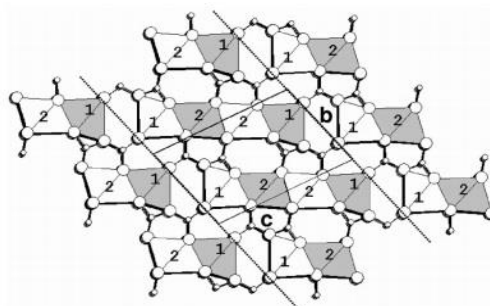
Figure 1.3. The structure of the pyroborates projected in the plane bc. The borate groups placed in the sides b and c of the unit cell. The largest circles refer oxygen ions while the smallest ones indicate the boron ions. The dashed lines indicate one column of ribbons (Freitas et al., 2003).
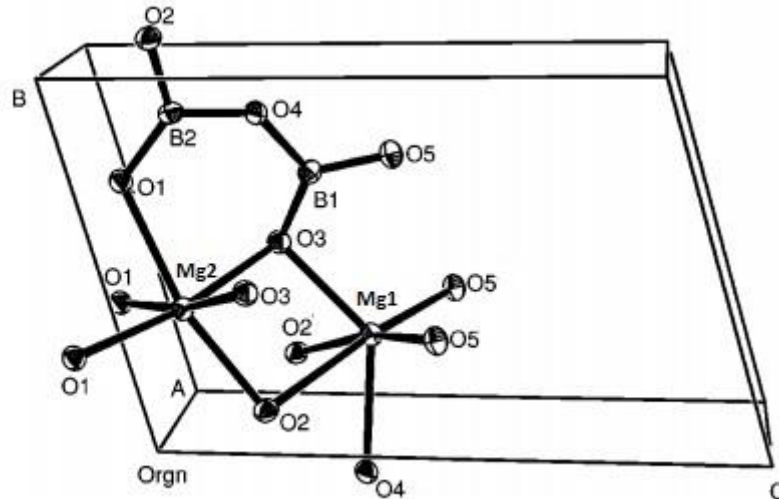
Figure 1.4. Structure fragment of pyroborate $Mg_2B_2O_5$ (Freitas et al., 2003).

The mineral type of magnesium pyroborate ($Mg_2B_2O_5$) called suanite was first discovered by Watanabe at Hol Kol mine in North Korea, as stringy form groups of monoclinic crystals. Synthetic $Mg_2B_2O_5$ was obtained as stratified and prismatic crystals. The synthetic $Mg_2B_2O_5$ was procured usually as a mixture of triclinic and monoclinic structure (Sakane et al., 1988). Suanite crystallizes in three crystallographic forms as a monoclinic phase, a monoclinic phase which having doubled unit cell volume and a triclinic phase (Kawano et al., 2009). Additionally, the type of suanite is white color and translucent and totally colourless in thin section. Its hardness is 5.5. Therefore, it is difficult to fuse (Watanabe T (1953) A new from Magnesium Hol Borate, Mineralogical Journal, Tokyo).

1.4   Synthesis Methods of Magnesium Pyroborate

Various different synthesis methods of magnesium pyroborate ($Mg_2B_2O_5$) are solid-state reaction techniques, solvothermal method under supercritical conditions technique, chemical vapor deposition (CVD) method technique, direct sintering process in vacuum technique, calcination method, flux method, sol-gel method and Solution Combustion Synthesis (SCS) method (Dosler et al., 2010; Gao et al., 2010; Yan et al., 2008; Dou et al., 2010; Chen et al., 2014; Ucyildiz et al., 2010; Xu et al., 2008; Zeng et al., 2008; Qasrawi et al., 2005; Elssfah et al., 2007; Jiang et al., 2006;

Oztas et al., 2009; Wang et al., 2009). Sol-gel processing, coprecipitation and hydrothermal methods as soft chemical methods, which used to obtain $Mg_2B_2O_5$ by including the reactions that take place in solution (Oztas et al., 2009).

Anhydrous triclinic and monoclinic $Mg_2B_2O_5$ compounds were synthesized by conventional heating, partial precipitation, chemical vapor deposition, microwave heating, high-energy milling, methods using different magnesium and boron-containing precursors (Ucyildiz et al., 2010). $Mg_2B_2O_5$ whiskers synthesized by various different synthesis methods, as explained above, have attracted considerable attention because these whiskers have excellent properties of mechanical and thermal, and which indicates high resistance to corrosion (Chen et al., 2014).

1.4.1   Solution Combustion Synthesis of $Mg_2B_2O_5$

Combustion Synthesis (CS) which is important technique for producing alloys, catalysts, advance ceramics and nanomaterials. CS does not need to further calcinations and repeated heating. It is an exothermic reaction and occurs with the evolution of heat and light (Ekambaram et al., 2005). CS depends on the nature of reactants which elements or compounds (solid, liquid or gas) and exothermicity. So, it is described as solution combustion synthesis, self-propagating high temperature synthesis (SHS); low-temperature combustion synthesis (LCS), emulsion combustion, volume combustion (thermal explosion), gel-combustion and sol-gel combustion (Patil et al., 2002).

Owing to having combination of combustion and a reactive solution, method is called solution combustion synthesis (SCS) method that includes self-sustained and highly exothermic reaction, which carry out between an aqueous metal nitrate and a fuel such as glycine, urea, citric acid, tartaric acid as shown in Figure 1.5. All these fuels are provided that the source of carbon and hydrogen which on the combustion form CO_2 and H_2O and liberate heat. They composes complexes with the metal ions producing homogeneous mixing of the cations in solution. Most important inorganic compounds such as ceramic oxides, borates, manganites, aluminates can obtain by SCS method (Desphande et al., 2004; Barron et al., 2016; Patil et al., 2002). Additionally, $Mg_2B_2O_5$ compounds can synthesize by solution combustion

6

synthesis, which used as a ferroelastic material, a nanorod or nanowire for use in nanomaterials and an allochromatic pigment (Ucyildiz et al., 2010; Oztas et al., 2009).

In the solution combustion calculations, the valency of the oxidizing elements which carbon and hydrogen was considered as positive and the reducing elements that metal cations as negative. The heat of combustion as oxidizer/fuel molar ratio (O/F) provided by 1, shown in Figure 1.6 (Patil et al., 2002).

Some remarkable properties of SCS process that firstly, the initial reaction environment existence in the liquid state (e.g. aqueous solution) allows mixing of the reactants at a molecular level, thus permitting exact and uniform formulation of the desired composition on the nanoscale. Secondly, the high reaction temperatures supply high product purity and crystallinity (Reddy et al., 2011).

Selection of ideal fuel is also important criteria for SCS. Fuels have to be water soluble, low ignition temperature and compatible with metal nitrates. According to these properties, urea and glycine fuels are available and are mostly used. Glycine nitrate process (GNP) represents mechanistic advantage over urea fuel. Alkaline and alkaline earth ions are more effectively complexed by carboxylic acid group. On the other hand, many transition metals and lanthanides are more effectively complexed by amino group (Patil et al., 2002; Chick et al., 1990).

Advantages of SCS method over other methods include fast speed, simplicity and cost-effectiveness, high yield (mass content), capability to achieve high purity crystalline materials. Additionally, SCS method provided that structure; composition, homogeneity and stoichiometry of products can control by this method (Barron et al., 2016; Patil et al., 2002).
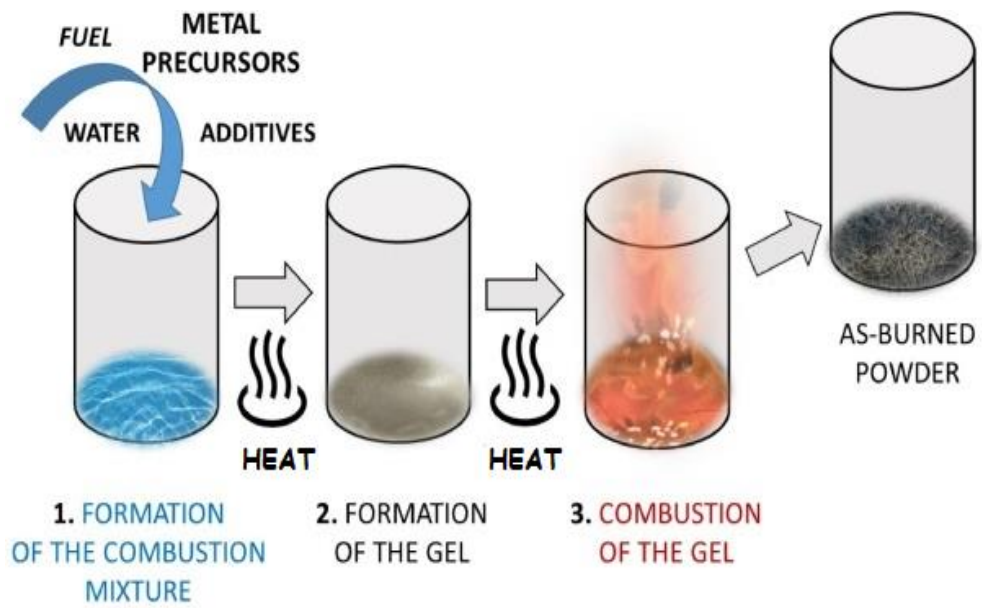
Figure 1.5. Schematic diagram of the synthesis process by solution combustion.
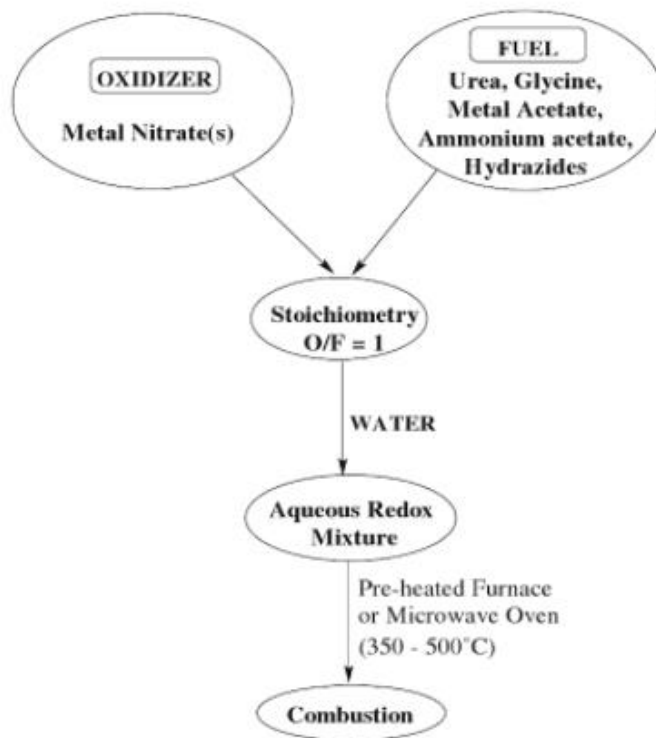
Figure 1.6. Flow diagram for solution combustion method (SCS) (Patil et al., 2002).

1.5   Effects of Rare Earth (RE) Elements

The using of rare earths as a dopant started since 1975. From that time, there have been several situations of formation the borate glasses with sufficiently rare-earth elements. Previous studies proved the typical ability of rare earth elements, not only on the enhancement of emitted light, but also on its capacity to create diverse optical properties as emission of wide spectral range. These optical properties are important to determine the laser properties of any material (Termizi et al., 2012).

There are several reasons for the use of rare-earth elements as dopants. These reasons about the behavior of rare-earth elements impurities in semiconductors possesses some severalizing properties such as the combination of low solubility with the capability of purifying the material. Such purification provided that a substantial decrease in the concentration of background impurities and defects and an increase in the charge-carrier mobility (Nemov et al., 2017).

Many rare earth (RE) ions displays that high luminescence efficiency in host borate crystals and glasses with various chemical compositions. As a result, combining rare earth dopants with the high thermal neutron capture cross-sections of Li or Mg and B may result in highly efficient neutron scintillators (Kelly et al., 2014).

The rare earth elements such as erbium which is of potential interest for telecommunications due to its photoluminescence (PL) emission. To achieve high-gain optical amplification in a few centimeter long waveguide, a high erbium concentration is required (Ibanez et al., 2011).

Figure 1.7. The rare-earth elements in the periodic table of elements (Righini et al., 2005).

Swapna et al., (2015) and Moorthy, (2007) said that among all the RE metal ions, Er^{3+} ions are considered to be the most important because of potential applications in the fields of optical fibre amplifiers, infrared lasers, erbium doped fibre amplifiers (EDFA) in the WDM System, microchip lasers, eye-safe lasers in medical fields.

The materials doped with RE ions became outstanding than crystals because of many advantages such as large RE^{3+} ion doping capacity, large in homogeneous line broadening and easy preparation, etc. This materials are also playing a significant role in producing highly efficient conversion lasers. It is well known that a host material with low phonon energies can suppress the nonradiative decay loss produced by multi-phonon relaxation and increases the luminescence efficiency (Swapna et al., 2015).

1.6   Doping Effects of Dy^{3+}, Ho^{3+} and Er^{3+}

In the studies of optical properties, Dy^{3+} doped borates are the available materials for yellow lighting applications in the visible range (Rao et al., 2015). Also, Dy^{3+} ions are well known as activator dopants for many different inorganic lattices producing white light emission by suitably adjusting the yellow and blue emission (Xiu et al., 2005).

According to Judd-Ofelt theory, the absorption spectra of rare-earth ions function as a basis for understanding their radiative properties. The sharp absorption lines arising from the 4f-4f electronic transitions can be magnetic dipole, electric dipole and electric quadrupole in character. As $4f$ electrons in the rare-earth atoms are well shielded by the outer $5s$ and $5p$ shells, the effective nuclear charge increases with increasing atomic number from Nd to Dy in rare earth elements, causing a reduction in the size of the $4f$ shell and a decrease in atomic or ionic radius from Nd to Dy. Consequently, the Dy-O distance is smaller than the Nd-O. This leads to an increase in the nephlauxetic effect, and an increase of Ω_2 as intensity parameter (Saisudha et al., 1996). Generally, Ω_2 is an indicator of the covalency of metal ligand bond. The Judd-Ofelt theory works well for the Ho^{3+} ion in study of all the mixed alkali borates. The Judd-Ofelt parameters, in particular Ω_2, are greater in mixed alkali borates than in the corresponding binary borates. The higher values of Ω_2 indicate higher covalency between holmium cation and oxide anions (Ratnakaram et al., 2003).

Rare-earth doped fiber is an optical fiber in which ions of a rare-earth element, such as Erbium or Holmium, have been indicated yielding high absorption with low loss in the visible, near-infrared spectral regions and included the glass core matrix. Rare earth ions are good applicant for active ions in laser materials because they demonstrates many absorption and fluorescence transitions in almost every region of the visible and the near-infrared range. Rare earths have another important characteristics in comparison to other optically active ions as well, the wavelengths of their emission and absorption transitions are relatively insensitive to host materials, the lifetimes of metastable states are long and the quantum efficiency tends to be high. These properties caused an excellent performance of rare earth ions in

many optical applications (Fibers optics for sale co, what are rare-earth doped fibers?)

Among the rare earths, Er^{3+} was chosen for study because its lower energy levels (40000 cm^{-1}) are well established in most crystals there are many fluorescing levels from which transitions occur involving a wide range of energies and between states of different character and it presents sufficient variety and complexity to provide an adequate test of any theory or treatment of radiative and nonradiative processes (Weber et al., 1967). So, in doping effect of Er^{3+}, the materials have more covalent character with higher symmetry which good host materials for broadband amplifiers and for laser applications in the near infrared region. Additionally, Er^{3+} ions are considered to be the most important because of potential applications in the fields of optical fibre amplifiers, infrared lasers, erbium doped fibre amplifiers (EDFA) in the WDM System, microchip lasers, eye-safe lasers in medical fields (Moorthy et al, 2007).

1.6.1 Literature Survey related with Dy-doped Studies

In study of (Santiago et al., 2011), Dy-doped strontium borates have been obtained by sol-gel method. The relationship of thermoluminescence and radioluminescence of the resulting borates have been examined. Thermoluminescence and Radioluminescence efficiency were increased with increasing of the concentration of doping metals involved in the luminescent studies.

Dysprosium doped strontium aluminates ($SrAl_2O_4:Dy^{3+}$) were synthesized by sol–gel combustion method. The effect of sol-gel combustion tempareture was investigated. As the sol–gel synthesis temperature increases from 600ºC to 800ºC, the green after glow of the ($SrAl_2O_4:Dy^{3+}$) phosphors becomes weaker in intensity and shorter in lifetime (Ma et al., 2015).

Dy^{3+} and Pr^{3+} co-doped lithium borate glasses were prepared by conventional melt quenching method. Among all rare earth doped glasses Dy^{3+} containing glasses are more interesting to study, because of its excessive emission in the visible region at 470-500 nm and around 570-600 nm. These emissions happen due to $^4F_{9/2} \rightarrow {}^6H_{15/2}$

(blue) and $^4F_{9/2} \rightarrow ^6H_{13/2}$ (yellow) transitions. Dy^{3+} doped glasses also shows one week emission band around 660-670 nm due to the transition $^4F_{9/2} \rightarrow ^6H_{11/2}$. These spectral transitions are necessary for white light emitting phosphor as well as glasses for W-LED application (Pawar et al., 2015).

Dy doped bismuth silicate single crystal was grown with high purity Dy_2O_3, SiO_2 and Bi_2O_3. At maximum doping concentration of Dy as 1.5%, the fluorescence intensity and lifetime were decreased (Xiong et al., 2017).

The Lead-free Dy^{3+}-doped zinc sodium bismuth borate were prepared by a melt-quench method. According to photoluminescence results, the triply ionized Dy^{3+} ions exhibit excitation bands in the near UV to blue region of the electromagnetic spectrum where most of the commercial UV and Blue LEDs have their emission wavelengths. Additionally, maximum absorption spectra was observed by ionic bond of Dy^{3+} ions with the surrounding O^{2-} ligands (Hegde et al., 2019).

Dy-doped lithium fluoroborate (LFB) was synthesized by melt-quench method. It was observed that density of the synthesized LFB-Dy glass was increased while the molar volume was decreased with increasing concentration of Dy^{3+} ions which proposed that the atoms are tightly bound, to each other, and are compact. The dysprosium ions with high density and high molecular mass replace borate ions with less density and low molecular mass, resulting in an increased density of the synthesized glasses (Zaman et al., 2019).

$Mg_2B_2O_5$ doped with Dy was synthesized by wet reaction. The Dy concentration was 0.01, 0.05, 0.1, 0.5, 1, 1.5 mol%. At concentration of 0.1 mol Dy, highest thermoluminescence response and excellent gamma rays and neutrons were found. Additionally, The largest peak was obtained at Dy 0.1% mol. For γ-rays, the peak was decreased with increasing the temperature. The same response was observed when the materials were exposed to neutrons (Cortes et al., 2019).

1.6.2   Literature Survey related with Ho-doped Studies

Mixed alkali effect (MAE) in $xNa_2O \cdot (30-x)K_2O \cdot 70B_2O_3$ (x = 5, 10, 15, 20 and 25) glasses doped with 0.5 Ho_2O_3 was investigated by measuring the optical properties of Ho^{3+}. According to the Judd-Ofelt parameters, the higher values of Ω_2 were obtained and which were indicated higher covalency between holmium cation and oxide anions in Ho^{3+} doped borate compound (Ratnakaram et al., 2003).

Ho^{3+} ion doped lead–zinc–borate glasses were synthesized by melting process. Large Ω_2 values were found and it was probably caused by relatively high covalency of the chemical bond in Ho^{3+} ion doped lead-zinc-borate structure (Hussain et al., 2006).

The phosphors of $Sr_{2.97}MgSi_2O_8:Eu^{2+}_{0.01},Ln^{3+}_{0.02}$ $(Ln^{3+}:Dy^{3+}$, Er^{3+} , $Ho^{3+})$ were synthesized with using small amount of H_3BO_3 as a flux by the solid-state reaction. The intensity of the emission was changed by different co-dopants. The afterglow properties of samples were enhanced with the Dy^{3+} , Er^{3+} or Ho^{3+} co-doping. Among these, the Dy^{3+} co-doped one showed the longest afterglow duration which had stronger thermoluminescence(TL) intensity (Nana et al., 2012).

The Ho^{3+} doped barium zinc boro tellurite glasses were prepared by conventional melt quenching technique at different concentrations. It is well known that rare earth ions doped materials display sharp excitation and emission bands. Highest emission intensity was found at 0.1 mol % which was found out that concentration quenching was occurred at 0.1 mol % doping concentration of Ho^{3+}. According to FTIR results, BO_4 units was present corresponding to Ho^{3+} ion (Rajaramakrishna et al., 2018).

$Ho^{3+}/Yb^{3+}/Er^{3+}$ tri-doped tellurite glasses have been prepared by melt-quenching method. According to spectroscopic results, the Ho^{3+} doped tellurite glass exhibits higher covalency between Ho–O bonds by considering Judd-Ofelt intensity parameters as Ω_2, Ω_4 and Ω_6. From the fluorescence emission spectra, it was found that the 2.0 μm band emission intensity of Ho^{3+} was enhanced greatly by increasing Er^{3+} doped concentration. The fluorescence decay behavior was investigated to exhibit the energy transfers existed in the doped rare-earth ions, and the energy

14

transfer mechanism was analyzed to find out the role of host phonon in the realization of energy transfers (Zhu et al., 2019).

Ho^{3+} single doped tellurite-borate glasses with various compositions were synthesized by solid state reaction technique. $^5I_8 \rightarrow ^5G_6$ transition of Ho^{3+} ion was steady with that of Judd-Ofelt parameter Ω_2 with increasing the B_2O_3 concentration, indicating that Ω_2 plays an important role of higher covalency character. Additionally, as the temperature increases the higher levels of the ground state are stayed and the absorption in lower energy regions were increased in transition of Ho^{3+} (Yanmin et al., 2015).

1.6.3   Literature Survey related with Er-doped Studies

Er-doped, Li-doped, and co-doped (Er, Li) ZnO nanocrystallites were synthesized by solution combustion method. According to the XRD results, the crystallite size was increased for Li^+ doping, while (Er + Li) co-doping was decreased the crystallite size. After annealing at 800ºC, all the samples were shown blue shift, due to erbium atom in the ZnO act as donors and increase the concentration of electrons in the conduction band (Sivasankari et al., 2013).

Borophosphate compound doped with Er which was synthesized by conventional melt-quenching method. According to photoluminescence results, photoluminescence(PL) lifetime and photoluminescence(PL) intensity were decreased with increasing B_2O_3 content. The addition of B_2O_3 was caused the formation of B-O-P, which wasresponsible for more rigid borophosphate network (Sdiri et al., 2014).

Er-doped lithium tetraborate compound was synthesized by solid state reaction. According to optical absorption, luminescence emission and excitation spectra of the investigated borate compounds f – f transitions of the Er^{3+} centers were observed, which was characterised by inhomogeneous broadening of the spectral lines caused by statistical distribution of the structural parameters (Er – O interatomic distances and coordination numbers to oxygen). In IR emission results, the lifetime for green emission band was decreased with increasing the Er

concentration that was related to the influence of the Er^{3+} – Er^{3+} pair centres, coupled by exchange interaction (Padlyak et al., 2016).

A novel erbium doped zinc borate compound were prepared and their transmission and photoluminescence properties were investigated for Er^{3+} ion doping concentrations. Narrow emission and absorption features were obtained due to 4f-4f electronic transitions in Er^{3+} ions superposed on the broad band host compound luminescence (Kostka et al., 2017).

2 mol% Dy ZnO, 2 mol% Er ZnO and 1 mol% Dy and 1 mol% Er co-doped ZnO nanoparticles were synthesized by combustion method. Due to the annealing effect, the enhancement of upconversion luminescence intensity in co-doped sample in green (535 nm) and red (665 nm) regions was observed at the 980 nm excitation. As a result, dysporsium and erbium metals as co-doping and annealing at high temperature with solution combustion method which were effected luminescence intensity as increasing values in nm regions (Kalaiezhily et al., 2018).

The Er^{3+} ions doped lithium borate was prepared by the melting quench method. As a result of the structural analysis by FTIR, which was confirmed the presence of bending vibration B-O-B in borate networks, B-O bond stretching of tetrahedral BO_4 units, and asymmetric stretching of the B-O vibrations in trigonal BO_3 units. This doping compound was demonstrated the great potential for infrared laser and optical amplifier applications (Rajagukguk et al., 2019).

Er^{3+} doped alkali borate and fluoroborate glasses have been synthesized by conventional melt quenching technique. The Er^{3+} ligand bond was ionic in nature and the degree of ionic character was changed with the change in chemical composition. The higher values of Ω_2 parameter were indicated the higher asymmetry nature of the ion site and were approved the less ionic character of the Er^{3+} ions with the surrounding ligands (Rayappan et al., 2013).

2. AIM AND SCOPE OF THE STUDY

The aim of this study is to synthesize rare earth metals doped $Mg_2B_2O_5$ nanoparticles by solution combustion synthesis method.

$Mg_2B_2O_5$: RE (Dy^{3+}, Ho^{3+}, Er^{3+}) nanoparticles were synthesized using different fuels such as glycine, tartaric acid, citric acid, urea and hexamethylenetetramine (HMTA).

RE (Dy^{3+}, Ho^{3+}, Er^{3+}) concentrations were varied as 0.005, 0.010, 0.020, 0.050 mol.

Firstly, RE doped $Mg_2B_2O_5$ nanoparticles obtained as gels were heated at 400^oC with 10min. for completing combustion process. Secondly, the prepared products were heated at 700^oC 2h., 800^oC 1h. and 900^oC 1h. to obtain pure and crystalline RE doped $Mg_2B_2O_5$ nanoparticles. Finally, the nanoparticles prepared through solution combustion synthesis process were characterized using IR, XRD and UV-VIS techniques for each concentration and temperature range.

The effect of temperature, type of rare earth ions and their various concentration on the optical characteristics of the products were investigated and how these parameters affected the crystallinity, crystallite size and purity of RE doped $Mg_2B_2O_5$ nanoparticles were also examined.

3. MATERIALS AND METHODS

3.1   Chemicals

The following chemicals were used in the synthesis of products:

$Mg(NO_3)_2.6H_2O$, Magnesium nitrate hexahydrate: Merck (pure 99.0%)

$Dy(NO_3)_3.5H_2O$, Dysprosium (III) nitrate pentahydrate: Aldrich (pure 99.5%)

$Ho(NO_3)_3.5H_2O$, Holmium (III) nitrate pentahydrate: Aldrich (pure 99.5%)

$Er(NO_3)_3. 5H_2O$, Erbium (III) nitrate pentahydrate: Aldrich (pure 99.5%)

$C_2H_5NO_2$, Glycine: Merck (pure $\geq$ 99.7%)

$C_4H_6O_6$, L(+)-Tartaric Acid: Merck (pure 99.0%)

CH_4N_2O, Urea: Merck (pure 99.5%)

$C_6H_8O_7.H_2O$, Citric Acid Monohydrate: Merck (pure 99.5%)

$C_6H_{12}N_4$, Hexamethylenetetramine: Merck (pure 99.0%)

H_3BO_3, Boric Acid: Fluka (pure 99.5%)

KBr: Spectroscopic grade and it was used for making IR pellets.

It was dried at 180°C before using.

3.2   Instruments

3.2.1 X-Ray Powder Diffractometer

X-ray powder diffraction patterns (XRD) were recorded on Rigaku miniflex, BD127412, and CuKα (30-40 kV, 10-20 mA, λ=1.54056 Å) radiation. Indexing of the XRD pattern was checked by Rigaku Programme.

3.2.2 Infrared Spectrophotometer

Shimadzu FT-IR-8400S Fourier Transform Infrared (FTIR) Spectrophotometer was used to obtain the spectra of the products in the region of the 4000-400 cm^{-1}. Spectra of solid samples were taken from KBr pellets using 0.0010:0.150 (wt/wt) product to KBr ratio.

3.2.3 Ultraviolet-Visible Spectrometer

Perkin Elmer Lambda 35 UV-VIS Spectroscopy was used to determine the optical properties of the samples. The spectra were recorded at wavelength range 200-900nm. The data was plotted by using Data Processor WinLab.

3.2.4 Furnaces

The reactions during the preparation of metal borates were carried out at heating range between 400-900ºC by the aid of Nuve MF 120 furnace.

3.3   Experimental Procedure

3.3.1   Synthesis of Rare Earth Metals (RE:Dy^{3+}, Ho^{3+}, Er^{3+}) doped $Mg_2B_2O_5$ using Gly, TA, CA, U and HMTA Fuels

Magnesium pyroborate ($Mg_2B_2O_5$) powders were synthesized with different amounts of Dy^{3+}, Ho^{3+}, Er^{3+} ions by solution combustion process. Dopant concentrations were used as x = 0.005, 0.01, 0.02, 0.05 mol to obtain $Mg_{(2-x)}RE_{(x)}B_2O_5$.

The raw materials, magnesium nitrate ($Mg(NO_3)_2.6H_2O$), boric acid (H_3BO_3) and dysprosium nitrate ($Dy(NO_3)_3.5H_2O$), holmium nitrate ($Ho(NO_3)_3.5H_2O$), erbium nitrate ($Er(NO_3)_3.5H_2O$) were the source of Mg, B, and Dy, Ho, Er respectively. Each RE metal was synthesized with Gly, TA, CA, U and HMTA fuels to obtain $Mg_2B_2O_5$:RE pyroborates. Stoichiometric proportion required for solution combustion synthesis was calculated considering total oxidizing and reducing valances of oxidizer and fuel.

Firstly, the process was performed by dissolving above reagents together in a minimum amount of distilled water and the concentration of the rare earth metal ions were changed in 0.005, 0.010, 0.020, 0.050 mol. Using a magnetic stirrer, the materials were evenly mixed in a porcelain evaporating dish and heated at 370°C until gel formation was obtained. Then, it was put in the preheated furnace adjusted at 400°C. The whole combustion process for producing RE metals (Dy, Ho and Er) doped $Mg_2B_2O_5$ material took 10 min. After 400°C furnace process, the prepared product was taken out from the furnace, cooled down to the room temperature and was crushed and blended well. Then, little amount of each samples were separated in sample dish for IR analysis.

Secondly, each crushed samples were put into crucible and again placed into the preheated furnace at 700°C for 2 hour, 800°C 1 hour and 900°C 1 hour to get rid of all organic compounds and to complete SCS process. At the end of each heating period including 400 °C 10 min. and 700°C 2 hour, 800°C 1 hour, 900°C 1 hour the samples were analysed with FTIR, XRD and UV-VIS.

The predicted general reactions with different fuels;

$(2-x)$ $Mg(NO_3)_2.6H_2O_{(s)}$ + x $Ln(NO_3)_2.5H_2O_{(s)}$ + $2H_3BO_{3(s)}$ + $fuel_{(s)} \rightarrow$
$Mg_{(2-x)}Ln_{(x)}B_2O_{5(s)}$ + $CO_{2\ (g)}$ + $H_2O_{(g)}$ + $NO_{2(g)}$
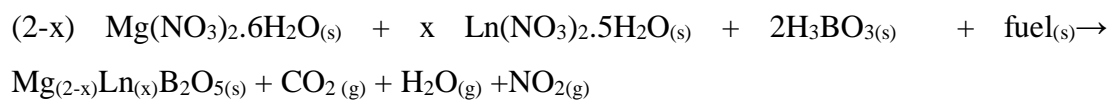
$(Ln= Dy^{3+}, Ho^{3+}, Er^{3+})$

(fuel= Glycine, tartaric acid, citric acid, urea and hexamethylenetetramine)

(x= 0.005, 0.010, 0.020 and 0.050 mol)
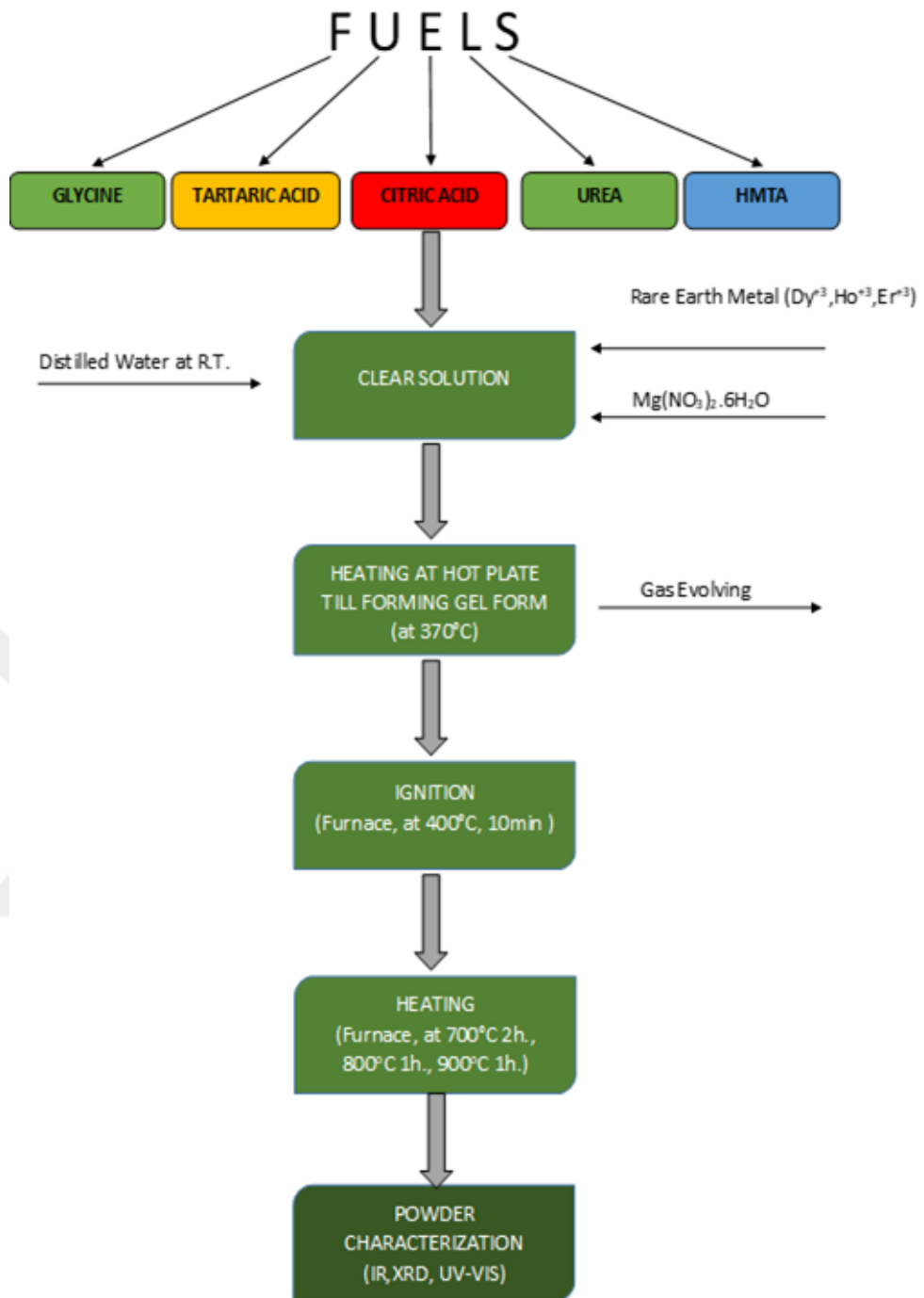
Figure 3.1. Procedure for RE metal (Dy^{3+}, Ho^{3+}, Er^{3+}) doped $Mg_2B_2O_5$ synthesis with SCS method.

4. RESULTS AND DISCUSSIONS

4.1 Rare Earth (RE: Dy^{3+}, Ho^{3+}, Er^{3+}) doped $Mg_2B_2O_5$ from Gly, TA, CA, U and HMTA fuels

$Mg_2B_2O_5$:Rare Earth (RE: Dy^{3+}, Ho^{3+}, Er^{3+}) pyroborates were prepared via solution combustion method exploiting magnesium nitrate, boric acid and different fuels such as Gly, TA, CA, U and HMTA. In this examination, it was figured out that dopant concentration, type of fuels and different temperature have significant affect on the crystallinity of the $Mg_2B_2O_5$ products. Furthermore, crystallinity of $Mg_2B_2O_5$ were investigated with different RE metals and concentrations.

In the synthesis of RE doped $Mg_2B_2O_5$, the yield of doped $Mg_2B_2O_5$ product is decreasing in the order of TA, CA, Gly, U and HMTA, respectively. When the HMTA and U were used as fuel, large amount of gas evolution was observed and the time duration needed for gel formation is faster than other fuels. When Gly used as fuel, the product was fluffy and light brown color after combustion process at $400^{o}C$ for 10 min., shown in Figure 4.2, Figure 4.3, Figure 4.4, Figure 4.5. When TA and CA used as fuel, the product was puffy and dark brown, cream color, respectively. On the other hand, $Mg_2B_2O_5$ product was not fluffy and white color when HMTA and U were used as fuel shown in Figure 4.2, Figure 4.3, Figure 4.4, Figure 4.5.

After the heating process of $700^{o}C$ 2h., the color of doped $Mg_2B_2O_5$ product was white when HMTA and U were used as fuel. The color of product was light grey when CA was used as fuel. And, when the TA was used as fuel, the product was grey color, shown in Figure 4.6. After $700^{o}C$ 2h. process, the heating processes of $800^{o}C$ 1h. and $900^{o}C$ 1 h. was completed.

The pictures that is shown below the products while gel formed.

Figure 4.1. The gelious form images of doping $Mg_2B_2O_5$ samples were synthesized with a) Gly, b) TA, c) CA, d) U, e) HMTA

4.2   Dy doped $Mg_2B_2O_5$

The stoichiometric mixture of reactants, $Mg(NO_3)_2.6H_2O$, $Dy(NO_3)_3.5H_2O$, H_3BO_3, fuels such as Gly, TA, CA, U, HMTA and distilled water were mixed and heated at $370^{\circ}C$ until gel form is obtained to produce $Mg_{(2-x)}Dy_{(x)}B_2O_5$ (x = 0.005, 0.010, 0.020, 0.050 mol). Then, it was put into furnace at $400^{\circ}C$ 10min. to acquire combustion. After that, it was heated to $700^{\circ}C$ for 2 hour to get best result of doped $Mg_2B_2O_5$ crystallinity.

The general reaction with different type of fuels;

$$(2-x)\ Mg(NO_3)_2.6H_2O_{(s)} + x\ Dy(NO_3)_2.5H_2O_{(s)} + 2H_3BO_{3(s)} + fuel_{(s)} \rightarrow$$

$$Mg_{(2-x)}Dy_{(x)}B_2O_{5(s)} + CO_{2\ (g)} + H_2O_{(g)} + NO_{2(g)}$$
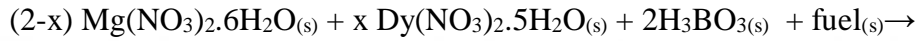
(fuel= Glycine, tartaric acid, citric acid, urea and hexamethylenetetramine)

(x= 0.005, 0.010, 0.020 and 0.050 mol)

In the combustion process of $Mg_2B_2O_5$ doped with Dy^{3+}, the intensity order of combustion highest to lowest was Gly, TA, CA, U and HMTA, respectively. Unlike the other fuels, when HMTA was used, the product's shape was speckled in 0.005, 0.010, 0.020, 0.050 mol, shown in Figure 4.2, Figure 4.3, Figure 4.4, Figure 4.5. The Dy^{3+} doped $Mg_2B_2O_5$ product was obtained more amount with Gly fuel and it was puffy and light brown color in 0.005, 0.010, 0.020, 0.050 mol Dy^{3+} concentrations at the end of $400^{\circ}C$ 10min. heating process, shown in the Figure 4.2, Figure 4.3, Figure 4.4, Figure 4.5. Additionally, the color of the gel form of the product was getting darker from light yellow to slightly light yellow with increasing concentrations. The color of the $Mg_2B_2O_5$ doped with Dy^{3+} that was synthesized with TA fuel was getting darker from brown to dark brown in 0.005, 0.010, 0.020, 0.050 mol Dy^{3+} concentrations after the $400^{\circ}C$, 10min., shown in the Figure 4.2, Figure 4.3, Figure 4.4, Figure 4.5. The product color was changed from brown to grey at the end heating process of $700^{\circ}C$ 2h., shown in Figure 4.6. While Dy^{3+} doped $Mg_2B_2O_5$ product with CA fuel was cream color and fluffy at $400^{\circ}C$ 10min., light grey color was observed after $700^{\circ}C$ 2h. On the other hand, the product was white

color with U and HMTA fuel and more gas evolution was observed compared with other fuels such as Gly, TA and CA.

The pictures that is shown below the products after 400°C 10min.
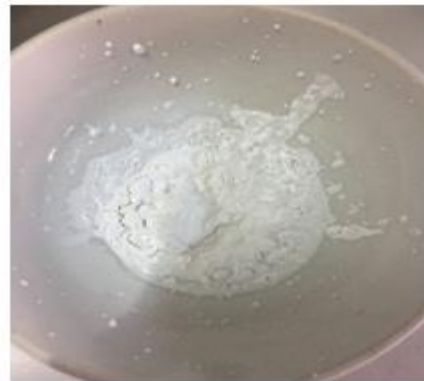
Figure 4.2. The images of $Mg_{2.995}Dy_{0.005}B_2O_5$ samples were synthesized with a) Gly, b) TA, c) CA, d) U, e) HMTA

Figure 4.3. The images of $Mg_{2.990}Dy_{0.010}B_2O_5$ samples were synthesized with a) Gly, b) TA, c) CA, d) U, e) HMTA
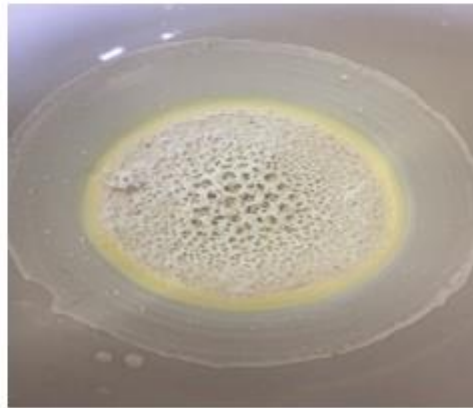
Figure 4.4. The images of $Mg_{2.980}Dy_{0.020}B_2O_5$ samples were synthesized with a) Gly, b) TA, c) CA, d) U, e) HMTA
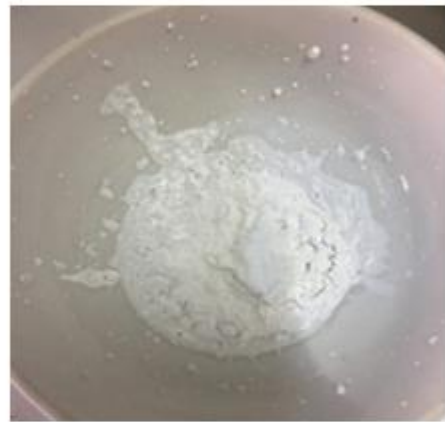
Figure 4.5. The images of $Mg_{2.950}Dy_{0.050}B_2O_5$ samples were synthesized with a) Gly, b) TA, c) CA, d) U, e) HMTA

The pictures that is shown below the products after 700°C 2h.
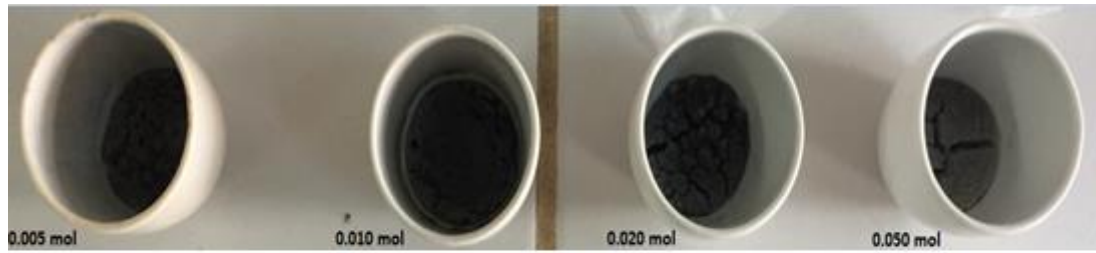
a
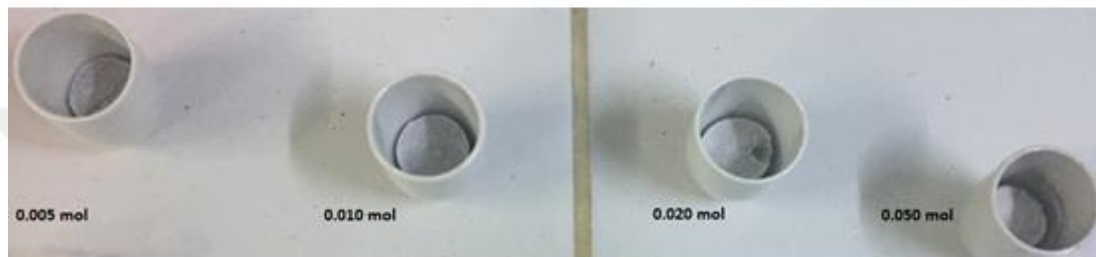
b

c
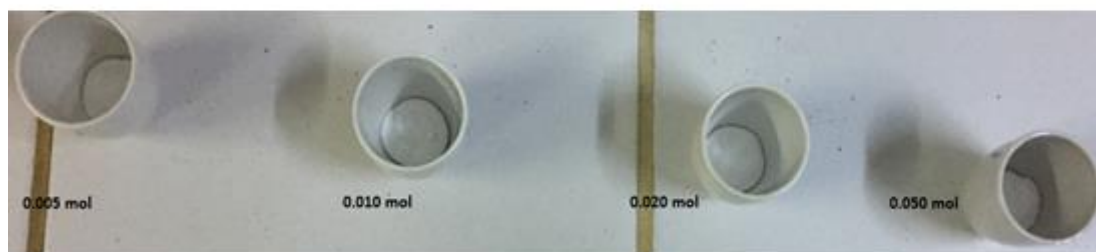
d

Figure 4.6. The images of $Mg_{(2-x)}Dy_{(x)}B_2O_5$ samples were synthesized as x = 0.005, 0.010, 0.020, 0.050 mol with a) TA, b) CA, c) U, d) HMTA

4.2.1   XRD Studies of Dy doped Mg₂B₂O₅

Figure 4.7, Figure 4.8, Figure 4.9 and Figure 4.10 shows powder X-ray diffraction patterns of Dy doped magnesium pyroborate synthesized from different fuels and at 700°C 2h. When all these figures considered, the intensity sequence from the highest to lowest is HMTA, U, Gly, CA, TA after the heating process of 700°C 2h. All these XRD peaks of doped compounds were matched with 15-0537 ICDD data card for triclinic $Mg_2B_2O_5$. The results exhibited that used different fuels gave doped $Mg_2B_2O_5$ products with different morphologies and crystallinity.

Dy doped $Mg_2B_2O_5$ synthesized with TA fuel has lowest crystallinity as 558.33 cps at 34.860 (2theta) and highest yield in all four concentrations (0.005, 0.010, 0.020, 0.050 mol) after the combustion process of 700°C 2h. Dy doped $Mg_2B_2O_5$ synthesized with HMTA fuel has highest crystallinity and lowest yield in considering all four concentrations (0.005, 0.010, 0.020, 0.050 mol) after the combustion process of 700°C 2h. The highest intensities of Dy doped $Mg_2B_2O_5$ are 995.83 cps at 34.940 (2theta) for 0.005 mol, 845.83 cps at 34.880 (2theta) for 0.010 mol, 841.68 cps at 35.040 (2theta) for 0.020 mol, 712.50 cps at 34.960 (2theta) for 0.050 mol by using HMTA fuel. When U is used as fuel, the intensities of product obtain as 937.50 cps at 34.860 (2theta) for 0.005 mol, 904.17 cps at 35.020 (2theta) for 0.010 mol, 683.34 cps at 34.840 (2theta) for 0.020 mol and 583.33 cps at 34.960 (2theta) for 0.050 mol. Apparently, the crystallinity is decreased as shifting the position of 2theta changes when the dopant concentration is increased. Consequently, HMTA and U are suitable fuels in our study because it produces $Mg_2B_2O_5$ with high crystalline.

Additionally, the crystallite size (D) of Dy^{3+} doped $Mg_2B_2O_5$ that was synthesized with different fuels were calculated from the XRD pattern according to Scherrer formula

$$D = \frac{K\lambda}{\beta Cos\theta}$$

where K is the constant, λ is the X-ray wavelength (0.15406 nm), β is the full-width at half maximum and θ is the diffraction angle.

Table 4.1. 0.005 mol Dy^{3+} doped $Mg_2B_2O_5$ crystallite size changing with fuels

FUELS	Crystallite size, nm (700°C, 2h.)
Gly	14,58
TA	11,34
CA	13,87
U	15,15
HMTA	18,72

Table 4.2. 0.010 mol Dy^{3+} doped $Mg_2B_2O_5$ crystallite size changing with fuels

FUELS	Crystallite size, nm (700°C, 2h.)
Gly	14,71
TA	13,31
CA	14,32
U	16,67
HMTA	18,86

Table 4.3. 0.020 mol Dy^{3+} doped $Mg_2B_2O_5$ crystallite size changing with fuels

FUELS	Crystallite size, nm (700°C, 2h.)
Gly	14,81
TA	13,46
CA	14,67
U	17,04
HMTA	18,98

Table 4.4. 0.05 mol Dy^{3+} doped $Mg_2B_2O_5$ crystallite size changing with fuels

FUELS	Crystallite size, nm (700°C, 2h.)
Gly	15,02
TA	13,84
CA	14,96
U	18,04
HMTA	19,11

Table 4.1, Table 4.2, Table 4.3 and Table 4.4 shows that while the crystallite size of Dy^{3+} doped $Mg_2B_2O_5$ synthesized with Gly, TA, CA, U and HMTA increases with increasing amount of moles. Otherwise, Dy^{3+} doped $Mg_2B_2O_5$ synthesized with HMTA has larger crystallite size when compared with other fuels.
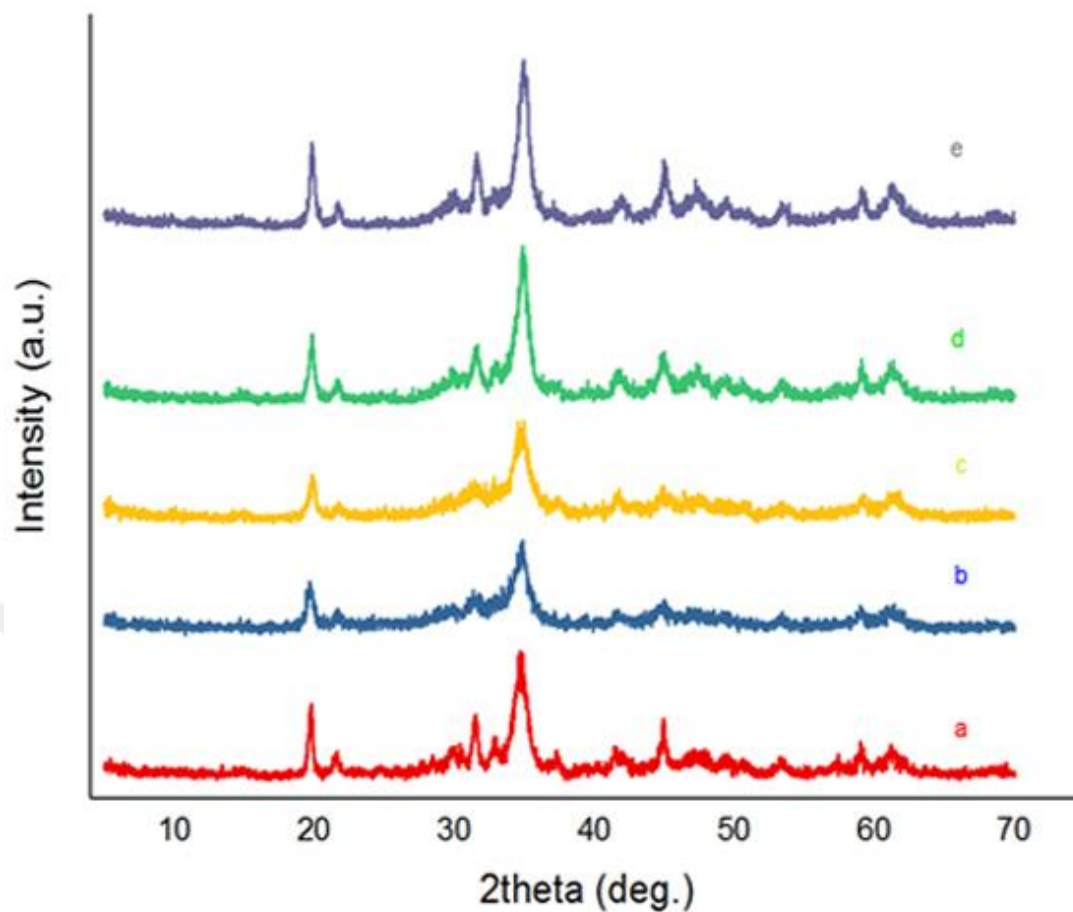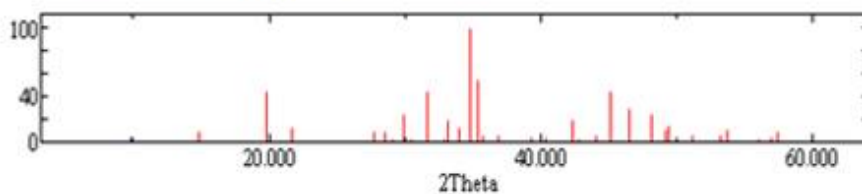
Figure 4.7. XRD patterns of 0.005 mol Dy doped $Mg_2B_2O_5$ at 700°C 2h., using a) Gly, b) TA, c) CA, d) U, e) HMTA with ICDD Data Card for 15-0537 Triclinic $Mg_2B_2O_5$
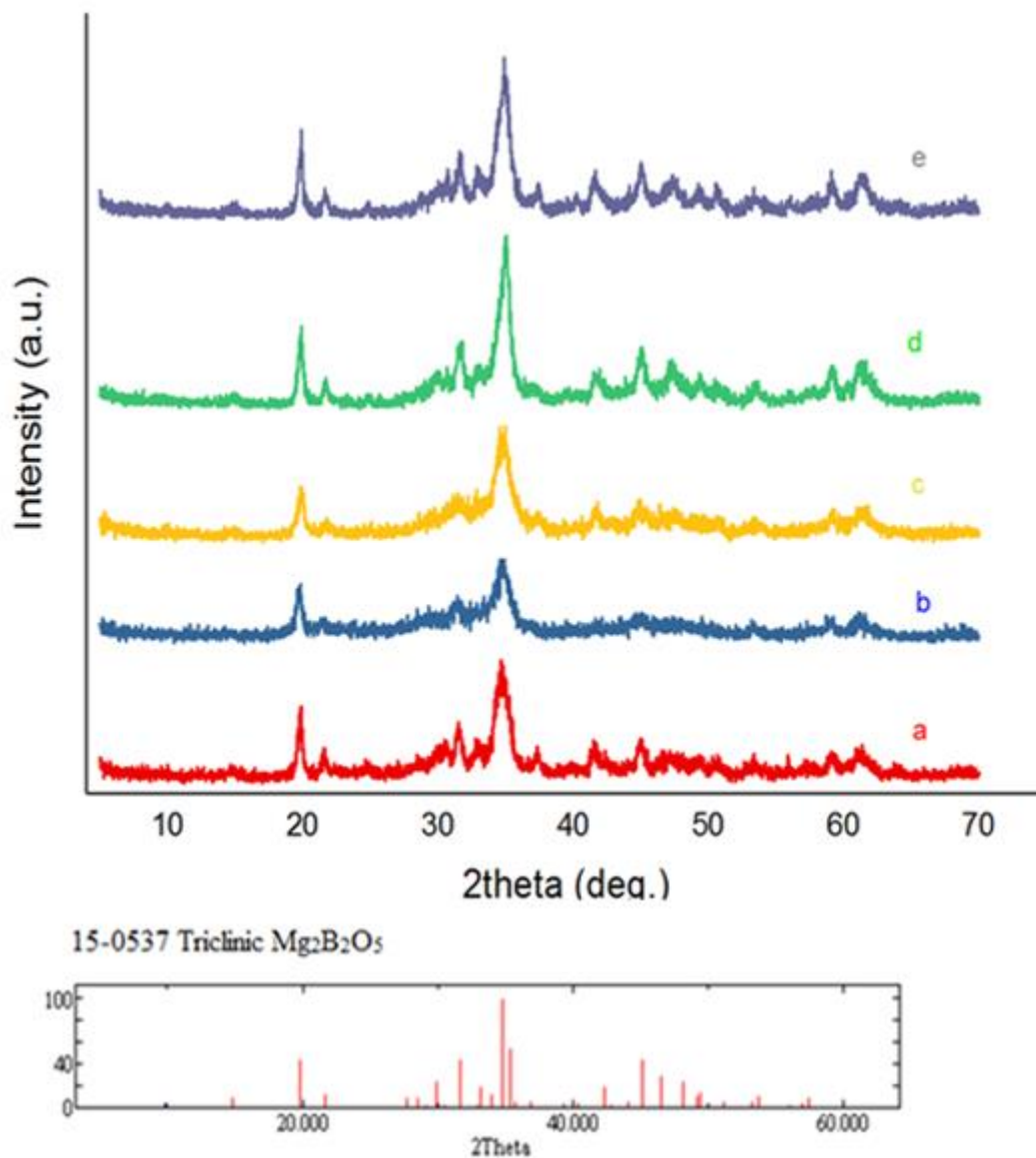
Figure 4.8. XRD patterns of 0.010 mol Dy doped $Mg_2B_2O_5$ at 700°C 2h., using a) Gly, b) TA, c) CA, d) U, e) HMTA with ICDD Data Card for 15-0537 Triclinic $Mg_2B_2O_5$
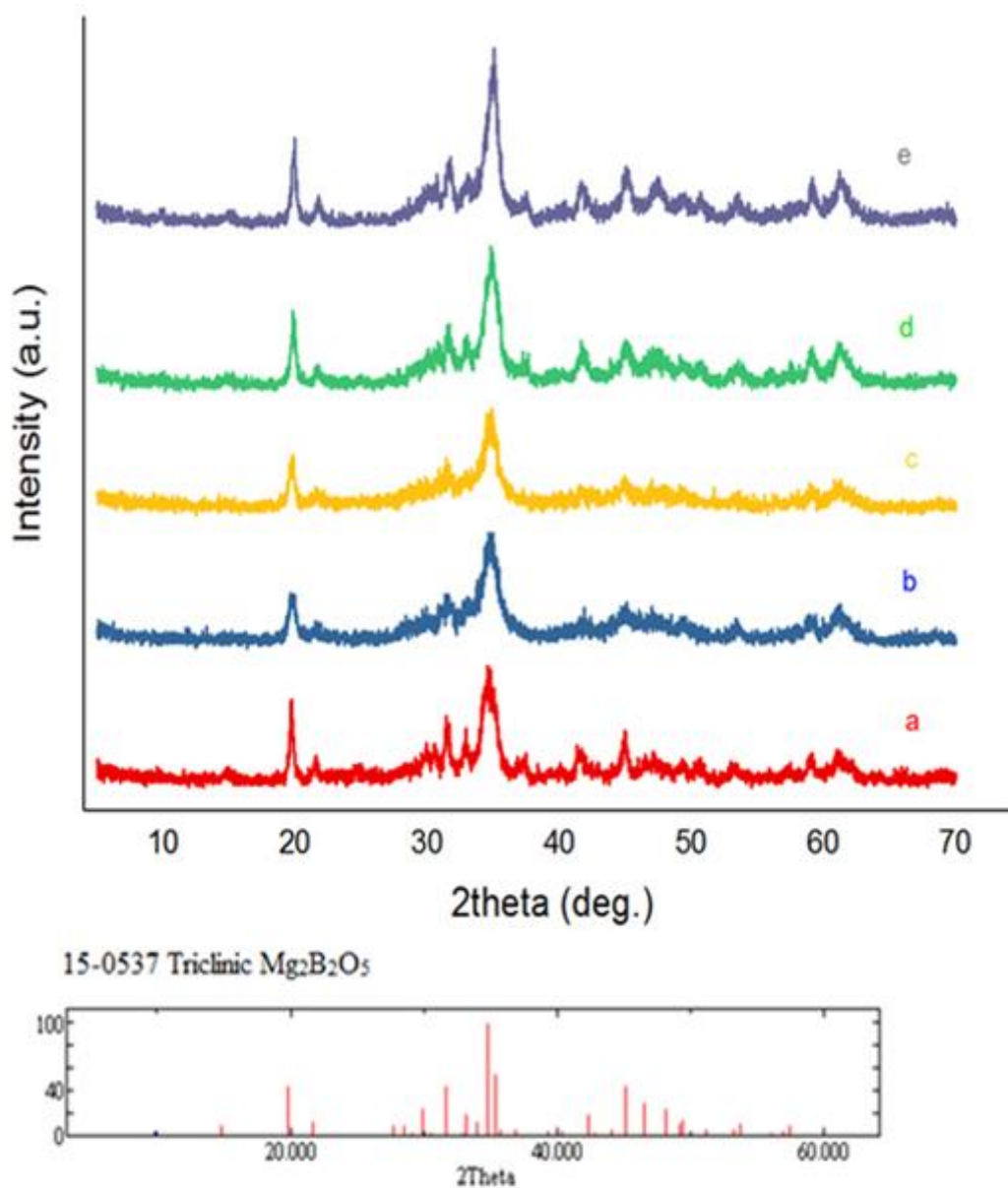
Figure 4.9. XRD patterns of 0.020 mol Dy doped $Mg_2B_2O_5$ at $700^{\circ}C$ 2h., using a) Gly, b) TA, c) CA, d) U, e) HMTA with ICDD Data Card for 15-0537 Triclinic $Mg_2B_2O_5$
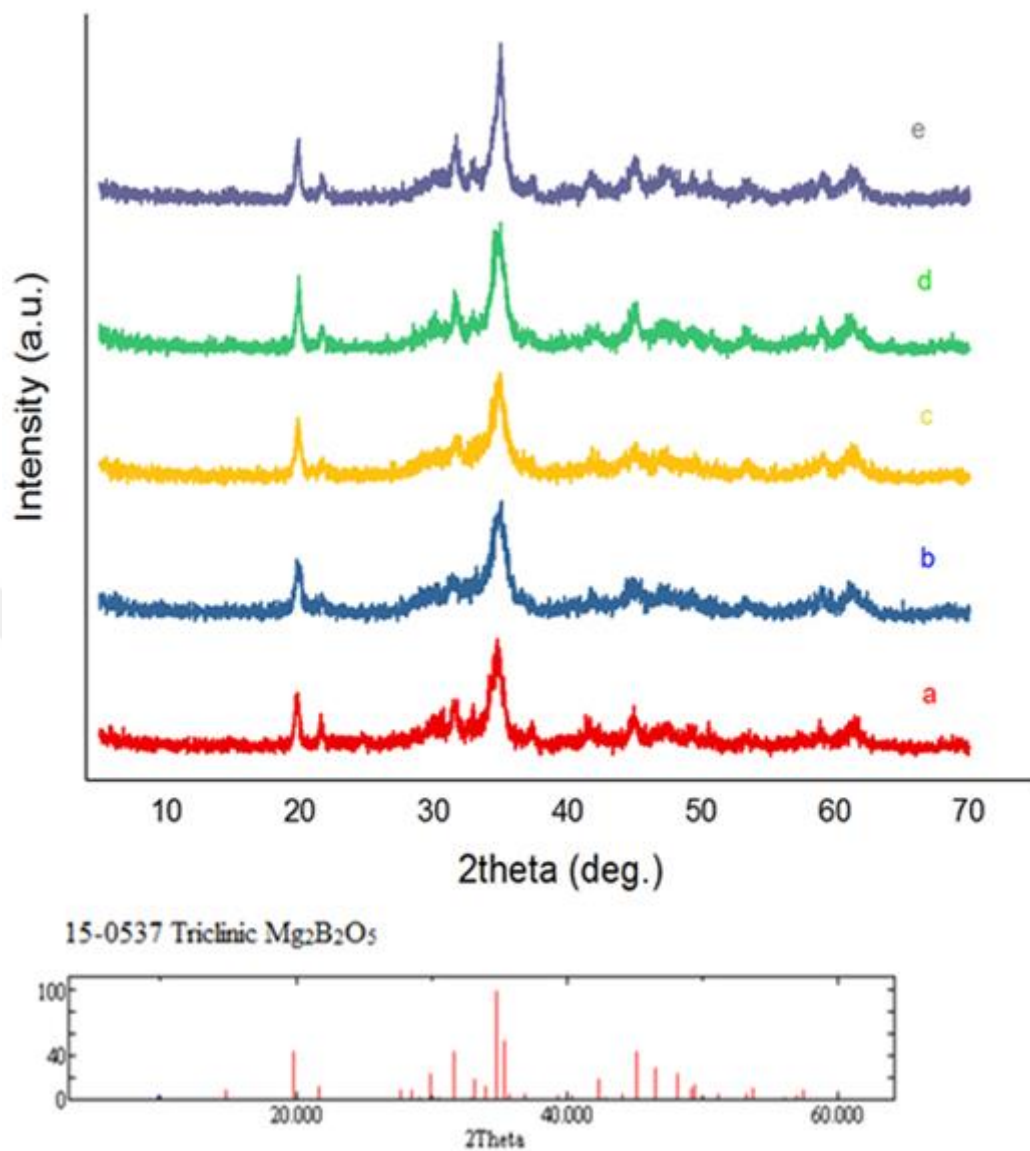
Figure 4.10. XRD patterns of 0.050 mol Dy doped $Mg_2B_2O_5$ at 700°C 2h., using a) Gly, b) TA, c) CA, d) U, e) HMTA with ICDD Data Card for 15-0537 Triclinic $Mg_2B_2O_5$

4.2.2 Infrared Spectroscopy Studies of Dy doped Mg₂B₂O₅

Fourier transform infrared (FTIR) spectra of Dy^{3+} doped $Mg_2B_2O_5$ samples synthesized with SCS method was recorded in the range 300-4000 cm⁻¹ using KBr pellets. IR spectra of $Mg_{(2-x)}Dy_{(x)}B_2O_5$ (x = 0.005, 0.010, 0.020, 0.050 mol) samples at 400°C for 10min. , 700°C 2h. , 800°C 1h. and 900°C 1h. were shown in below. The strong bonds at 1450-1550 cm⁻¹ and 600-750 cm⁻¹ was correlated with characteristic vibrational of $Mg_2B_2O_5$. When the heating process increased from 400°C to 900°C, the absorption of 600-750 cm⁻¹ spectrum was became clear. In the pyroborate, the group of bands between 1100 cm⁻¹ and 1450 cm⁻¹ are strong, broad, and very strongly dependent on isotopic mass (Weir et al.,1964).

The absorption peak at 1150–1200 cm⁻¹ can be assigned to antisymmetric stretching vibrations of the BOB groups in pyroborates (Guo et al., 2014). The spectra of synthetic triclinic suanite exhibited a single band at 610 cm⁻¹ (Oztas et al., 2009).
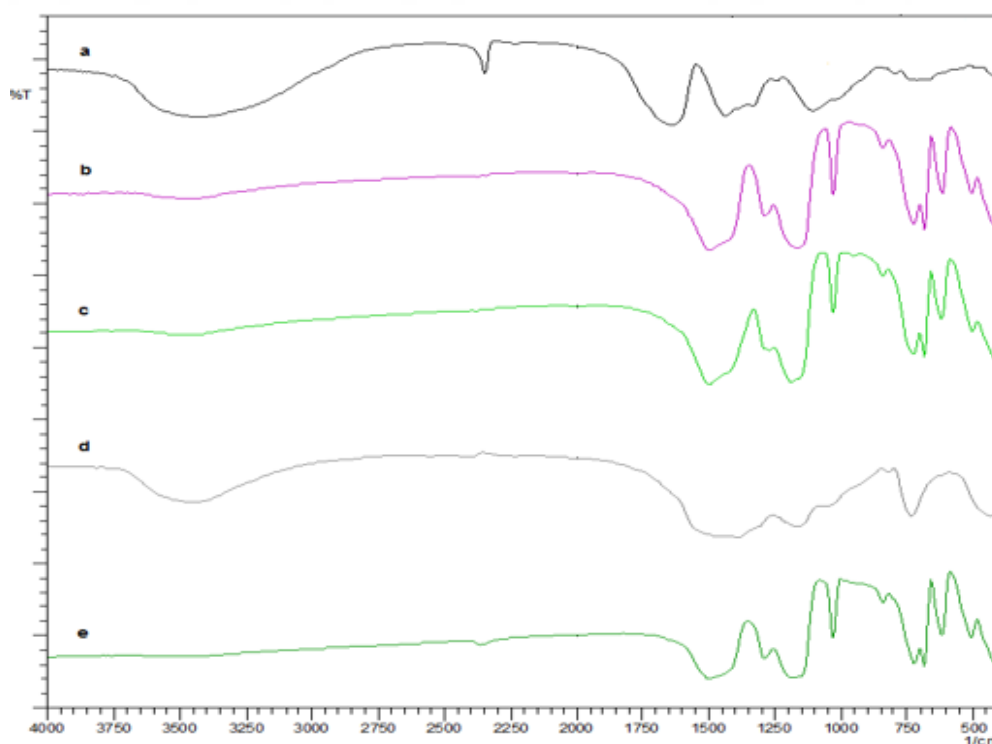
Figure 4.11. IR spectra of 0.005 mol Dy doped $Mg_2B_2O_5$ at 400°C 10 min. using a) Gly, b) U, c) CA, d) TA, e) HMTA

39
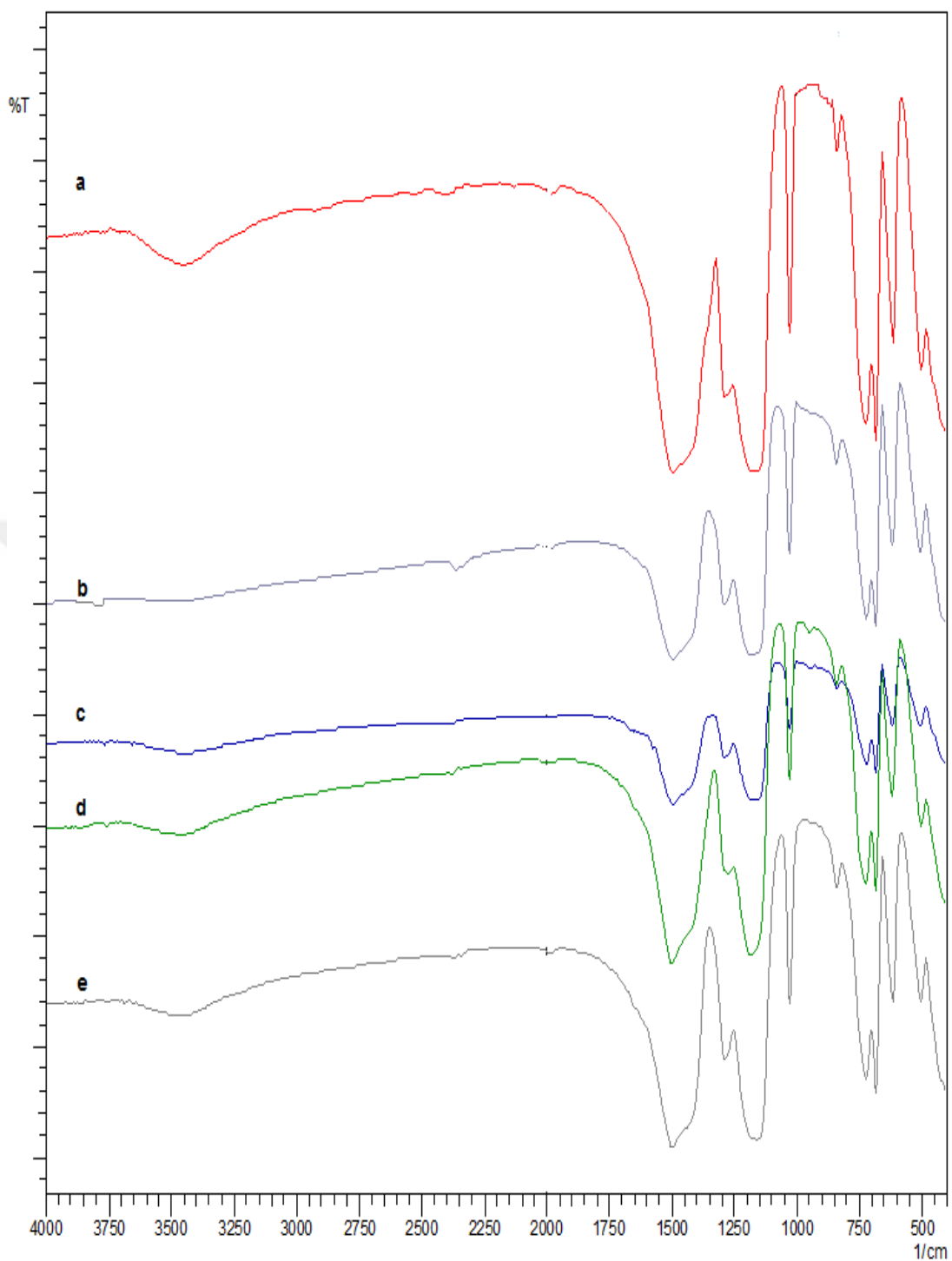
Figure 4.12. IR spectra of 0.005 mol Dy doped $Mg_2B_2O_5$ at 700°C 2h. using
a) Gly, b) TA, c) CA, d) U, e) HMTA
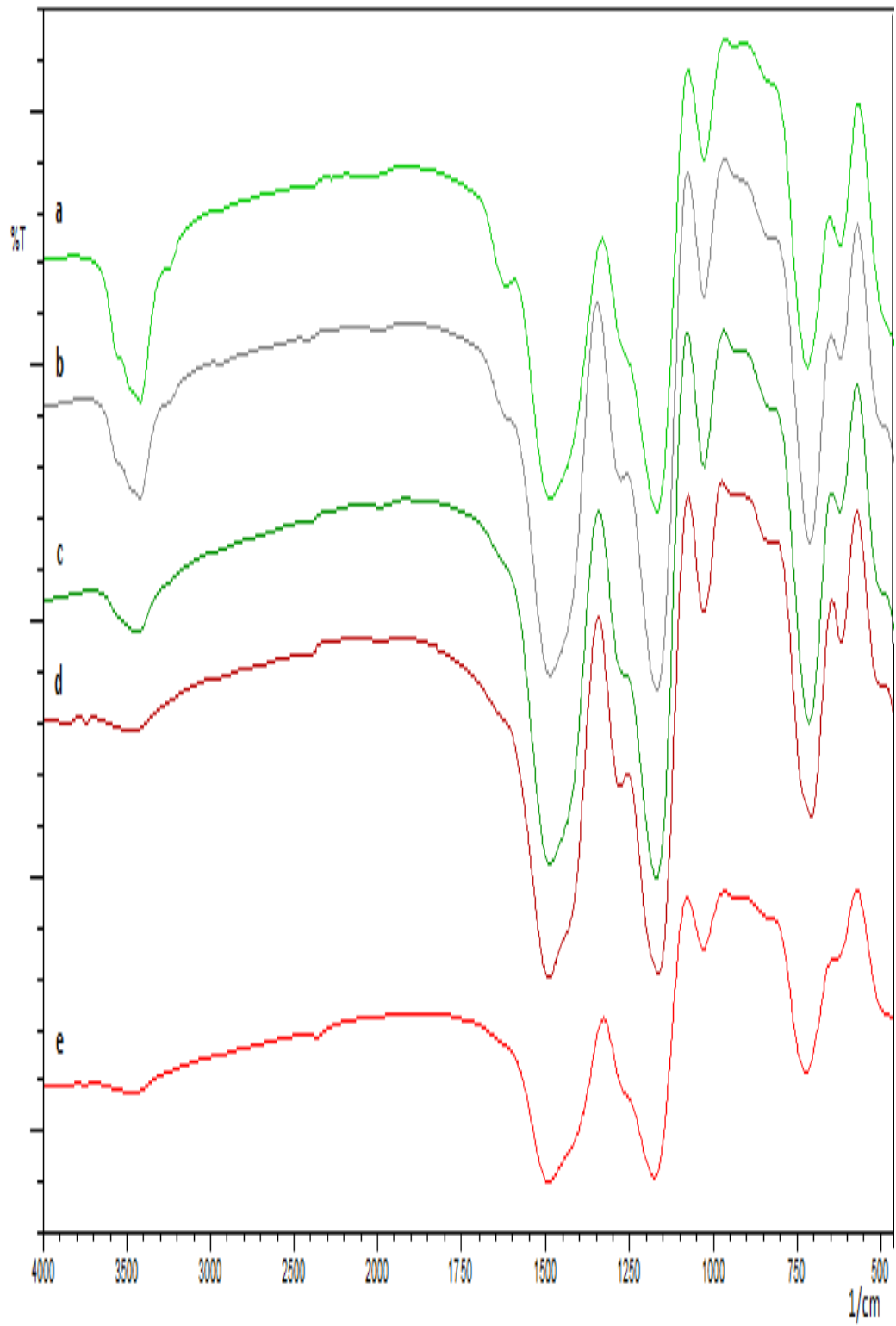
Figure 4.13. IR spectra of 0.005 mol Dy doped $Mg_2B_2O_5$ at 800°C 1h. using
a) Gly, b) HMTA, c) U, d) TA, e) CA
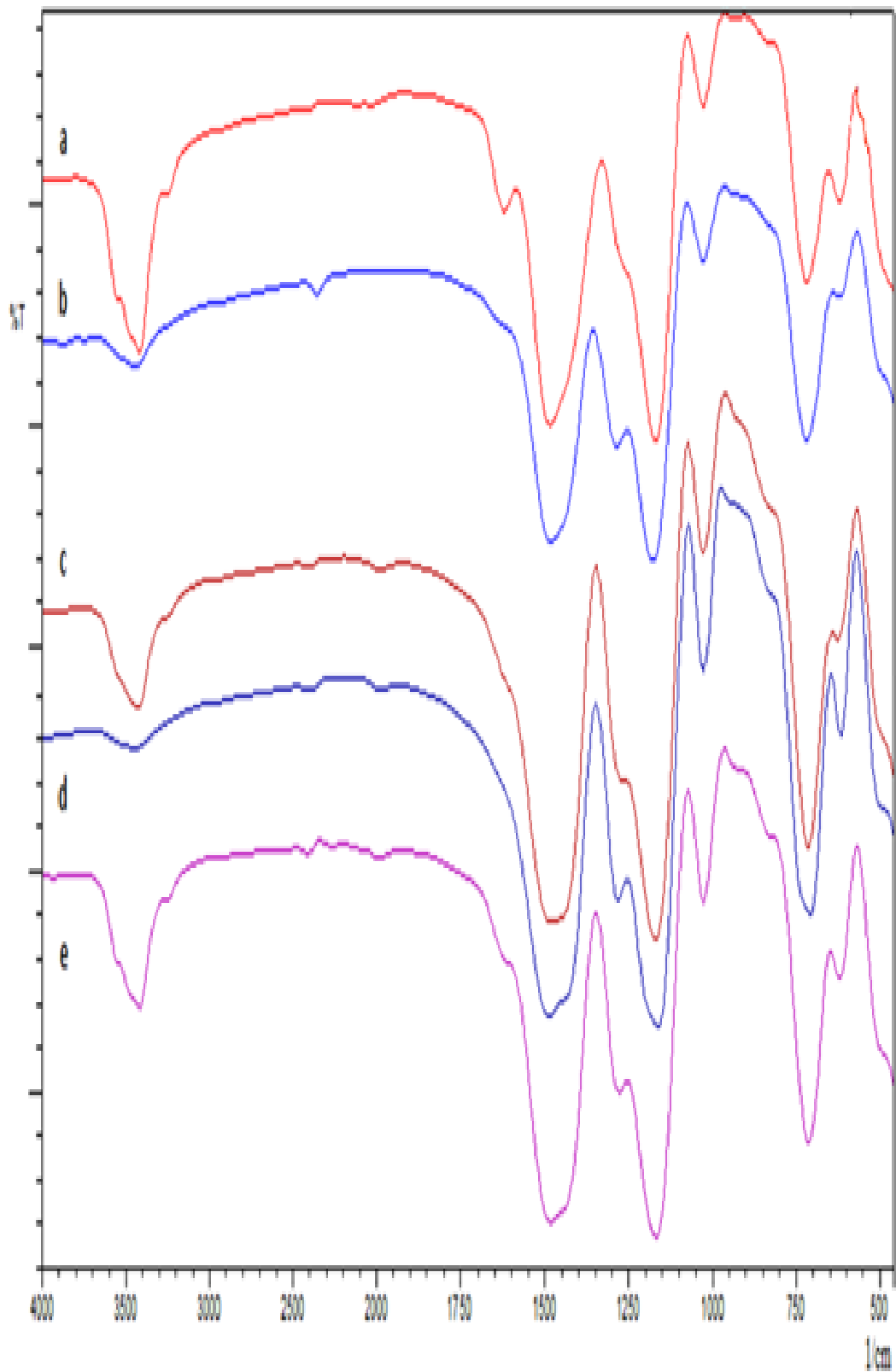
Figure 4.14. IR spectra of 0.005 mol Dy doped $Mg_2B_2O_5$ at 900°C 1h. using a) CA, b) Gly, c) HMTA, d) TA, e) U
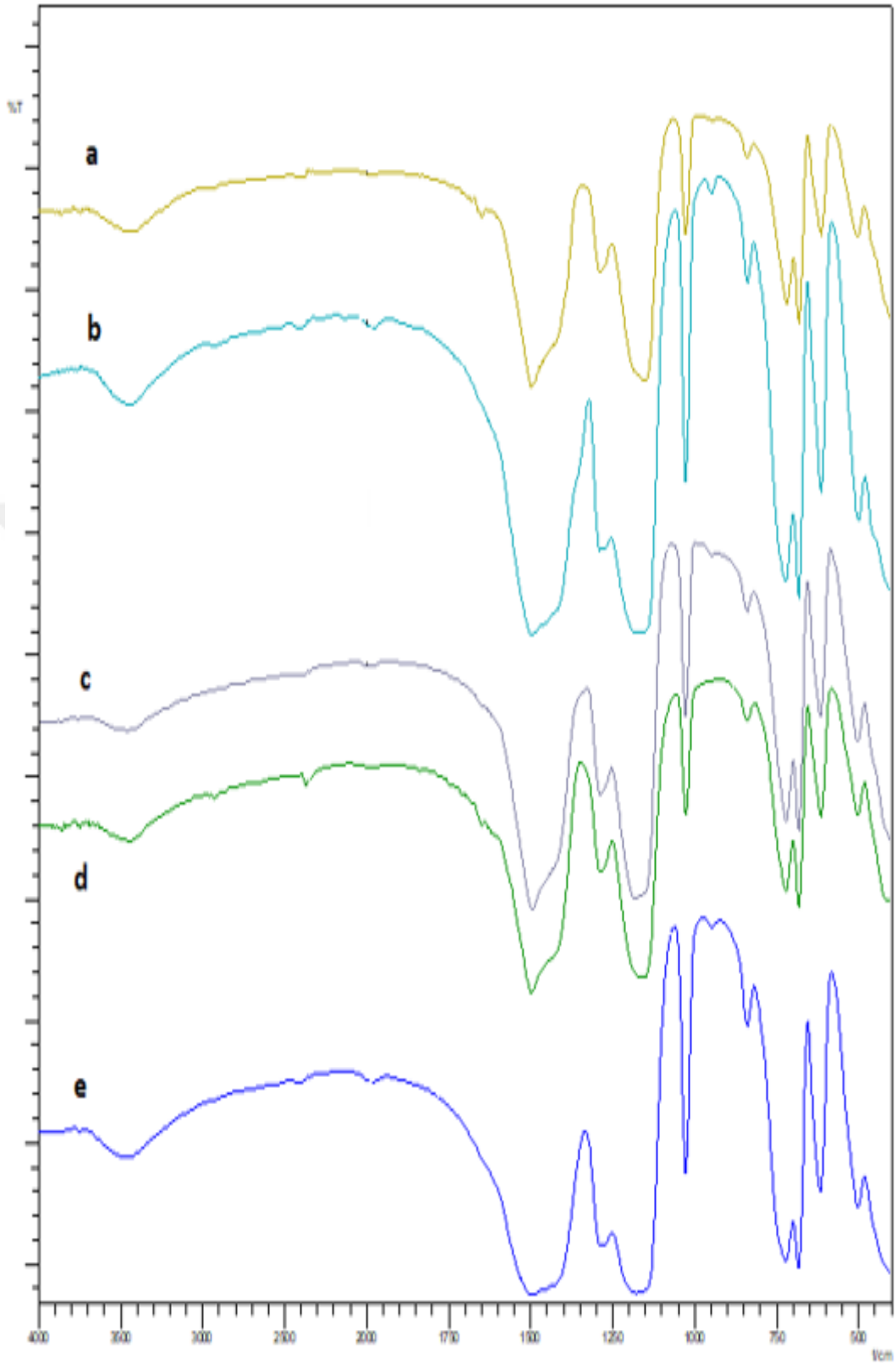
Figure 4.15. IR spectra of 0.010 mol Dy doped $Mg_2B_2O_5$ at 700°C 2h. using a) TA, b) U, c) HMTA, d) CA, e) Gly
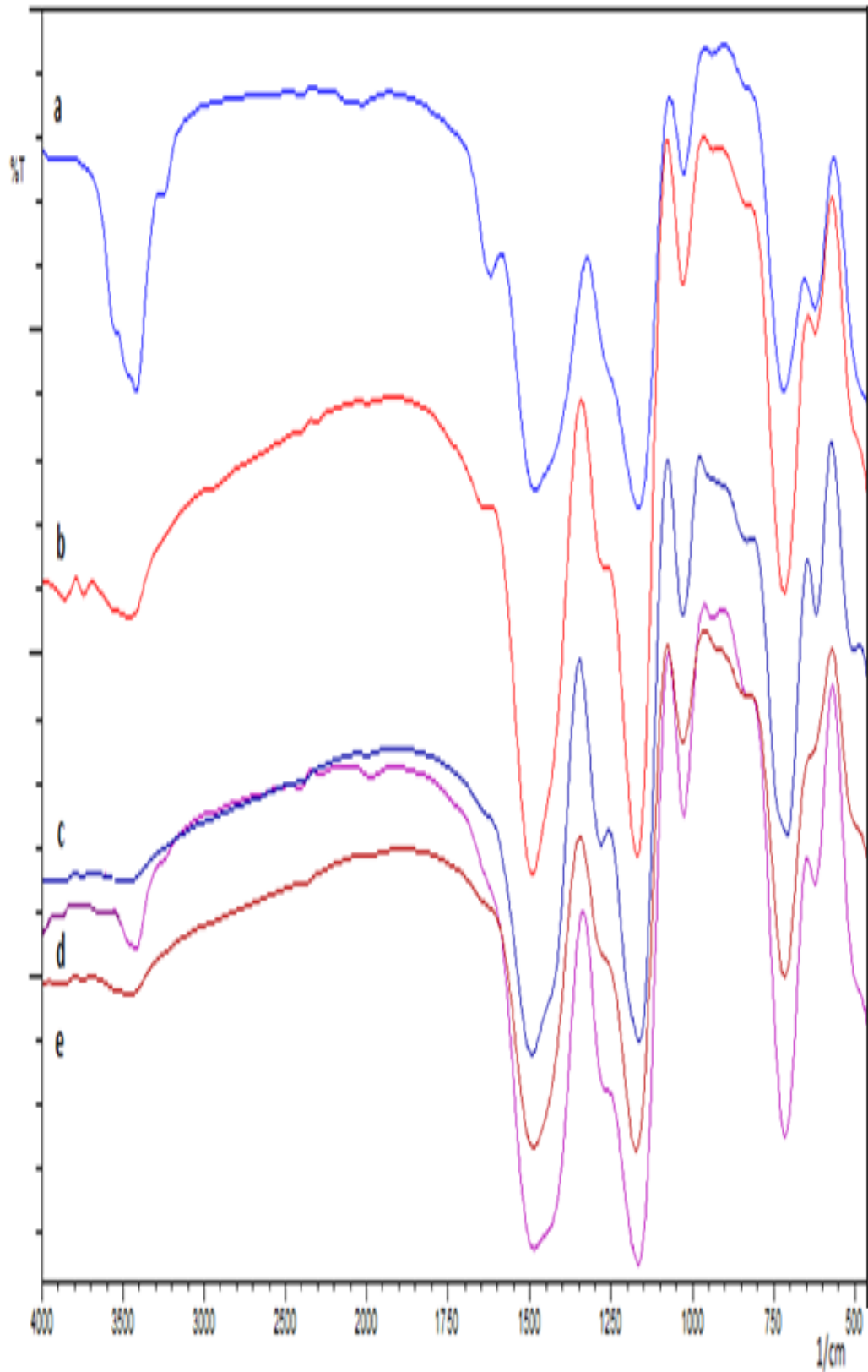
Figure 4.16. IR spectra of 0.050 mol Dy doped $Mg_2B_2O_5$ at 800°C 1h. using a) Gly, b) CA, c) TA, d) U, e) HMTA
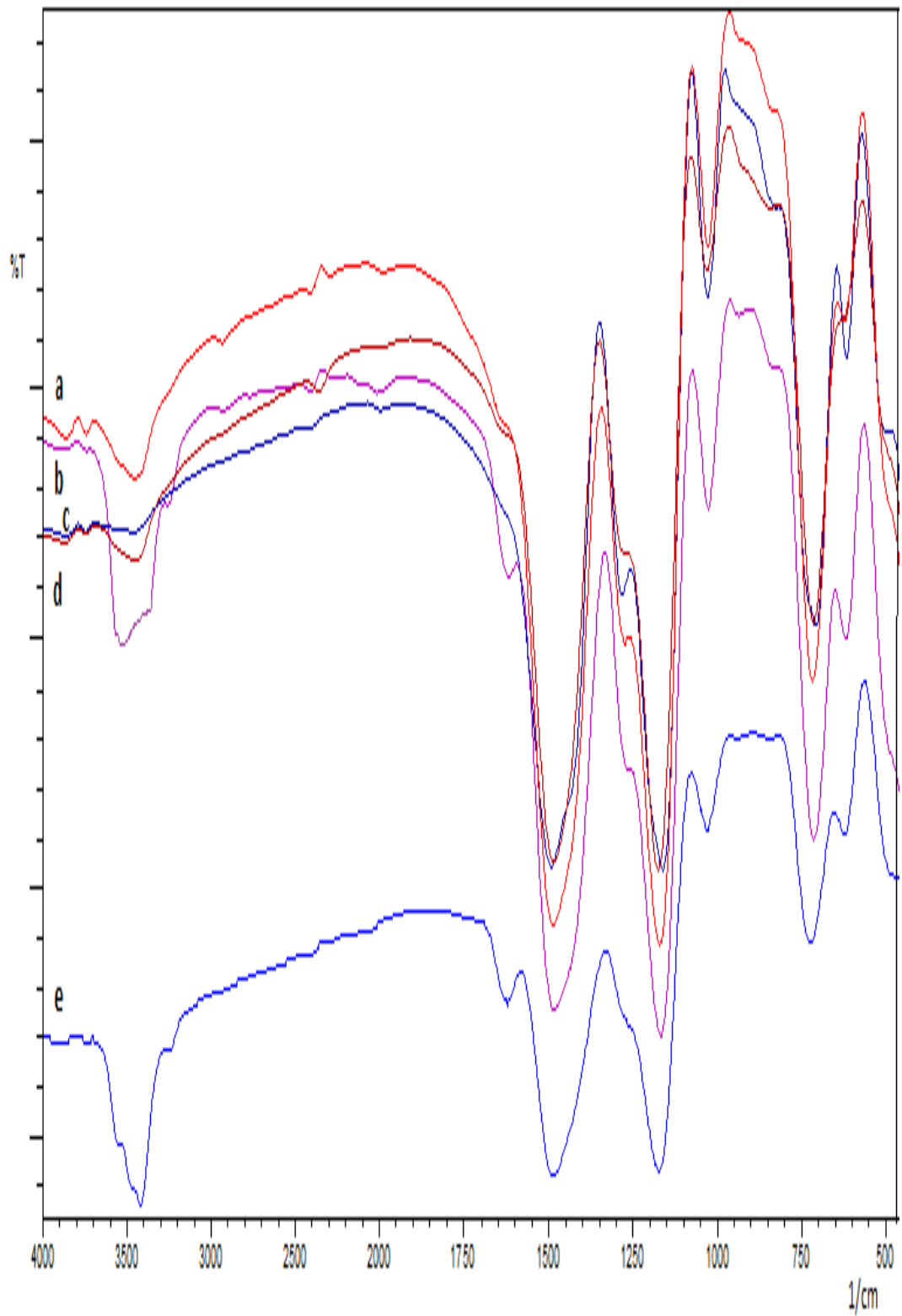
Figure 4.17. IR spectra of 0.050 mol Dy doped $Mg_2B_2O_5$ at 900°C 1h. using a) Gly, b) CA, c) TA, d) U, e) HMTA

4.2.1 Ultraviolet Visible Studies of Dy doped Mg$_2$B$_2$O$_5$

Optical properties of samples were determined with UV-VIS Spectroscopy. Absorbance and Reflectance of UV-VIS spectrum of Mg$_{(2-x)}$Dy$_x$B$_2$O$_5$ (x = 0.005, 0.010, 0.020, 0.050 mol) samples at 700ºC 2h., 800ºC 1h. and 900ºC 1h with HMTA and Urea fuel were shown below. When the doping amount moles of Dy were increased, the absorbance of material was increased. On the other hand, when the doping amount moles of Dy were increased, the reflectance of material was decreased at 700ºC and 800ºC. At 900ºC, the absorbance of materials was increased with decreasing doping amounts of Dy. Otherwise, the reflectance of materials was increased with increasing doping amounts of Dy.

In the consideration of 0.005 mol Dy^{3+} and 0.010 mol Dy^{3+} doping with HMTA fuel, blue shift obtained with increasing temperature and wavelength. On the other hand, 0.020 mol Dy^{3+} and 0.050 mol Dy^{3+} mol Dy^{3+} doping with HMTA fuel, red shift obtained with increasing temperature as 700 ºC, 800 ºC and 900ºC and with decreasing wavelength. Red shift also obtained with Urea fuel in four different concentrations with increasing temperature as 700ºC and 800ºC and decreasing wavelength.
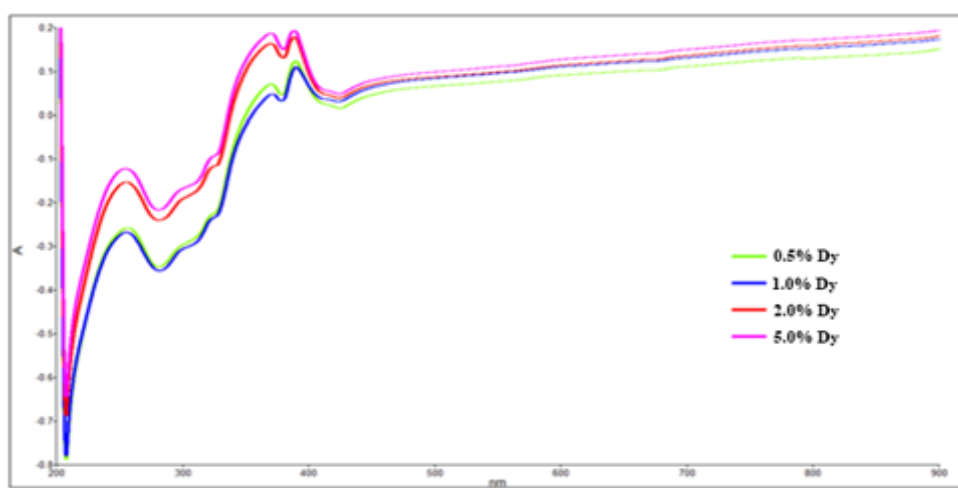
Figure 4.18. Absorbance UV-VIS Spectrum of 0.005(0.5%) mol, 0.010(1%) mol, 0.020(2%) mol and 0.5(5%) mol Dy doped Mg$_2$B$_2$O$_5$ at 700ºC 2h. using HMTA fuel
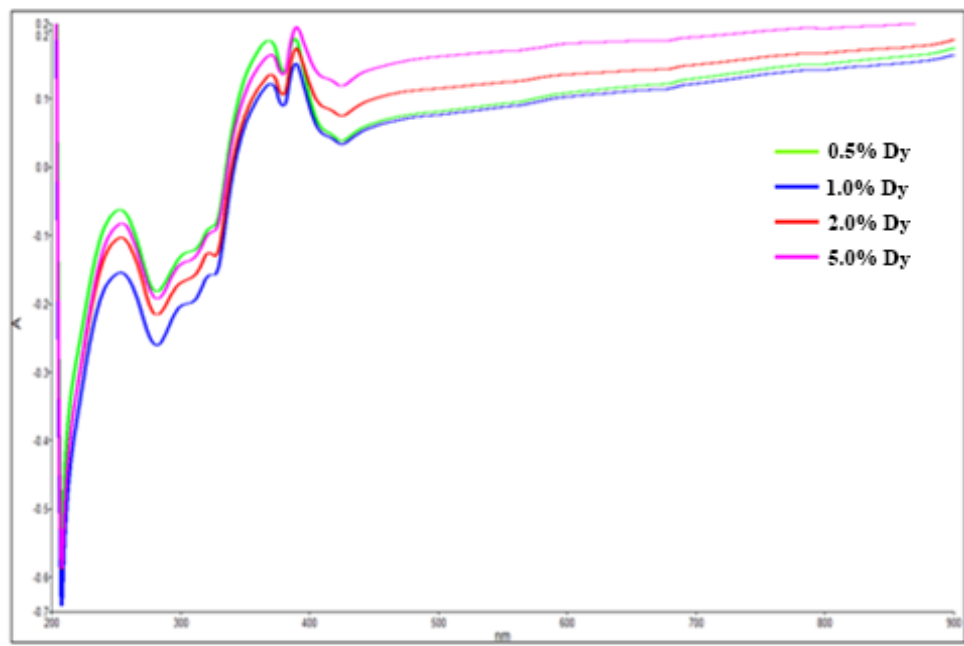
Figure 4.19. Absorbance UV-VIS Spectrum of 0.005(0.5%) mol, 0.010(1%) mol, 0.020(2%) mol and 0.5(5%) mol Dy doped $Mg_2B_2O_5$ at 700°C 2h. using Urea fuel
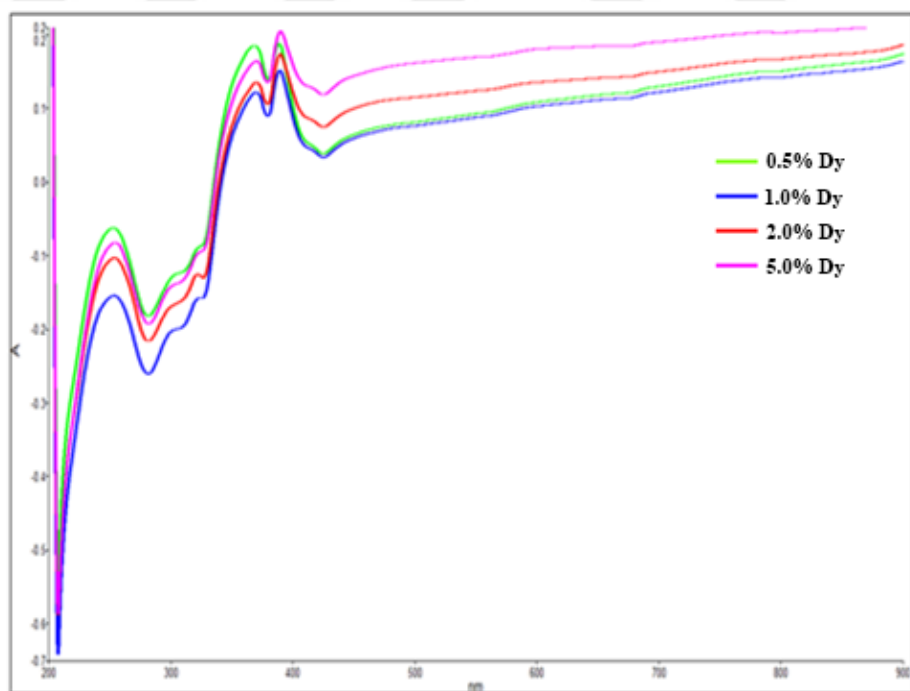
Figure 4.20. Reflectance UV-VIS Spectrum of 0.005(0.5%) mol, 0.010(1%) mol, 0.020(2%) mol and 0.5(5%) mol Dy doped $Mg_2B_2O_5$ at 700°C 2h. using HMTA fuel
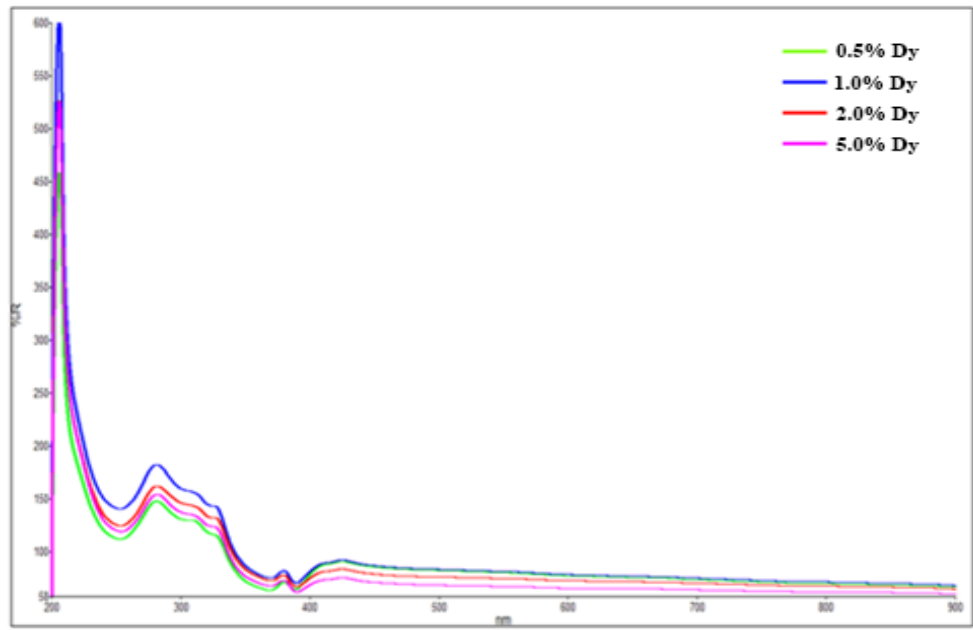
Figure 4.21. Reflectance UV-VIS Spectrum of 0.005(0.5%) mol, 0.010(1%) mol, 0.020(2%) mol and 0.5(5%) mol Dy doped $Mg_2B_2O_5$ at 700ºC 2h. using Urea fuel
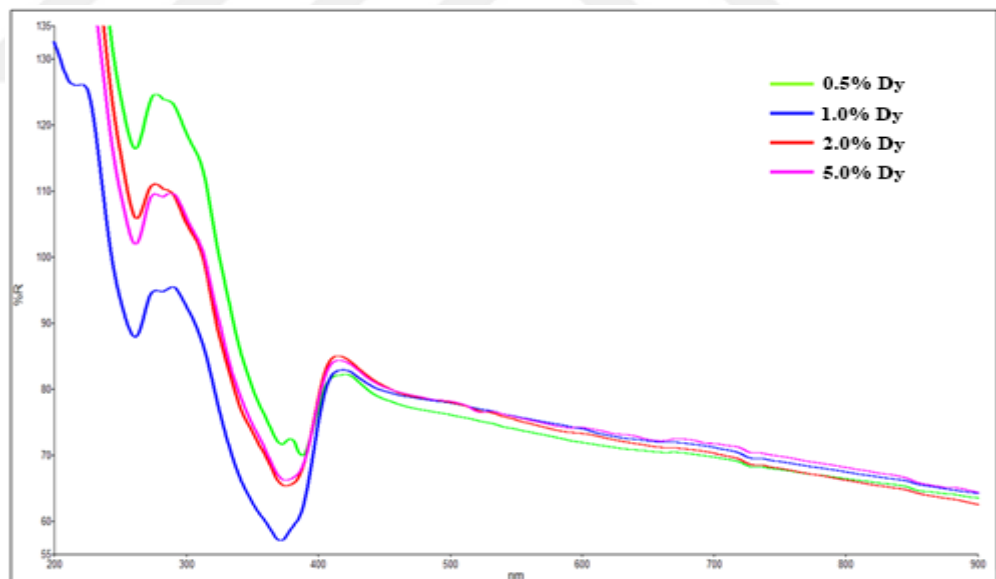
Figure 4.22. Absorbance UV-VIS Spectrum of 0.005(0.5%) mol, 0.010(1%) mol, 0.020(2%) mol and 0.5(5%) mol Dy doped $Mg_2B_2O_5$ at 800ºC 1h. using HMTA fuel
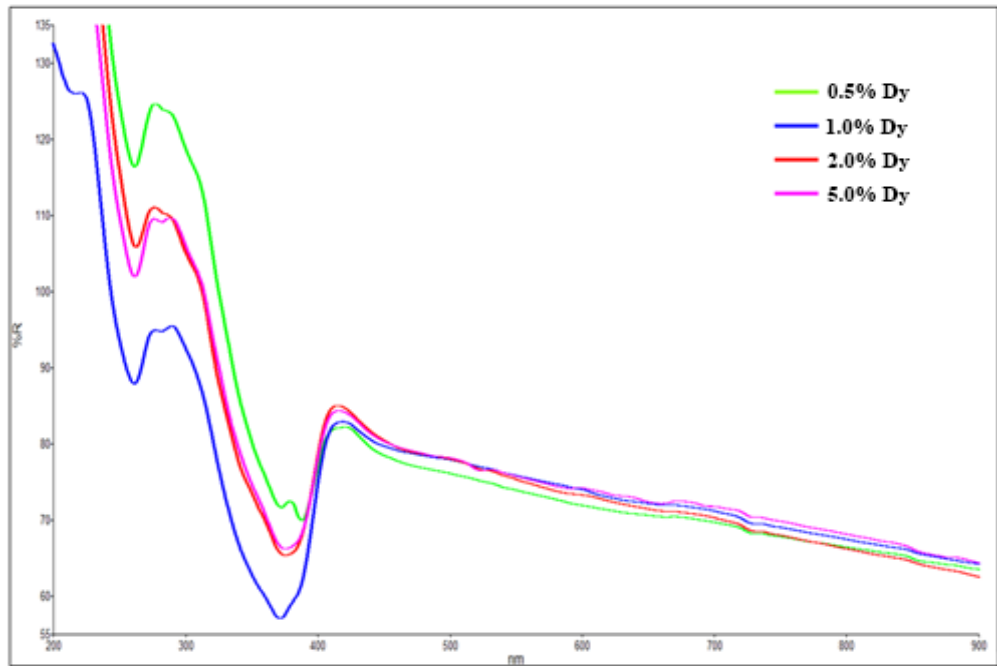
Figure 4.23. Absorbance UV-VIS Spectrum of 0.005(0.5%) mol, 0.010(1%) mol, 0.020(2%) mol and 0.5(5%) mol Dy doped $Mg_2B_2O_5$ at 800°C 1h. using Urea fuel
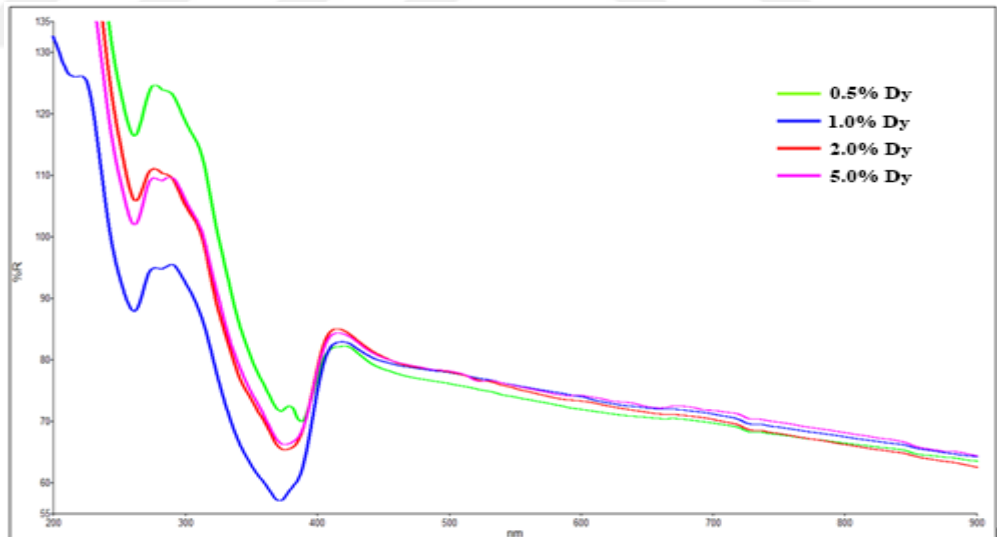
Figure 4.24. Reflectance UV-VIS Spectrum of 0.005(0.5%) mol, 0.010(1%) mol, 0.020(2%) mol and 0.5(5%) mol Dy doped $Mg_2B_2O_5$ at 800°C 1h. using HMTA fuel
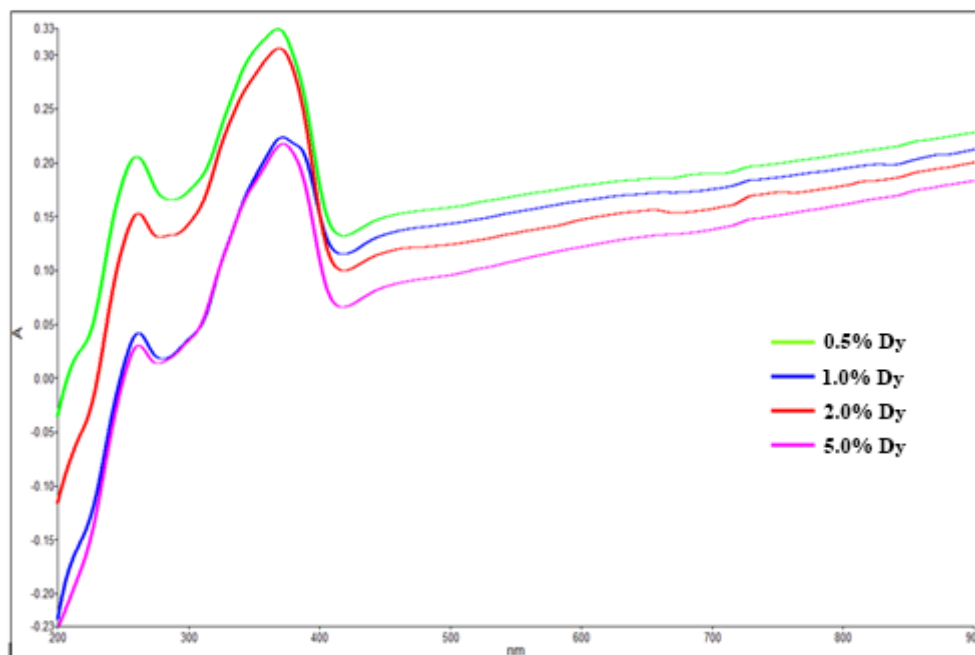
Figure 4.25. Reflectance UV-VIS Spectrum of 0.005(0.5%) mol, 0.010(1%) mol, 0.020(2%) mol and 0.5(5%) mol Dy doped $Mg_2B_2O_5$ at 800ºC 1h. using Urea fuel
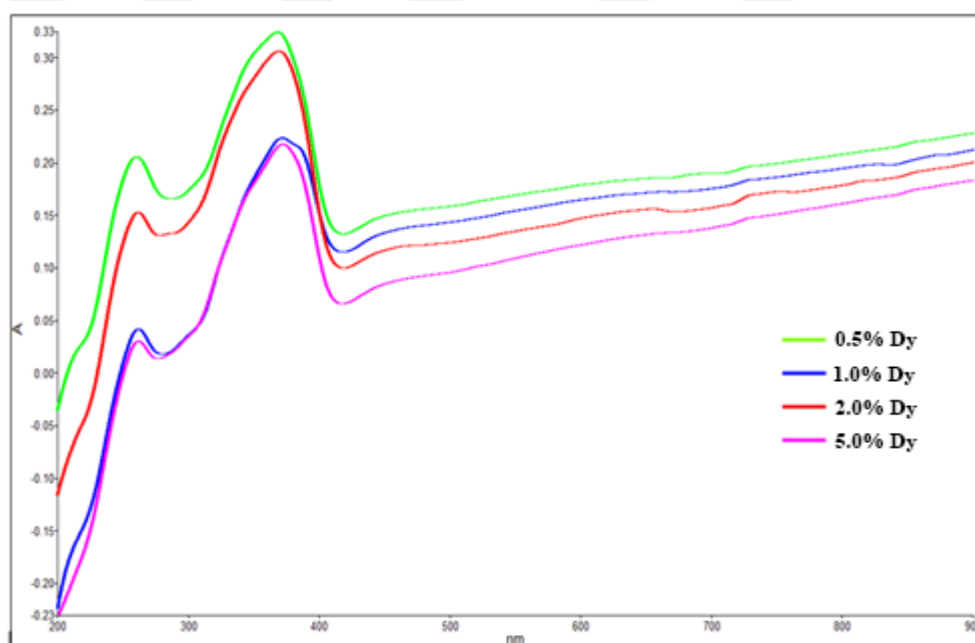
Figure 4.26. Absorbance UV-VIS Spectrum of 0.005(0.5%) mol, 0.010(1%) mol, 0.020(2%) mol and 0.5(5%) mol Dy doped $Mg_2B_2O_5$ at 900ºC 1h. using HMTA fuel
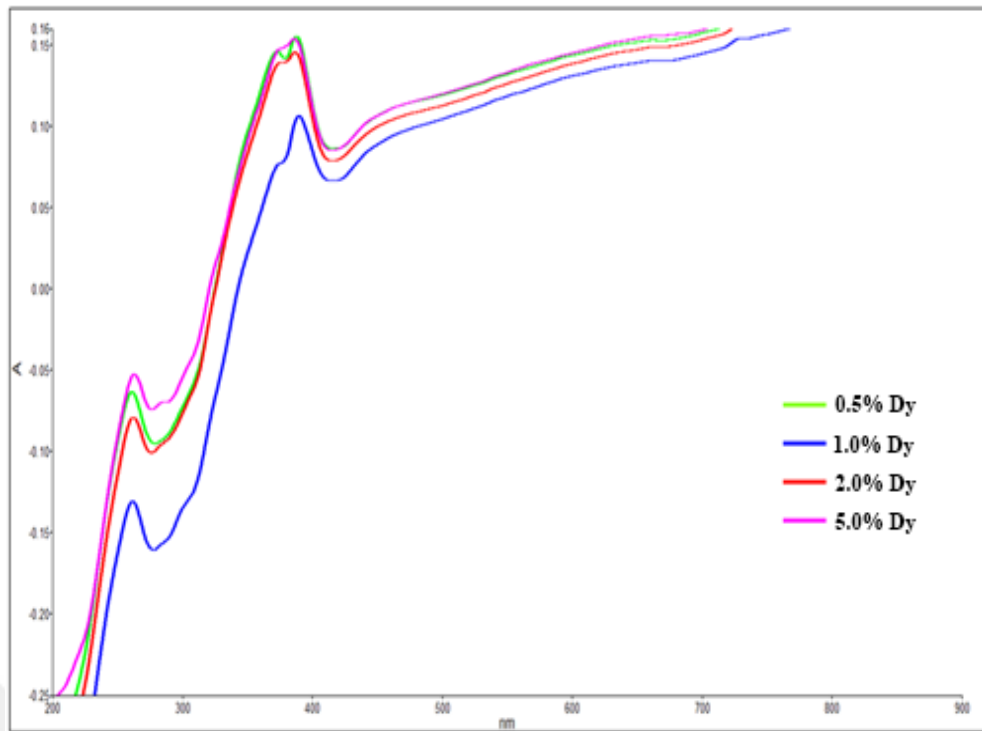
Figure 4.27. Reflectance UV-VIS Spectrum of 0.005(0.5%) mol, 0.010(1%) mol, 0.020(2%) mol and 0.5(5%) mol Dy doped $Mg_2B_2O_5$ at 900°C 1h. using HMTA fuel

4.3   Ho doped $Mg_2B_2O_5$

A series of $Mg_2B_2O_5$: Ho^{3+} (0.005, 0.010, 0.020, 0.050 mol) doping pyroborates were synthesized by solution combustion method. Firstly, heated at 370°C until gel form is obtained to produce $Mg_{(2-x)}Ho_{(x)}B_2O_5$ (x = 0.005, 0.010, 0.020, 0.050 mol). Then, it was put into furnace at 400°C 10min. to acquire combustion. After that, it was heated to 700°C for 2 hour to get best result of doped $Mg_2B_2O_5$ crystallinity.

The general reaction with different type of fuels;

$(2-x) Mg(NO_3)_2.6H_2O_{(s)} + x Ho(NO_3)_2.5H_2O_{(s)} + 2H_3BO_{3(s)} + fuel_{(s)} \rightarrow$

$Mg_{(2-x)}Ho_{(x)}B_2O_{5(s)} + CO_{2(g)} + H_2O_{(g)} + NO_{2(g)}$
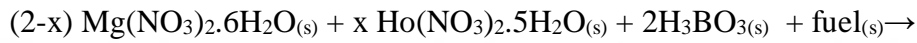
(fuel= Glycine, tartaric acid, citric acid, urea and hexamethylenetetramine)

(x= 0.005, 0.010, 0.020 and 0.050 mol)

In the combustion process of $Mg_2B_2O_5$ doped with Ho^{3+} the intensity order of combustion highest to lowest was Gly, TA, CA, U and HMTA, respectively, as in Dy doped $Mg_2B_2O_5$. Unlike the other fuels, when HMTA was used, the product's shape was speckled in 0.005, 0.010, 0.020, 0.050 mol, shown in Figure 4.28, Figure 4.29, Figure 4.30, Figure 4.31. The 0.010 mol Ho doping compound was partial combustion, dark brown color after the process of 400°C 10min. by using TA fuel, shown in Figure 4.29, and became dark after the process of 700°C 2h, shown in Figure 4.32. The reason of this situation was that the compound needed more heating process to achieve best result of $Mg_2B_2O_5$ compound. When Gly was used as fuel, the product was fluffy and light brown color at 400°C 10min. Additionally, while CA was used as fuel, the compound was puffy and cream color after the combustion process of 400°C 10min., its color turned from cream to light grey after 700°C 2h. On the other hand, the product was white color and low yield with U and HMTA fuel and more gas evolution was observed compared with other fuels such as Gly, TA and CA.

The pictures that is shown below the products after 400ºC 10min.
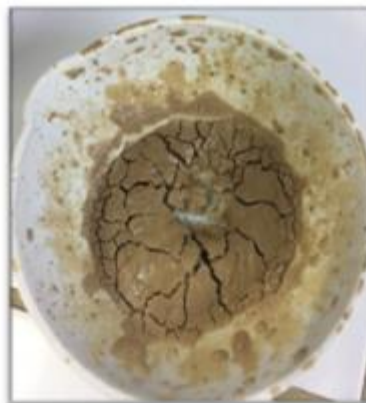
Figure 4.28. The images of $Mg_{2.995}Ho_{0.005}B_2O_5$ samples were synthesized with a) Gly, b) TA, c) CA, d) U, e) HMTA

Figure 4.29. The images of $Mg_{2.990}Ho_{0.010}B_2O_5$ samples were synthesized with a) Gly, b) TA, c) CA, d) U, e) HMTA

Figure 4.30. The images of $Mg_{2.980}Ho_{0.020}B_2O_5$ samples were synthesized with a) Gly, b) TA, c) CA, d) U, e) HMTA

Figure 4.31. The images of $Mg_{2.950}Ho_{0.050}B_2O_5$ samples were synthesized with a) Gly, b) TA, c) CA, d) U, e) HMTA

The pictures that is shown below the products after 700°C 2h.
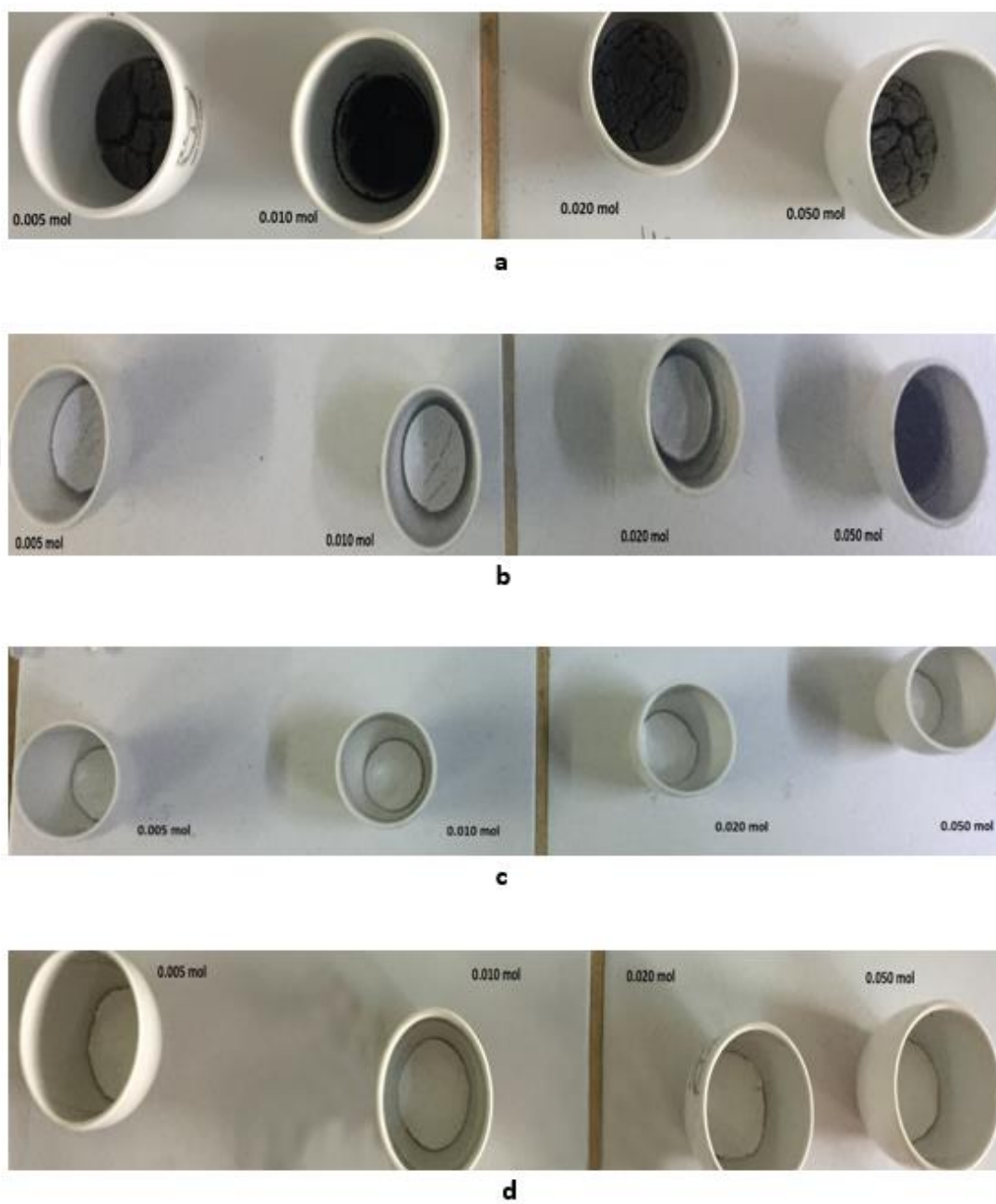
Figure 4.32. The images of $Mg_{(2-x)}Ho_{(x)}B_2O_5$ samples were synthesized as x = 0.005, 0.010, 0.020, 0.050 mol with a) TA, b) CA, c) U, d) HMTA

4.3.1 XRD Studies of Ho doped $Mg_2B_2O_5$

Figure 4.33, Figure 4.34, Figure 4.35 and Figure 4.36 shows powder X-ray diffraction patterns of Ho doped magnesium pyroborate synthesized from different fuels and at 700°C 2h. When all these figures considered, the intensity sequence from the highest to lowest is HMTA, U, Gly, CA, TA after the heating process of 700°C 2h. All these XRD peaks of doped compounds were matched with 15-0537 ICDD data card for triclinic $Mg_2B_2O_5$. The results exhibited that used different fuels gave doped $Mg_2B_2O_5$ products with different morphologies and crystallinity.

0.010 mol Ho^{3+} doped $Mg_2B_2O_5$ product synthesized with TA fuel was obtained amorph phase as 304.17 cps at 24.700 (2theta) . The reason of this situation was that the doped compound was needed more heating process to obtain best results of $Mg_2B_2O_5$. Generally, Ho doped $Mg_2B_2O_5$ synthesized with TA fuel has lowest crystallinity as 679.17 cps at 34.860 (2theta) and highest yield in considering all four concentrations (0.005, 0.010, 0.020, 0.050 mol) after the combustion process of 700 °C 2h. Ho doped $Mg_2B_2O_5$ synthesized with HMTA fuel has highest crystallinity and lowest yield in all four concentrations (0.005, 0.010, 0.020, 0.050 mol) after the combustion process of 700 °C 2h. The highest intensities of Ho doped $Mg_2B_2O_5$ are 987.50 cps at 34.940 (2theta) for 0.005 mol, 900.00 cps at 34.940 (2theta) for 0.010 mol, 945.83 cps at 35.000 (2theta) for 0.020 mol, 870.83 cps at 35.140 (2theta) for 0.050 mol by using HMTA fuel. Additionally, when U is used as fuel, the intensities of product obtain as 883.33 cps at 34.960 (2theta) for 0.005 mol, 808.33 cps at 35.160 (2theta) for 0.010 mol, 791.67 cps at 35.100 (2theta) for 0.020 mol and 704.17 cps at 34.880 (2theta) for 0.050 mol. Apparently, the crystallinity is decreased as shifting the position of 2theta changes when the dopant concentration is increased. Consequently, HMTA and U are suitable fuels in our study because it produces $Mg_2B_2O_5$ with high crystalline.

Additionally, the crystallite size (D) of Ho^{3+} doped $Mg_2B_2O_5$ that was synthesized with different fuels were calculated from the XRD pattern according to Scherrer formula

$$D = \frac{K\lambda}{\beta Cos\theta}$$

where K is the constant, λ is the X-ray wavelength (0.15406 nm), β is the full-width at half maximum and θ is the diffraction angle.

Table 4.5. 0.005 mol Ho^{3+} doped $Mg_2B_2O_5$ crystallite size changing with fuels

FUELS	Crystallite size, nm (700°C, 2h.)
Gly	15,03
TA	11,34
CA	13,87
U	16,03
HMTA	17,98

Table 4.6. 0.010 mol Ho^{3+} doped $Mg_2B_2O_5$ crystallite size changing with fuels

FUELS	Crystallite size, nm (700°C, 2h.)
Gly	15,12
TA	-
CA	13,91
U	16,18
HMTA	18,21

Table 4.7. 0.020 mol Ho^{3+} doped $Mg_2B_2O_5$ crystallite size changing with fuels

FUELS	Crystallite size, nm (700°C, 2h.)
Gly	16,47
TA	12,86
CA	14,28
U	16,89
HMTA	18,49

Table 4.8. 0.05 mol Ho3+ doped Mg2B2O5 crystallite size changing with fuels

FUELS	Crystallite size, nm (700°C, 2h.)
Gly	16,59
TA	12,97
CA	15,03
U	17,46
HMTA	18,94

Table 4.5, Table 4.6, Table 4.7 and Table 4.8 shows that while the crystallite size of Ho^{+3} doped $Mg_2B_2O_5$ synthesized with Gly, TA, CA, U and HMTA increases with increasing amount of moles. Otherwise, Dy^{3+} doped $Mg_2B_2O_5$ synthesized with HMTA has larger crystallite size when compared with other fuels. On the other hand, 0.010 mol Ho^{+3} doped $Mg_2B_2O_5$ synthesized with TA, the crystallite size of this compound was not calculated significantly.
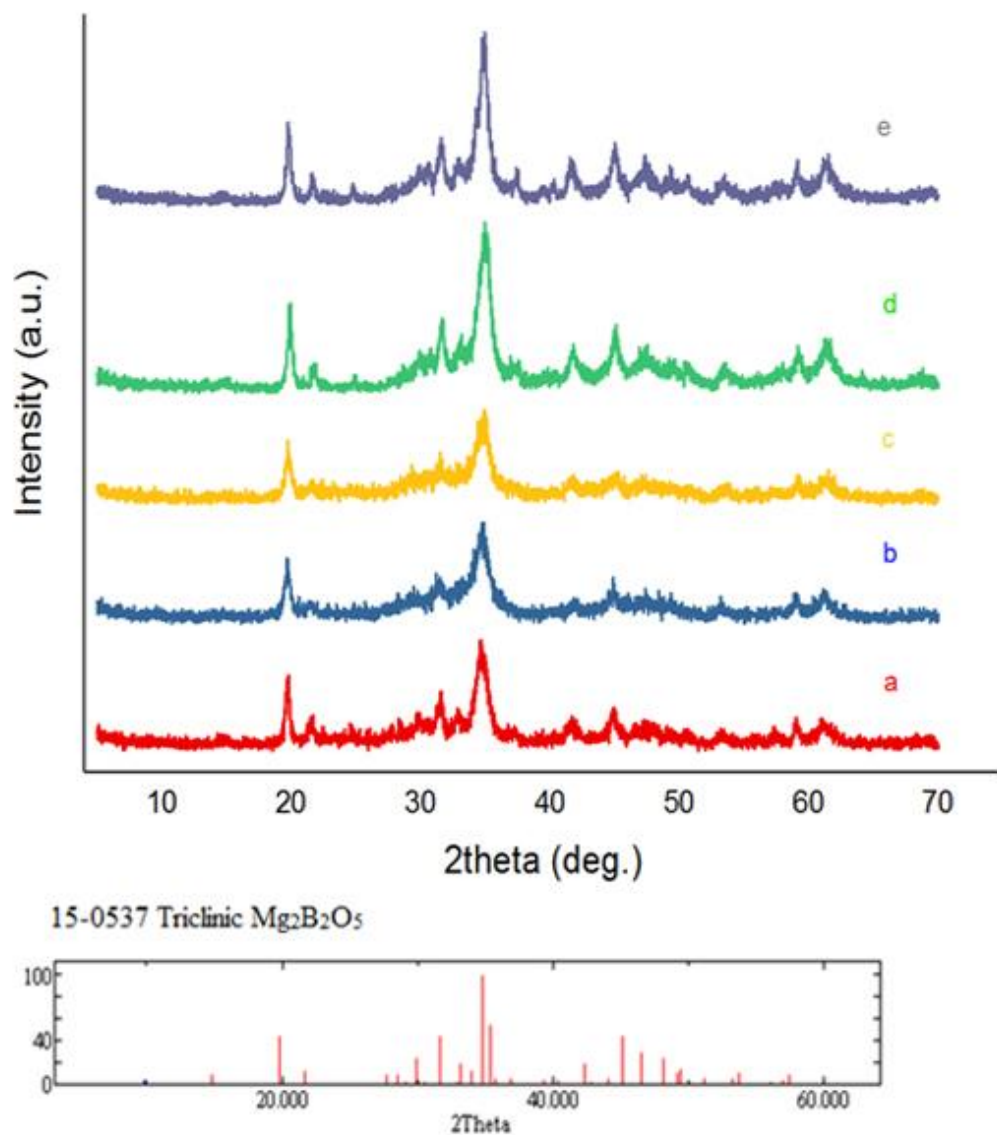
Figure 4.33. XRD patterns of 0.005 mol Ho doped $Mg_2B_2O_5$ at 700°C 2h., using a) Gly, b) TA, c) CA, d) U, e) HMTA with ICDD Data Card for 15-0537 Triclinic $Mg_2B_2O_5$
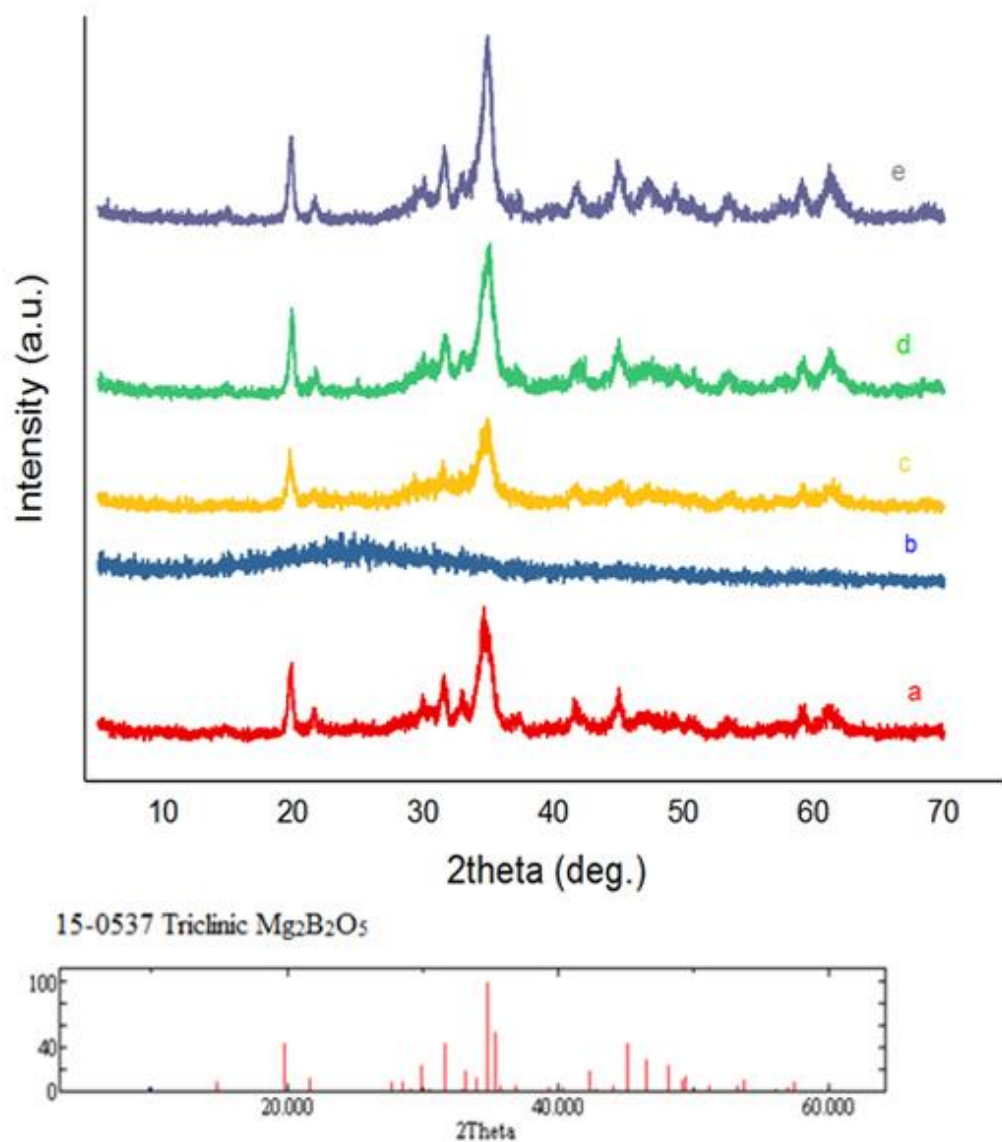
Figure 4.34. XRD patterns of 0.010 mol Ho doped $Mg_2B_2O_5$ at 700°C 2h., using a) Gly, b) TA, c) CA, d) U, e) HMTA with ICDD Data Card for 15-0537 Triclinic $Mg_2B_2O_5$
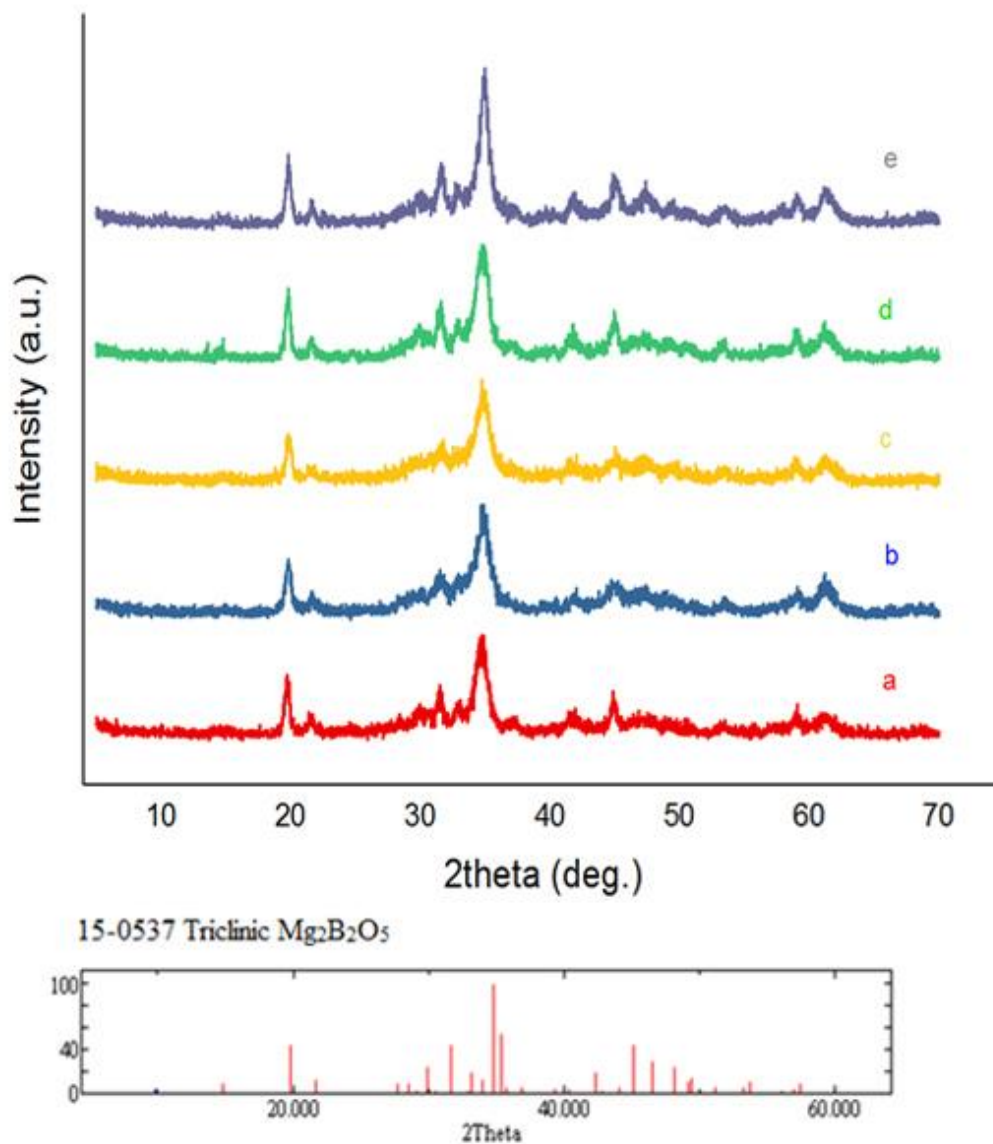
Figure 4.35. XRD patterns of 0.020 mol Ho doped Mg_2B_2O5 at 700ºC 2h., using a) Gly, b) TA, c) CA, d) U, e) HMTA with ICDD Data Card for 15-0537 Triclinic $Mg_2B_2O_5$
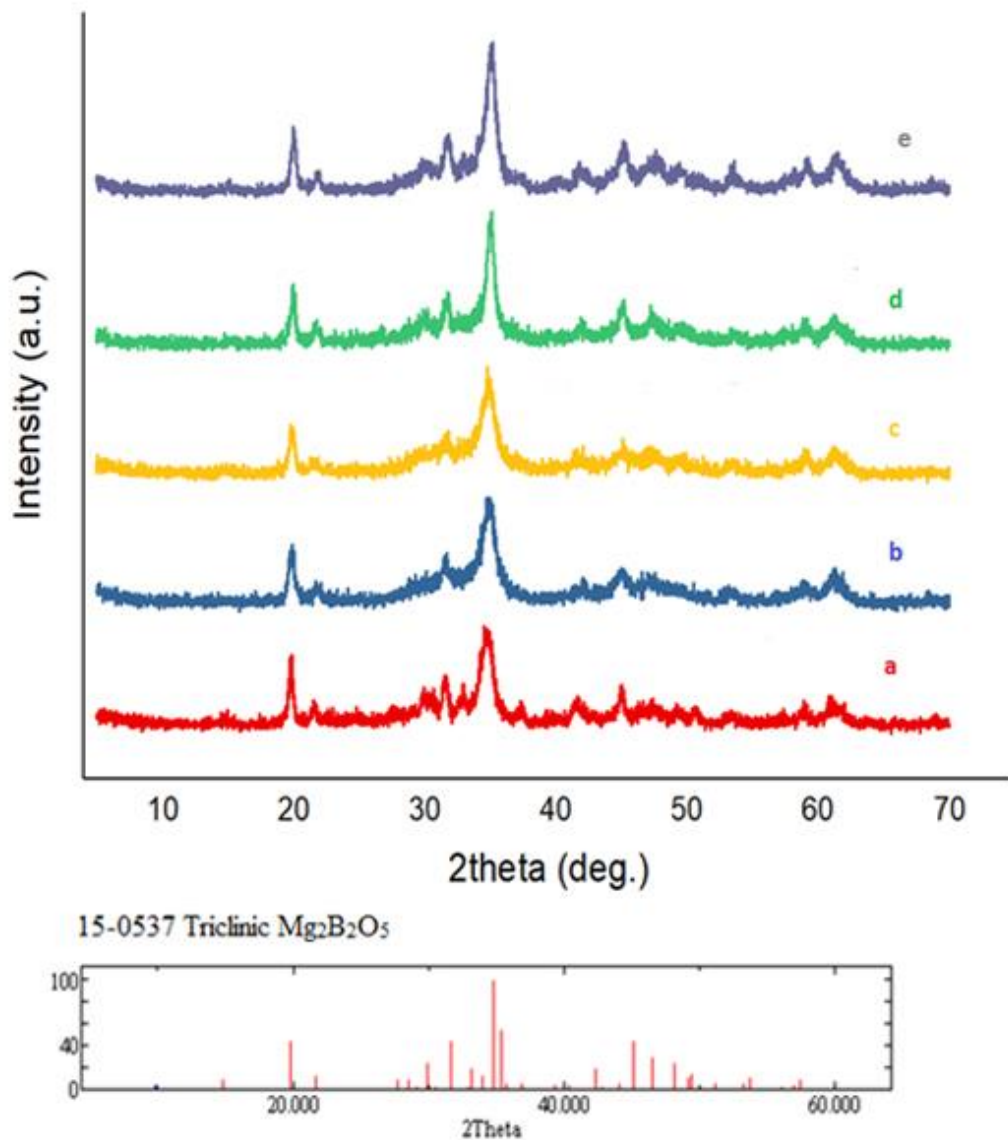
Figure 4.36. XRD patterns of 0.050 mol Ho doped $Mg_2B_2O_5$ at 700ºC 2h., using a) Gly, b) TA, c) CA, d) U, e) HMTA with ICDD Data Card for 15-0537 Triclinic $Mg_2B_2O_5$

4.3.2 Infrared Spectroscopy Studies of Ho doped $Mg_2B_2O_5$

Fourier transform infrared (FTIR) spectra of Ho^{3+} doped $Mg_2B_2O_5$ samples synthesized with SCS method was recorded in the range 300-4000 cm^{-1} using KBr pellets. IR spectra of $Mg_{(2-x)}Ho_{(x)}B_2O_5$ (x = 0.005, 0.010, 0.020, 0.050 mol) samples at 400°C for 10min. and 700°C 2h. were shown in below.

In the heating process of 400°C 10min., peaks at 3700-3200 cm^{-1} observed as O-H stretching mode of hydroxyl group due to surface moisturising. After 700°C process, these peaks were not observed. The strong bonds at 1450-1550 cm^{-1} and 600-750 cm^{-1} was correlated with characteristic vibrational of $Mg_2B_2O_5$. When the heating process increased from 400°C to 700°C, the absorption of 600-750 cm^{-1} spectrum was became clear. In the pyroborate, the group of bands between 1100 cm^{-1} and 1450cm^{-1} are strong, broad, and very strongly dependent on isotopic mass (Weir et al., 1964). The absorption peak at 1150–1200 cm^{-1} can be assigned to antisymmetric stretching vibrations of the BOB groups in pyroborates (Guo et al., 2014). The spectra of synthetic triclinic suanite exhibited a single band at 610 cm^{-1} (Oztas et al., 2009). When 0.010 mol Ho^{3+} doped $Mg_2B_2O_5$, the major peaks in the range of 1450-1550 cm^{-1} due to B-O stretching vibrations were not obtained strongly because of amorph type of pyroborate.
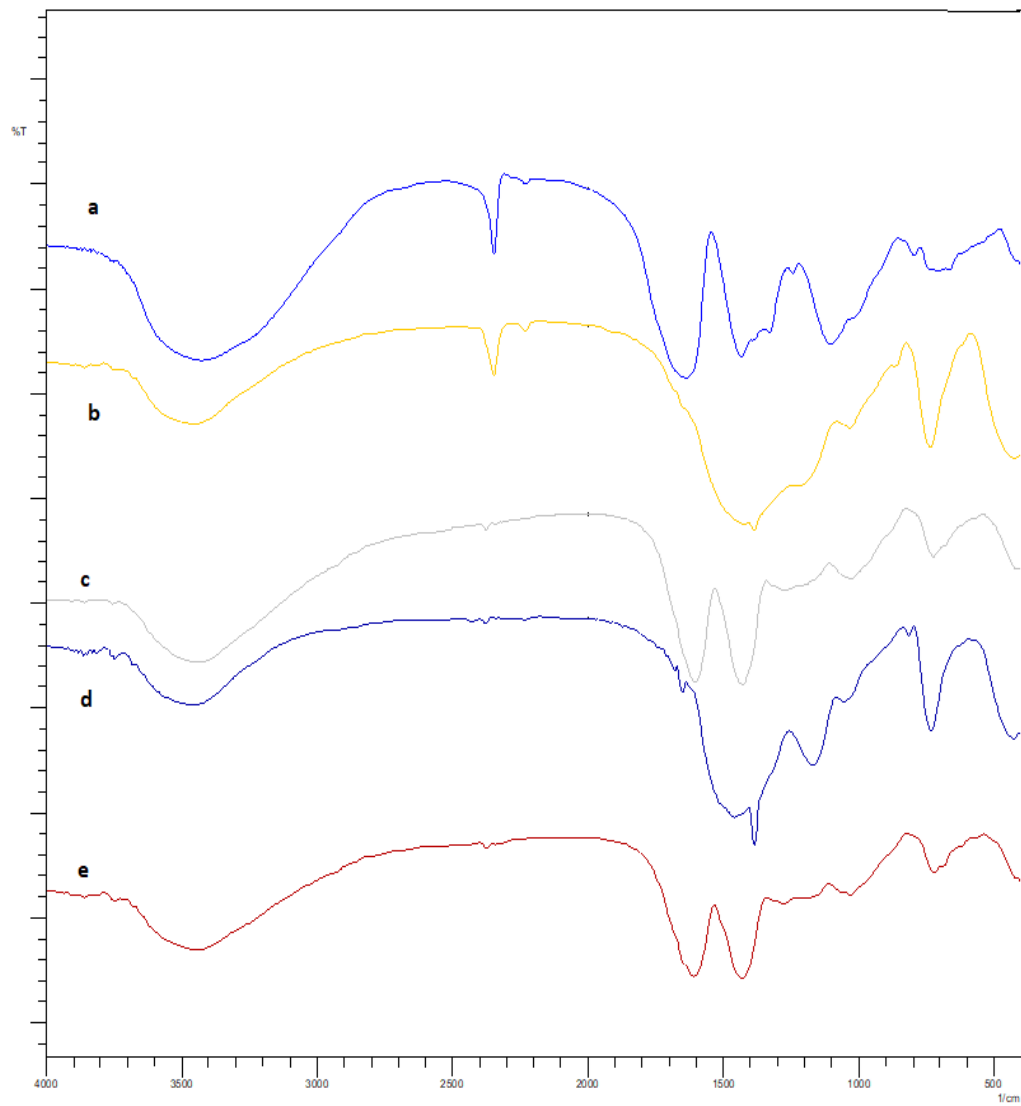
Figure 4.37. IR spectra of 0.005 mol Ho doped $Mg_2B_2O_5$ at 400°C 2h. using
a) Gly, b) U, c) CA, d) TA, e) HMTA
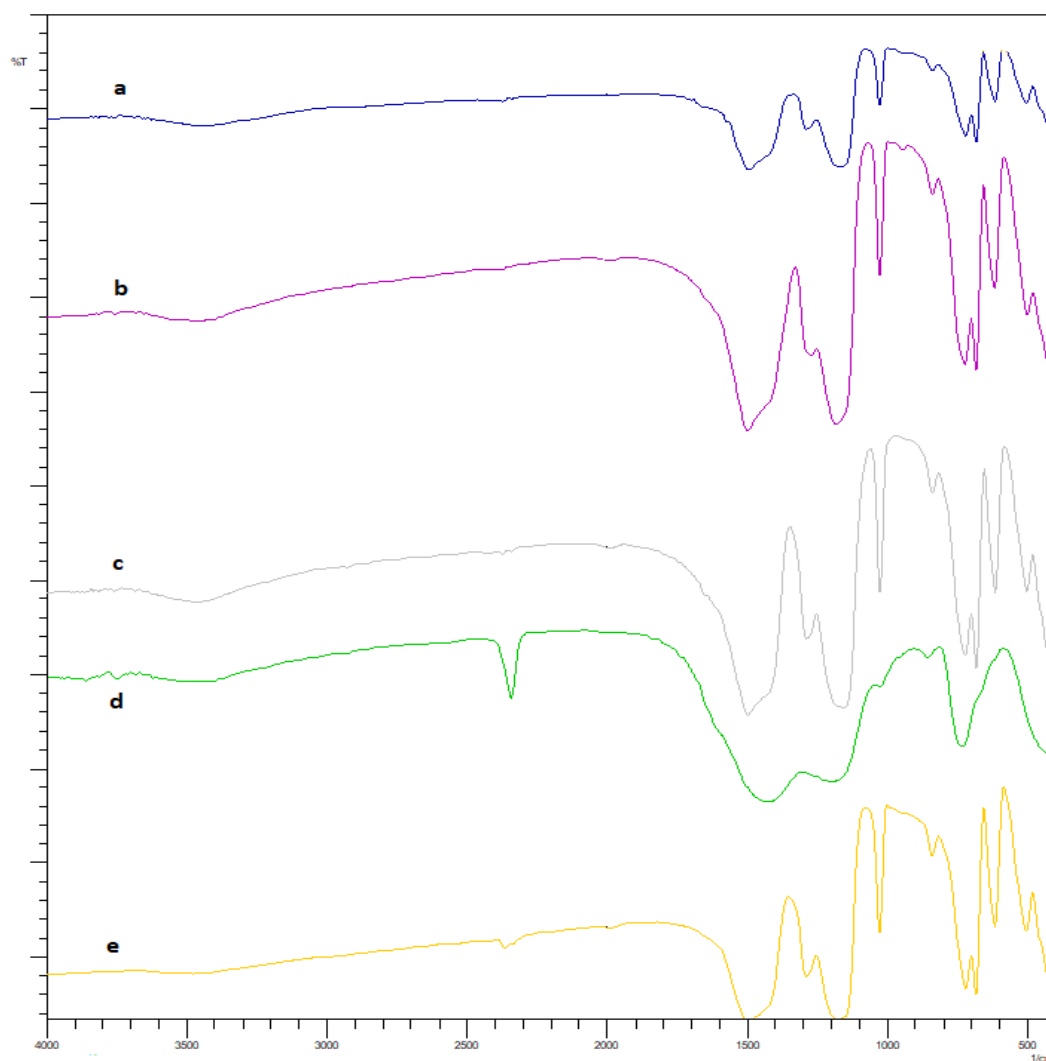
Figure 4.38. IR spectra of 0.005 mol Ho doped $Mg_2B_2O_5$ at 700°C 2h. using a) Gly, b) U, c) CA, d) TA, e) HMTA
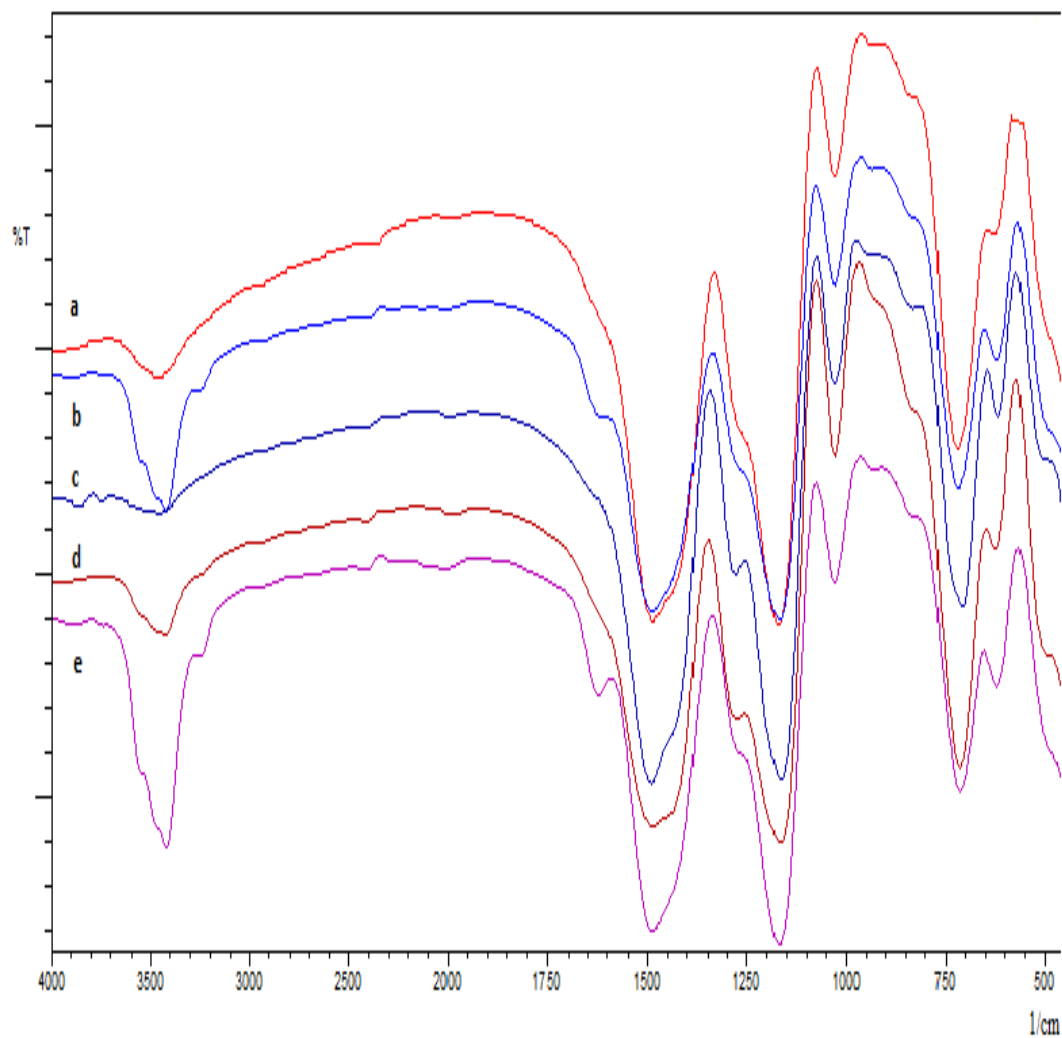
Figure 4.39. IR spectra of 0.005 mol Ho doped $Mg_2B_2O_5$ at 800°C 1h. using a) CA b) Gly, c) HMTA, d) TA, e) U
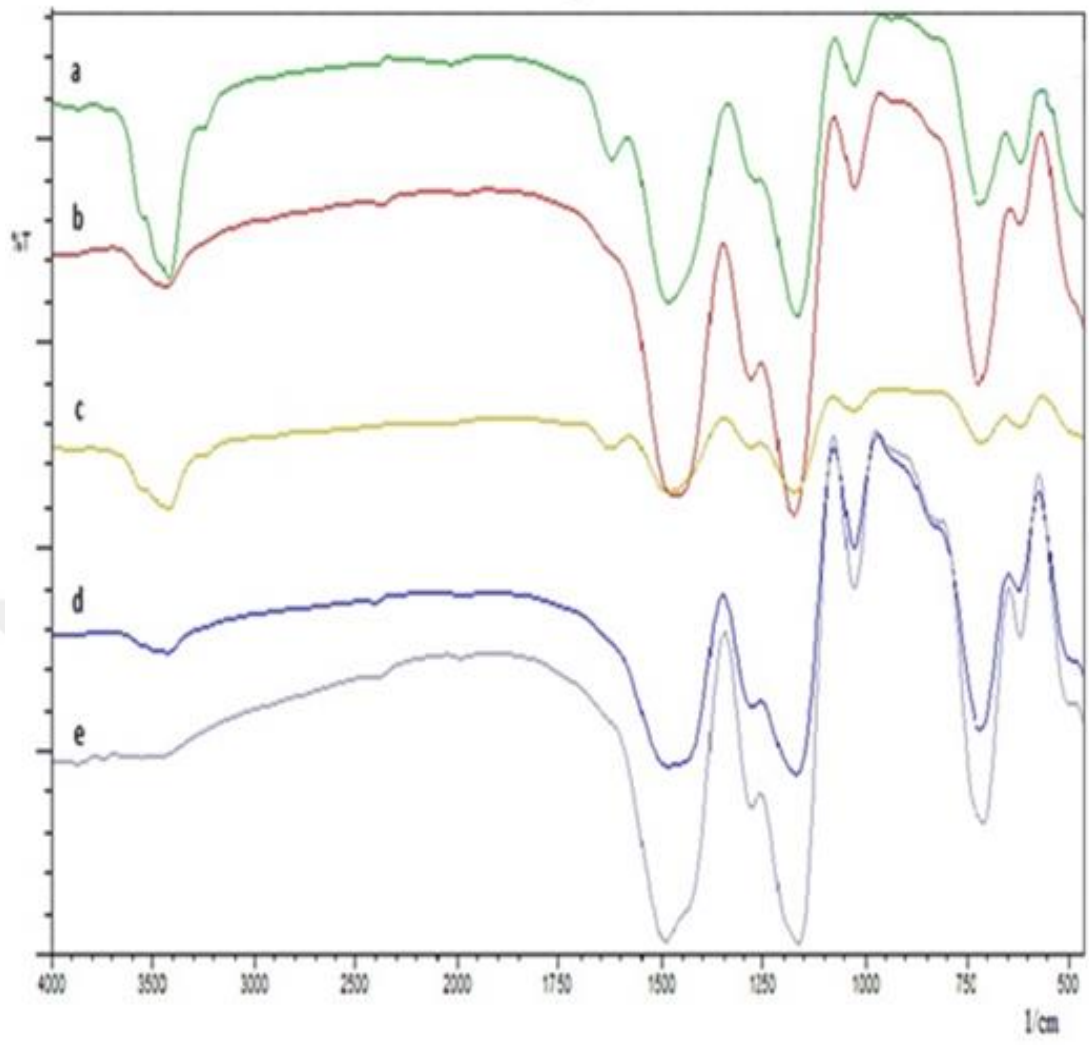
Figure 4.40. IR spectra of 0.005 mol Ho doped $Mg_2B_2O_5$ at 900°C 1h. using a) CA b) Gly, c) HMTA, d) TA, e) U
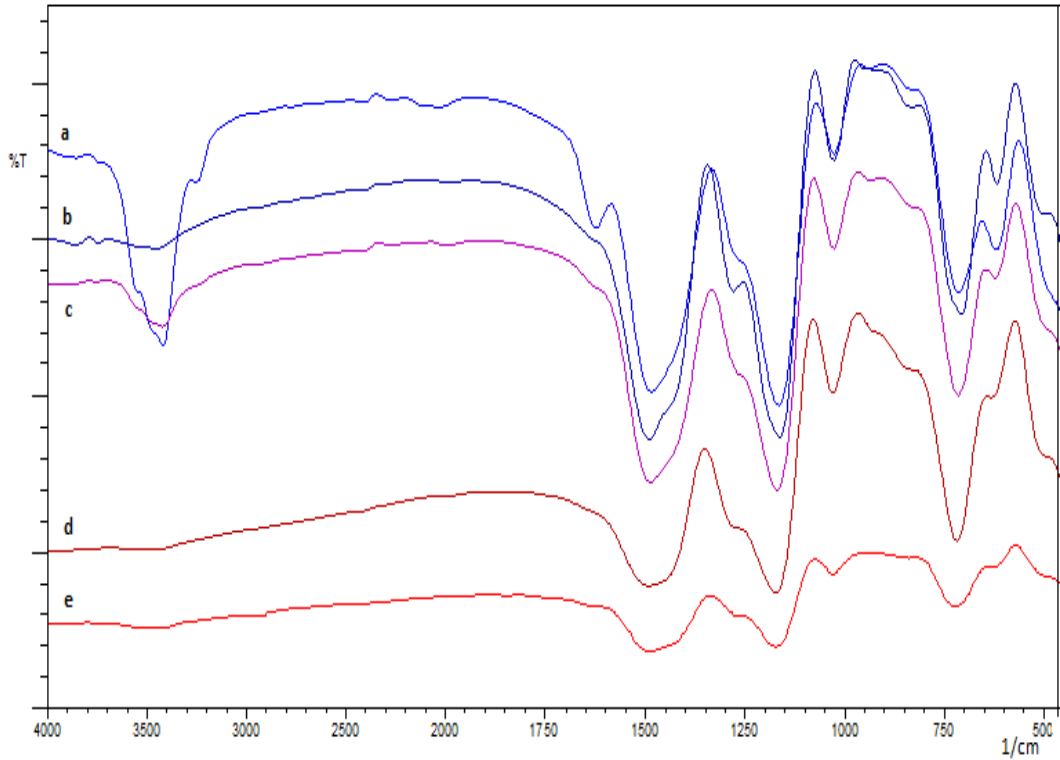
Figure 4.41. IR spectra of 0.020 mol Ho doped $Mg_2B_2O_5$ at 800°C 1h. using
a) Gly b) TA, c) U, d) HMTA, e) TA
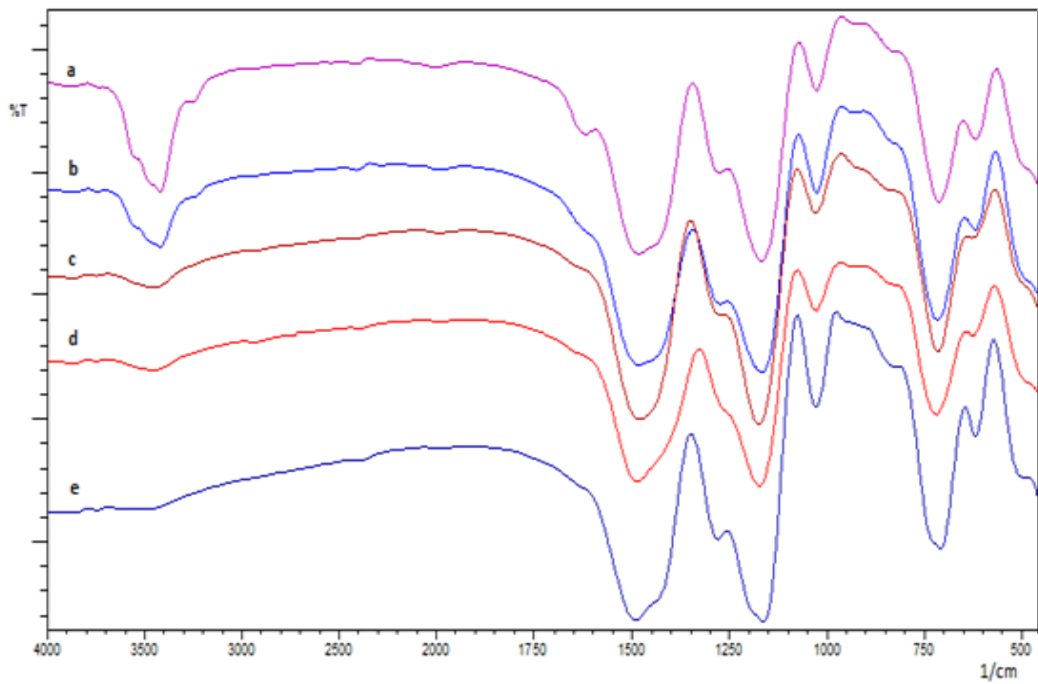
Figure 4.42. IR spectra of 0.020 mol Ho doped $Mg_2B_2O_5$ at 900°C 1h. using
a) Gly b) TA, c) U, d) HMTA, e) TA

4.3.3 Ultraviolet Visible Studies of Ho doped $Mg_2B_2O_5$

Optical properties of samples were determined with UV-VIS Spectroscopy. Absorbance and Reflectance of UV-VIS spectrum of $Mg_{(2-x)}Ho_{(x)}B_2O_5$ (x = 0.005, 0.010, 0.020, 0.050 mol) samples at 700ºC 2h., 800ºC 1h. and 900ºC 1h with HMTA and Urea fuel were shown in below. When the doping amount moles of Ho were increased, the absorbance of material was increased. On the other hand, when the doping amount moles of Ho were increased, the reflectance of material was decreased at 700ºC and 800ºC. At 900ºC, the absorbance of materials was increased with decreasing doping amounts of Ho. Otherwise, the reflectance of materials was increased with increasing doping amounts of Ho.

In the consideration of 0.005 mol Ho^{3+}, 0.010 mol Ho^{3+} and 0.050 mol Ho^{3+} doping with HMTA fuel, blue shift obtained with increasing temperature and wavelength. On the other hand, 0.020 mol Ho^{3+} doping with HMTA fuel, red shift obtained with increasing temperature as 700ºC, 800ºC and 900ºC and with decreasing wavelength. 0.05 mol Ho^{3+} doping with Urea fuel, blue shift obtain with increasing temperature and wavelength. In reverse case, red shift obtained with Urea fuel in 0.010, 0.020 and 0.050 mol concentrations with increasing temperature as 700ºC and 800ºC and decreasing wavelength.
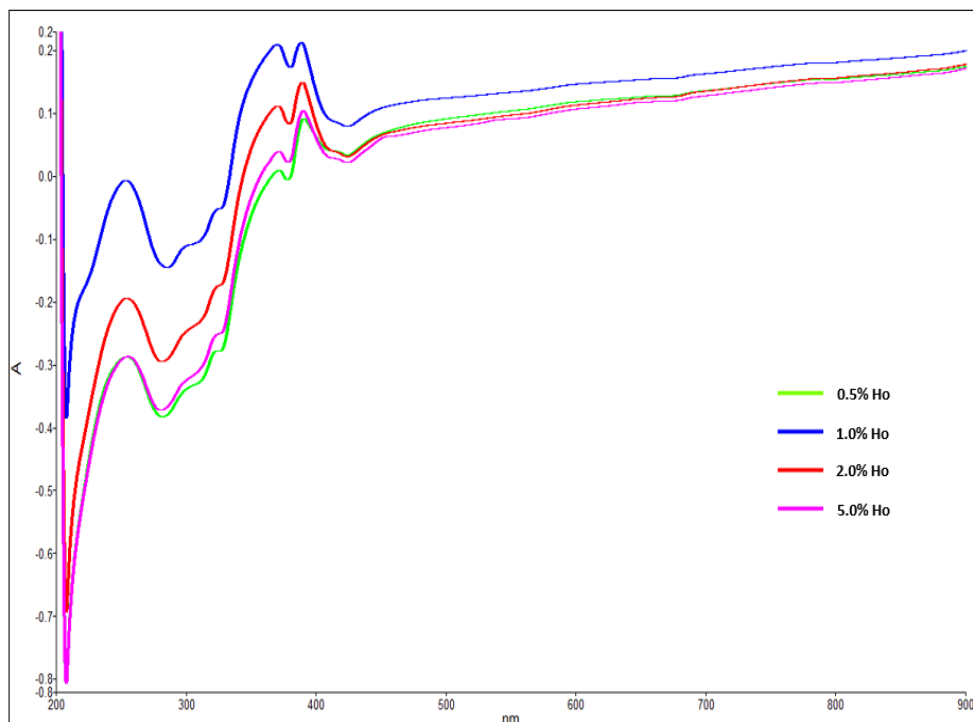
Figure 4.43. Absorbance UV-VIS Spectrum of 0.005(0.5%) mol, 0.010(1%) mol, 0.020(2%) mol and 0.5(5%) mol Ho doped $Mg_2B_2O_5$ at 700°C 2h. using HMTA fuel
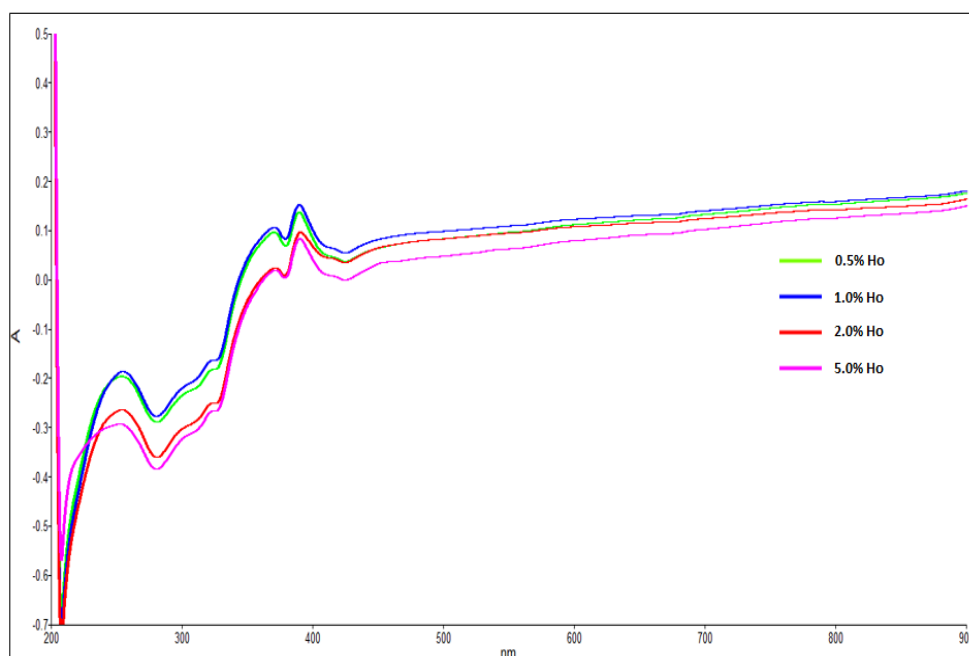
Figure 4.44. Absorbance UV-VIS Spectrum of 0.005(0.5%) mol, 0.010(1%) mol, 0.020(2%) mol and 0.5(5%) mol Ho doped $Mg_2B_2O_5$ at 700°C 2h. using Urea fuel

73
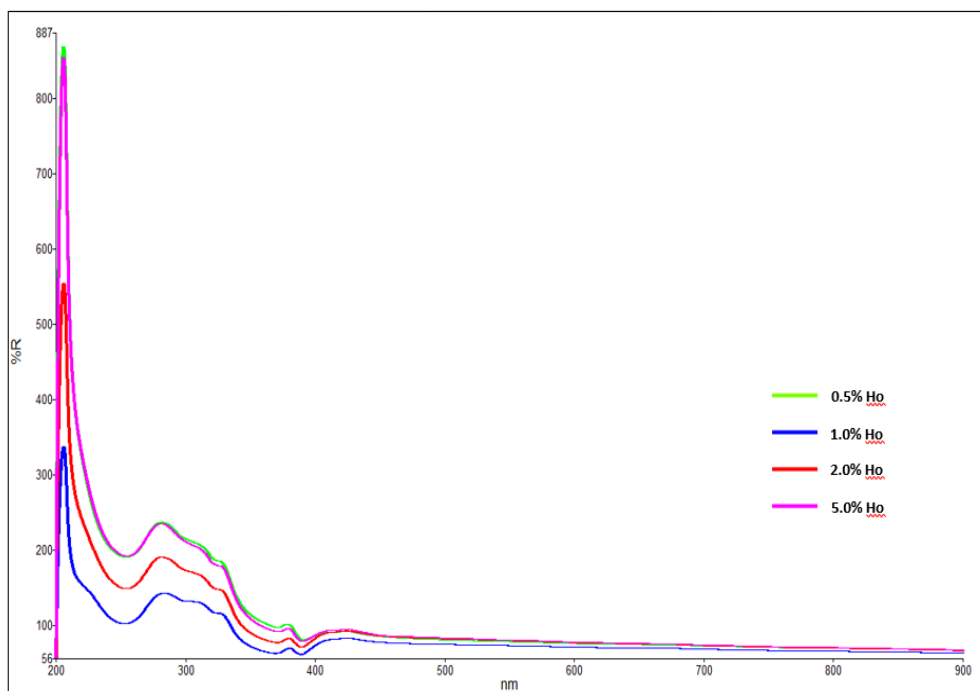
Figure 4.45. Reflectance UV-VIS Spectrum of 0.005(0.5%) mol, 0.010(1%) mol, 0.020(2%) mol and 0.5(5%) mol Ho doped $Mg_2B_2O_5$ at 700ºC 2h. using HMTA fuel
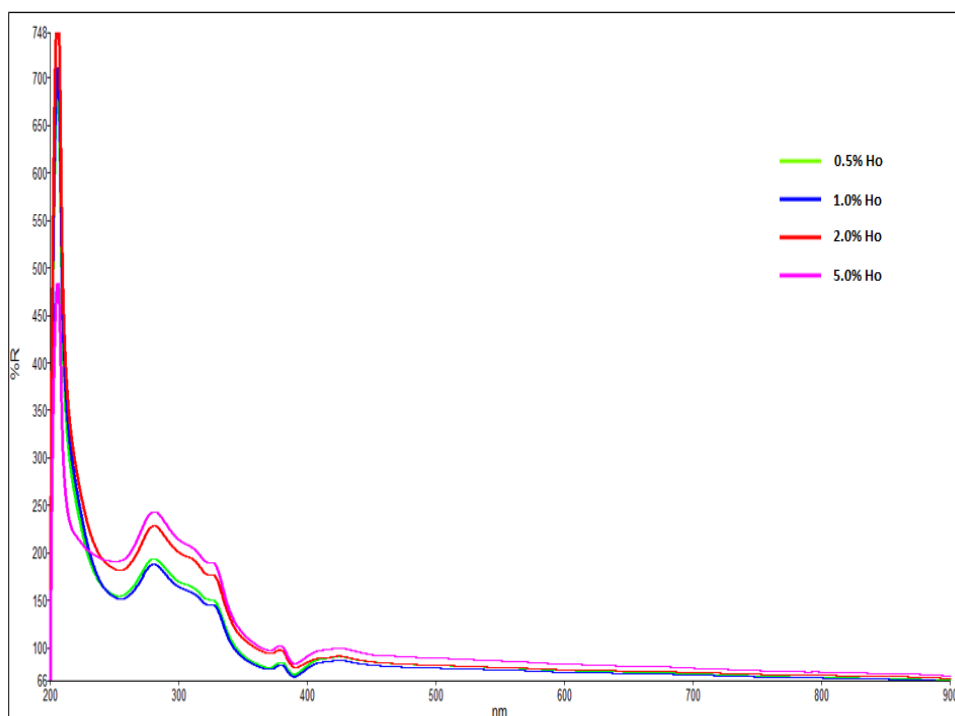
Figure 4.46. Reflectance UV-VIS Spectrum of 0.005(0.5%) mol, 0.010(1%) mol, 0.020(2%) mol and 0.5(5%) mol Ho doped $Mg_2B_2O_5$ at 700ºC 2h. using Urea fuel
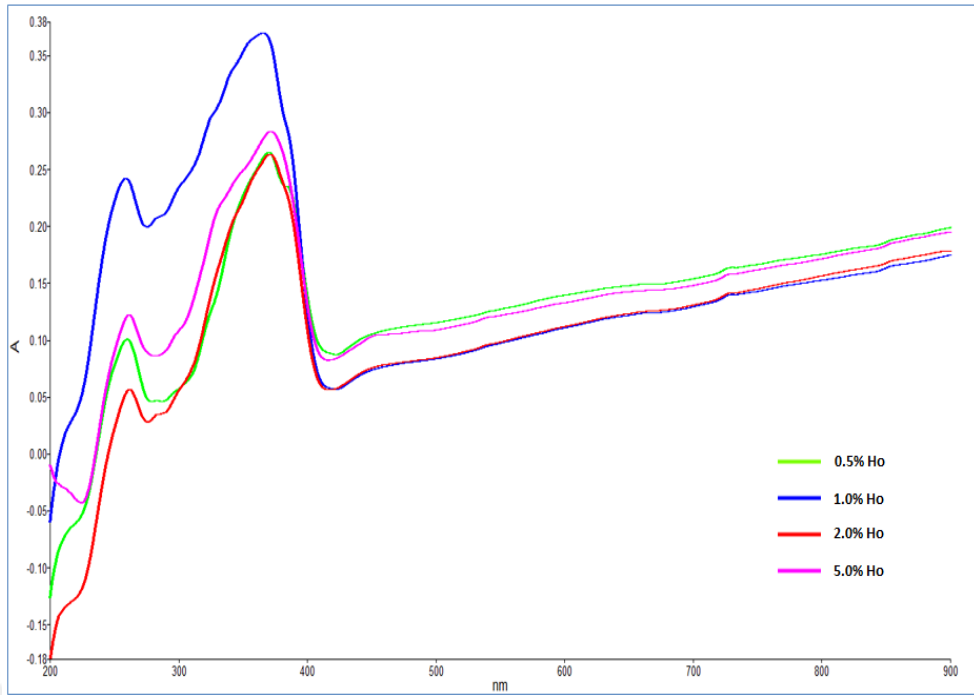
Figure 4.47. Absorbance UV-VIS Spectrum of 0.005(0.5%) mol, 0.010(1%) mol, 0.020(2%) mol and 0.5(5%) mol Ho doped $Mg_2B_2O_5$ at 800°C 1h. using HMTA fuel
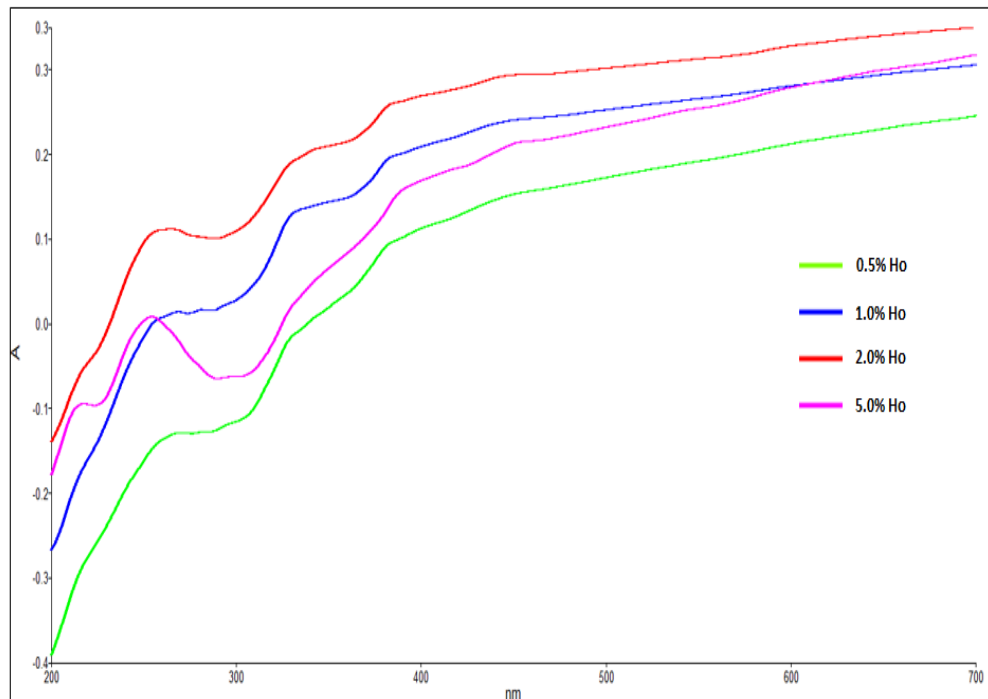
Figure 4.48. Absorbance UV-VIS Spectrum of 0.005(0.5%) mol, 0.010(1%) mol, 0.020(2%) mol and 0.5(5%) mol Ho doped $Mg_2B_2O_5$ at 800°C 1h. using Urea fuel
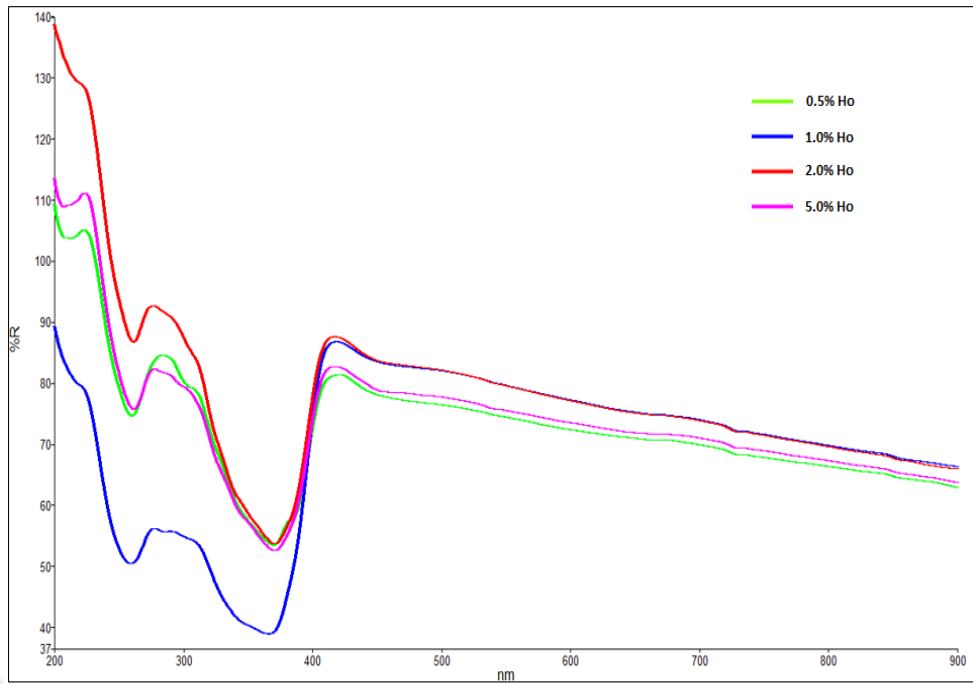
Figure 4.49. Reflectance UV-VIS Spectrum of 0.005(0.5%) mol, 0.010(1%) mol, 0.020(2%) mol and 0.5(5%) mol Ho doped $Mg_2B_2O_5$ at 800ºC 1h. using HMTA fuel
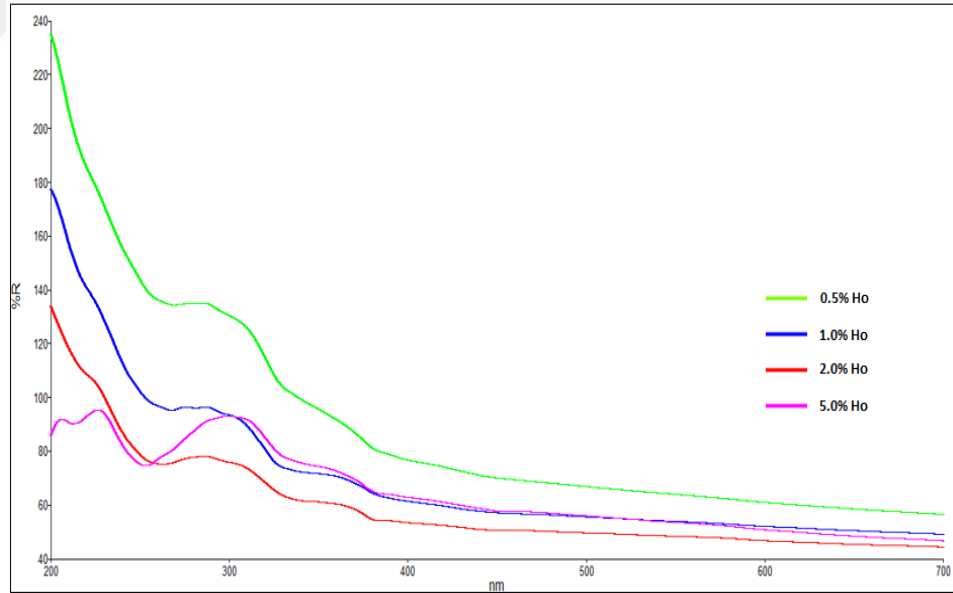
Figure 4.50. Reflectance UV-VIS Spectrum of 0.005(0.5%) mol, 0.010(1%) mol, 0.020(2%) mol and 0.5(5%) mol Ho doped $Mg_2B_2O_5$ at 800ºC 1h. using Urea fuel
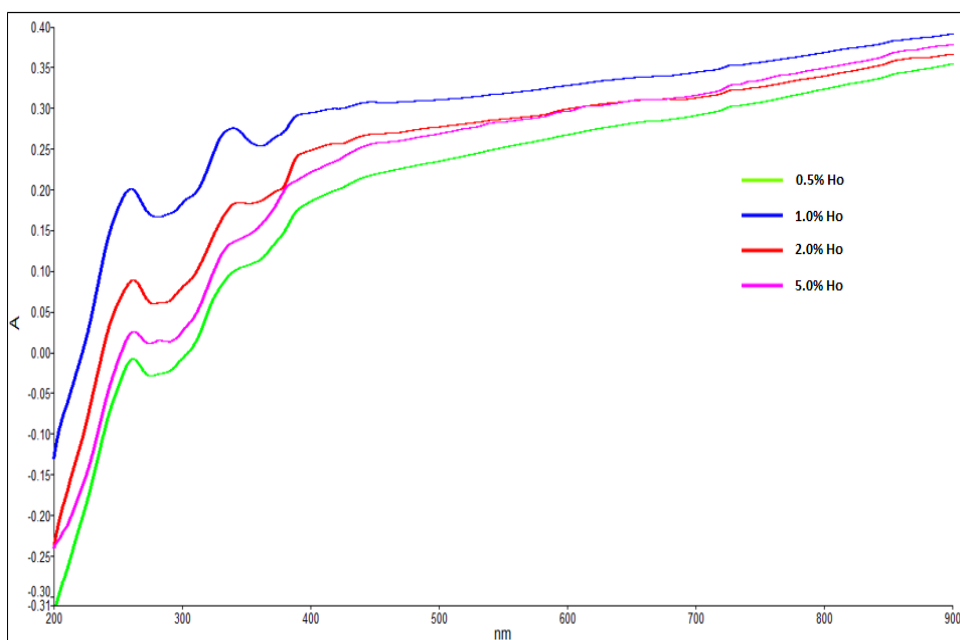
Figure 4.51. Absorbance UV-VIS Spectrum of 0.005(0.5%) mol, 0.010(1%) mol, 0.020(2%) mol and 0.5(5%) mol Ho doped $Mg_2B_2O_5$ at 900ºC 1h. using HMTA fuel
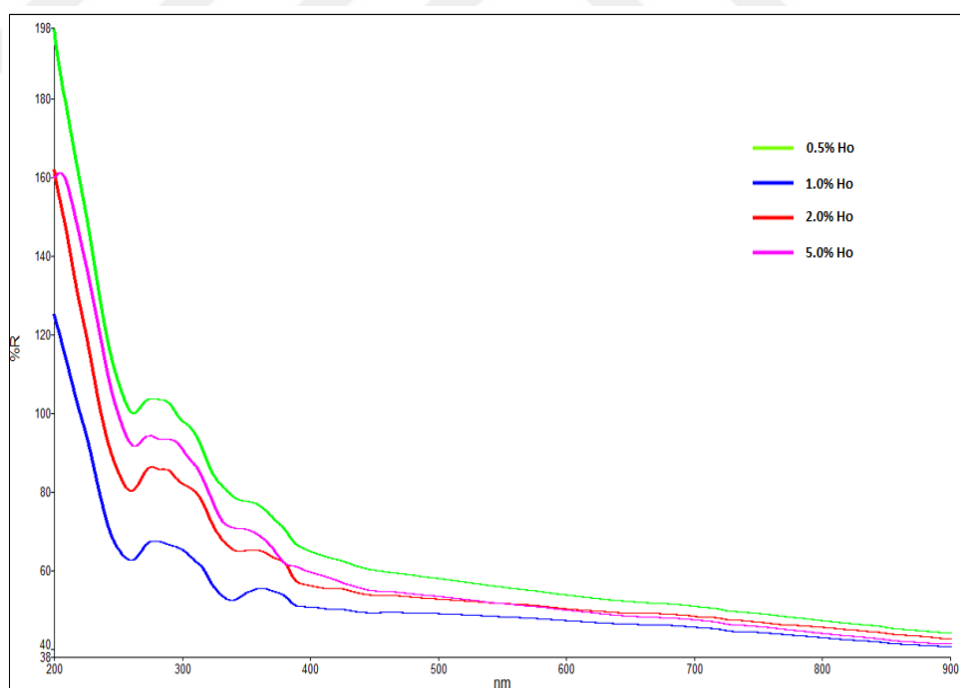
Figure 4.52. Reflectance UV-VIS Spectrum of 0.005(0.5%) mol, 0.010(1%) mol, 0.020(2%) mol and 0.5(5%) mol Ho doped $Mg_2B_2O_5$ at 900ºC 1h. using HMTA fuel

77

4.4   Er doped $Mg_2B_2O_5$

A series of $Mg_2B_2O_5$: Er^{3+} (0.005, 0.010, 0.020, 0.050 mol) doping pyroborates were synthesized by solution combustion method. Firstly, heated at 370°C until gel form is obtained to produce $Mg_{2-x}Er_xB_2O_5$ (x = 0.005, 0.010, 0.020, 0.050 mol). At the end of gelious part, gelious form was pink like color in considering all fuels, shown in Figure 4.1. Then, it was put into furnace at 400°C 10min. to acquire combustion. After that, it was heated to 700°C for 2 hour to get best result of doped $Mg_2B_2O_5$ crystallinity.

The general reaction with different type of fuels;

$(2-x)$ $Mg(NO_3)_2.6H_2O_{(s)}$ + x $Er(NO_3)_2.5H_2O_{(s)}$ + $2H_3BO_{3(s)}$ + $fuel_{(s)} \rightarrow$

$Mg_{(2-x)}Er_{(x)}B_2O_{5(s)}$ + $CO_{2\ (g)}$ + $H_2O_{(g)}$ + $NO_{2(g)}$
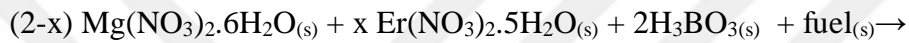
(fuel= Glycine, tartaric acid, citric acid, urea and hexamethylenetetramine)

(x= 0.005, 0.010, 0.020 and 0.050 mol)

In the combustion process of $Mg_2B_2O_5$ doped with Er^{3+} the intensity order of combustion highest to lowest was Gly, TA, CA, U and HMTA, respectively, as in Dy doped $Mg_2B_2O_5$. Unlike the other fuels, when HMTA was used, the product's shape was speckled in 0.005, 0.010, 0.020, 0.050 mol, shown in Figure 4.53, Figure 4.54, Figure 4.55, Figure 4.56. After the heating process of 700°C, The color of 0.005 mol and 0.010 mol doping compounds were changed from brown to dark grey by using TA fuel. Also, the color of 0.020 mol Er and 0.050 mol Er doping compounds were changed from brown to black after the process of 700°C 2h. shown in Figure 4.57. The reason of this situation was that the compound needed more heating process to achieve best result of $Mg_2B_2O_5$ compound. While CA was used as fuel, the compound was puffy and cream color after the combustion process of 400°C 10min., its color turned from cream to light grey after 700°C 2h. Additionally, When Gly was used as fuel, the product was fluffy and light brown color at 400°C 10min. Unlike the other fuels, U and HMTA made the $Mg_2B_2O_5$ white color and low yield.

78

The pictures that is shown below the products after 400ºC 10min.

Figure 4.53. The images of $Mg_{2.995}Er_{0.005}B_2O_5$ samples were synthesized with a) Gly, b) TA, c) CA, d) U, e) HMTA

Figure 4.54. The images of $Mg_{2.990}Er_{0.010}B_2O_5$ samples were synthesized with a) Gly, b) TA, c) CA, d) U, e) HMTA

Figure 4.55. The images of $Mg_{2.980}Er_{0.020}B_2O_5$ samples were synthesized with a) Gly, b) TA, c) CA, d) U, e) HMTA

Figure 4.56. The images of $Mg_{2.950}Er_{0.050}B_2O_5$ samples were synthesized with a) Gly, b) TA, c) CA, d) U, e) HMTA

The pictures that is shown below the products after 700°C 2h.

a

b
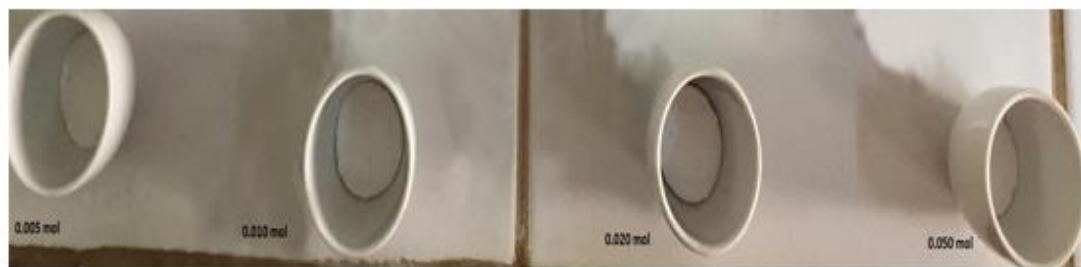
c
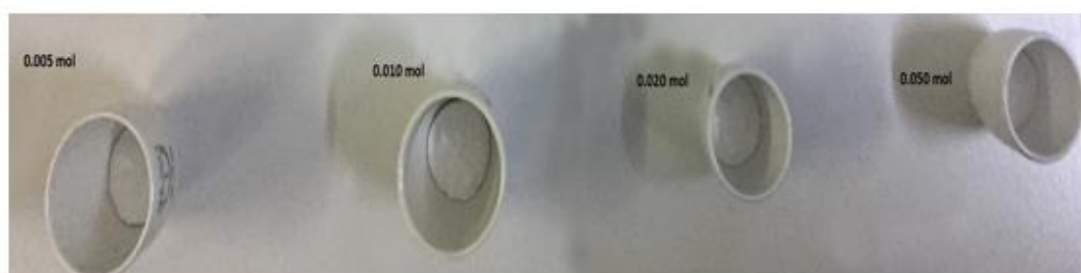
d

Figure 4.57. The images of $Mg_{(2-x)}Er_{(x)}B_2O_5$ samples were synthesized as x = 0.005, 0.010, 0.020, 0.050 mol with a) TA, b) CA, c) U, d) HMTA

4.4.1 XRD Studies of Er doped Mg$_2$B$_2$O$_5$

The results exhibited that used different fuels gave doped Mg$_2$B$_2$O$_5$ products with different morphologies and crystallinity. Figure 4.58, Figure 4.59, Figure 4.60 and Figure 4.61 shows powder X-ray diffraction patterns of Er doped magnesium pyroborate synthesized from different fuels and at 700°C 2h. When all these figures considered, the intensity sequence from the highest to lowest is HMTA, U, Gly, CA, TA after the heating process of 700°C 2h. All these XRD peaks of doped compounds were matched with 15-0537 ICDD data card for triclinic Mg$_2$B$_2$O$_5$.

0.020 mol and 0.050 mol Er^{3+} doped Mg$_2$B$_2$O$_5$ product synthesized with TA fuel was obtained amorph phase as 362.17 cps at 35.040 (2theta) and 358.14 cps at 34.700 (2theta), respectively. The reason of this situation was that the doped compound was needed more heating process to obtain best results of Mg$_2$B$_2$O$_5$. Er doped Mg$_2$B$_2$O$_5$ synthesized with HMTA fuel has highest crystallinity and lowest yield in all four concentrations (0.005, 0.010, 0.020, 0.050 mol) after the combustion process of 700 $^{\circ}$C 2h. The highest intensities of Er doped Mg$_2$B$_2$O$_5$ are 1087.00 cps at 34.960 (2theta) for 0.005 mol, 1004.17 cps at 35.060 (2theta) for 0.010 mol, 891.67 cps at 34.900 (2theta) for 0.020 mol, 737.50 cps at 34.960 (2theta) for 0.050 mol by using HMTA fuel. Unlike other doping RE metals as Dy and Ho, Er doped Mg$_2$B$_2$O$_5$ has highest intensities with HMTA fuel. Not only HMTA fuel but also U fuel was suitable fuel as highest intensity as 795.83 cps at 34.760 (2theta). As a result, the crystallinity is decreased as shifting the position of 2theta changes when the dopant concentration is increased.

Additionally, the crystallite size (D) of the Er^{3+} doped Mg$_2$B$_2$O$_5$ that was synthesized with different fuels were calculated from the XRD pattern according to Scherrer formula

$$D = \frac{K\lambda}{\beta Cos\theta}$$

where K is the constant, λ is the X-ray wavelength (0.15406 nm), β is the full-width at half maximum and θ is the diffraction angle.

Table 4.9. 0.005 mol Er^{3+} doped $Mg_2B_2O_5$ crystallite size changing with fuels

FUELS	Crystallite size, nm (700°C, 2h.)
Gly	16,73
TA	10,34
CA	13,96
U	17,21
HMTA	18,21

Table 4.10. 0.010 mol Er^{3+} doped $Mg_2B_2O_5$ crystallite size changing with fuels

FUELS	Crystallite size, nm (700°C, 2h.)
Gly	16,84
TA	11,04
CA	14,09
U	17,58
HMTA	19,36

Table 4.11. 0.020 mol Er^{3+} doped $Mg_2B_2O_5$ crystallite size changing with fuels

FUELS	Crystallite size, nm (700°C, 2h.)
Gly	16,86
TA	-
CA	13,91
U	16,21
HMTA	19,14

Table 4.12. 0.05 mol Er^{3+} doped $Mg_2B_2O_5$ crystallite size changing with fuels

FUELS	Crystallite size, nm (700°C, 2h.)
Gly	17,73
TA	-
CA	13,86
U	17,35
HMTA	19,68

Table 4.9, Table 4.10, Table 4.11 and Table 4.12 shows that while the crystallite size of Er^{+3} doped $Mg_2B_2O_5$ synthesized with Gly, TA, CA, U and HMTA increases with increasing amount of moles. Otherwise, Er^{3+} doped $Mg_2B_2O_5$ synthesized with HMTA has larger crystallite size when compared with other fuels. On the other hand, 0.020 mol and 0.050 mol Er^{+3} doped $Mg_2B_2O_5$ synthesized with TA, the crystallite size of this compound was not calculated significantly.
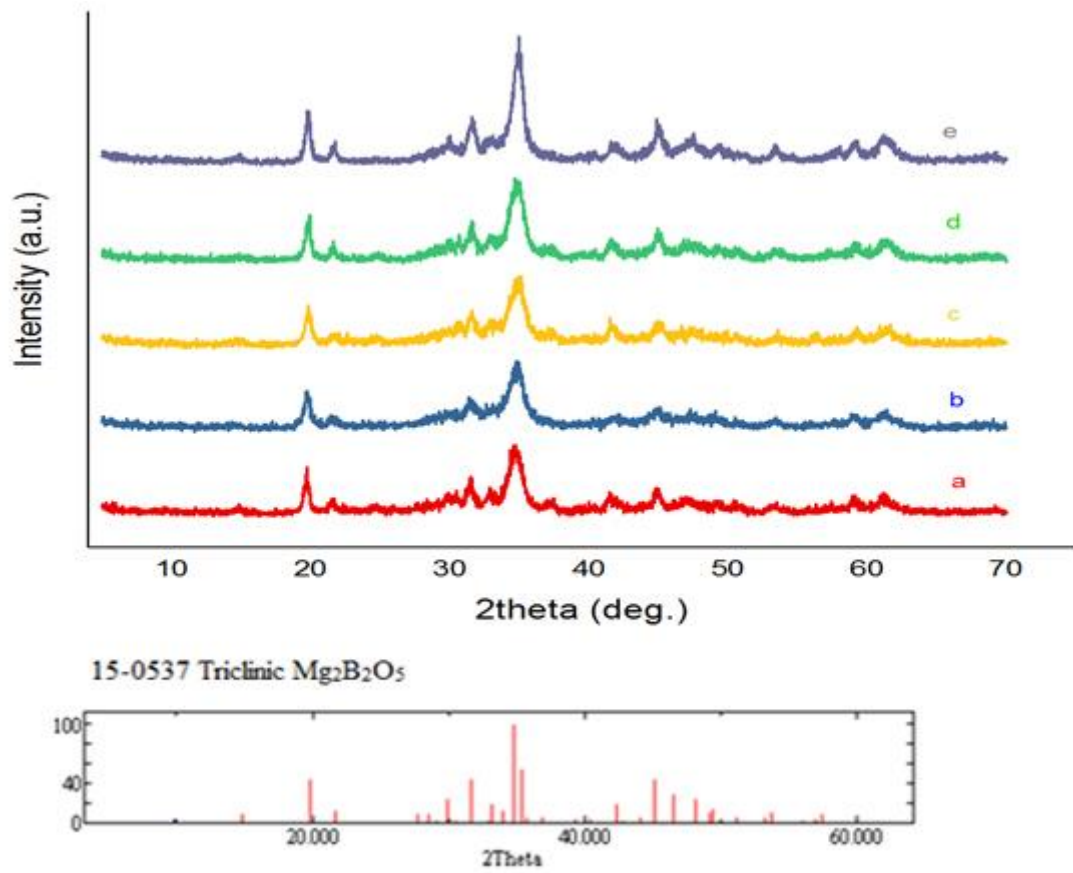
Figure 4.58. XRD patterns of 0.005 mol Er doped $Mg_2B_2O_5$ at 700°C 2h., using a) Gly, b) TA, c) CA, d) U, e) HMTA with ICDD Data Card for 15-0537 Triclinic $Mg_2B_2O_5$
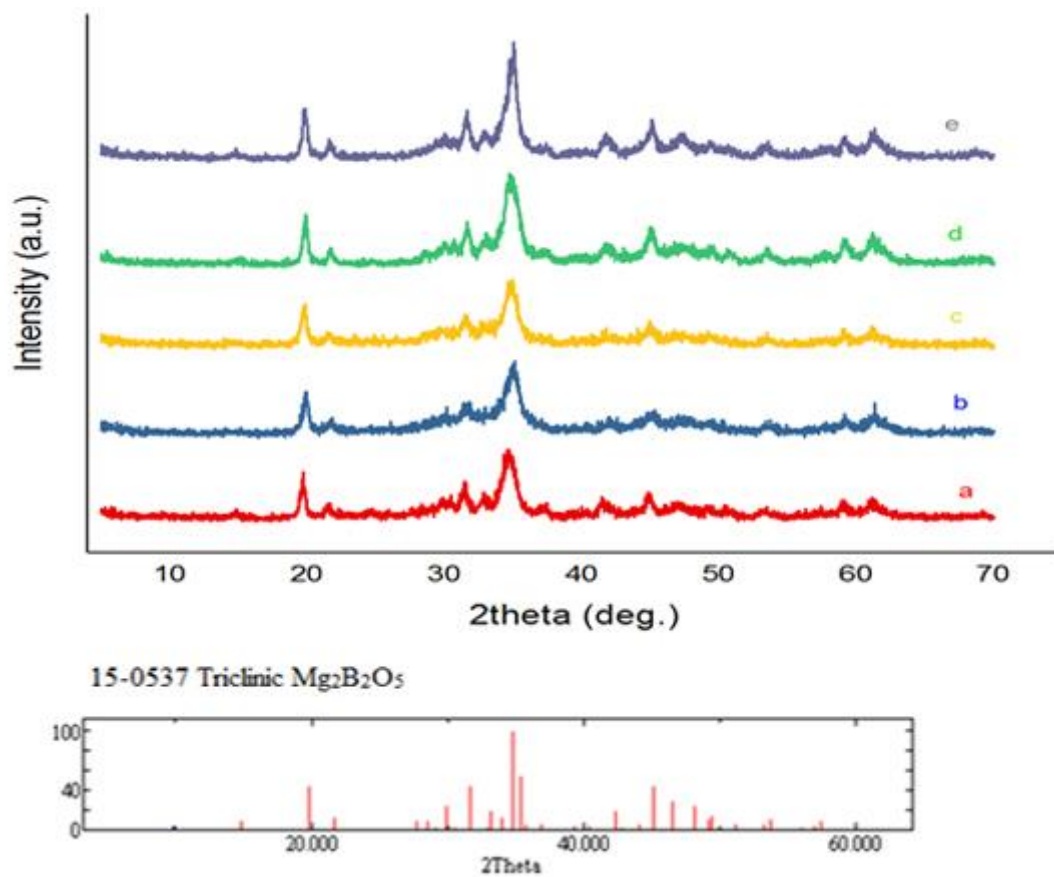
Figure 4.59. XRD patterns of 0.010 mol Er doped $Mg_2B_2O_5$ at 700°C 2h., using a) Gly, b) TA, c) CA, d) U, e) HMTA with ICDD Data Card for 15-0537 Triclinic $Mg_2B_2O_5$
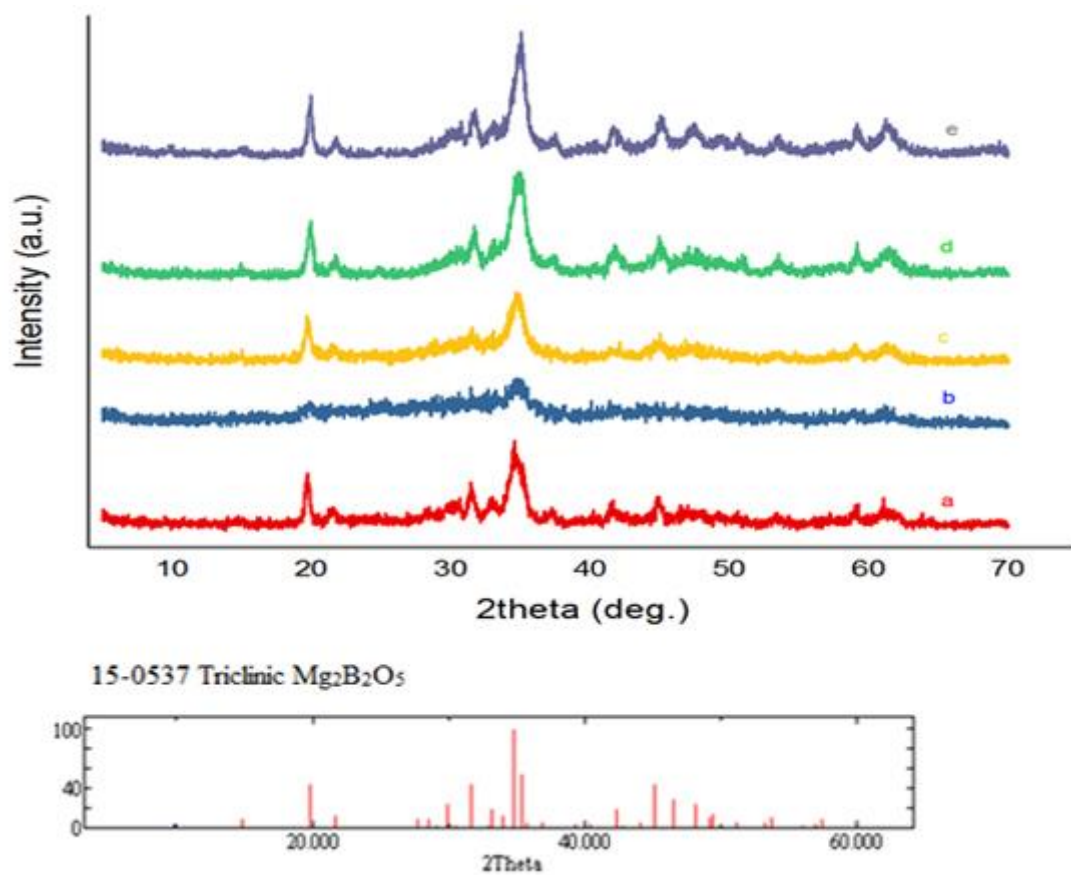
Figure 4.60. XRD patterns of 0.020 mol Er doped $Mg_2B_2O_5$ at 700°C 2h., using a) Gly, b) TA, c) CA, d) U, e) HMTA with ICDD Data Card for 15-0537 Triclinic $Mg_2B_2O_5$
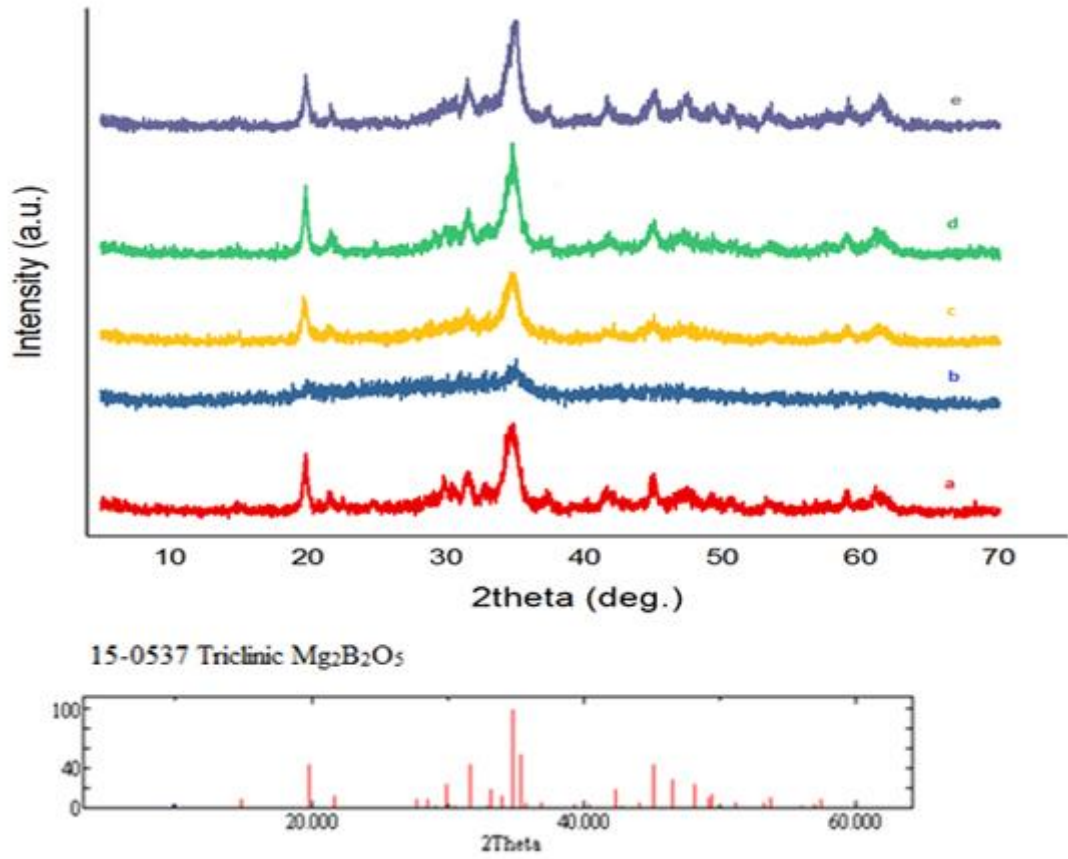
Figure 4.61. XRD patterns of 0.050 mol Er doped $Mg_2B_2O_5$ at 700°C 2h., using a) Gly, b) TA, c) CA, d) U, e) HMTA with ICDD Data Card for 15-0537 Triclinic $Mg_2B_2O_5$

91

4.4.2 Infrared Spectroscopy Studies of Er doped Mg$_2$B$_2$O$_5$

Fourier transform infrared (FTIR) spectra of Er^{3+} doped Mg$_2$B$_2$O$_5$ samples synthesized with SCS method was recorded in the range 300-4000 cm^{-1} using KBr pellets. IR spectra of Mg$_{(2-x)}$Er$_x$B$_2$O$_5$ (x = 0.005, 0.010, 0.020, 0.050 mol) samples at 400ºC for 10min. and 700ºC 2h. were shown in below. The strong bonds at 1450-1550 cm^{-1} and 600-750 cm^{-1} was correlated with characteristic vibrational of Mg$_2$B$_2$O$_5$. In the heating process of 400ºC 10min., peaks at 3700-3200 cm^{-1} observed as O-H stretching mode of hydroxyl group due to surface moisturising. After 700ºC process, these peaks were not observed. When the heating process increased from 400ºC to 700ºC, the absorption of 600-750 cm^{-1} spectrum was became clear. In the pyroborate, the group of bands between 1100 cm^{-1} and 1450 cm^{-1} are strong, broad, and very strongly dependent on isotopic mass (Weir et al., 1964). The absorption peak at 1150–1200 cm^{-1} can be assigned to antisymmetric stretching vibrations of the BOB groups in pyroborates (Guo et al., 2014). The spectra of synthetic triclinic suanite exhibited a single band at 610 cm^{-1} (Oztas et al., 2009). When 0.020 mol and 0.050 mol Er^{3+} doped Mg$_2$B$_2$O$_5$, the major peaks in the range of 1450-1550 cm^{-1} due to B-O stretching vibrations were not obtained strongly because of amorph type of pyroborate.
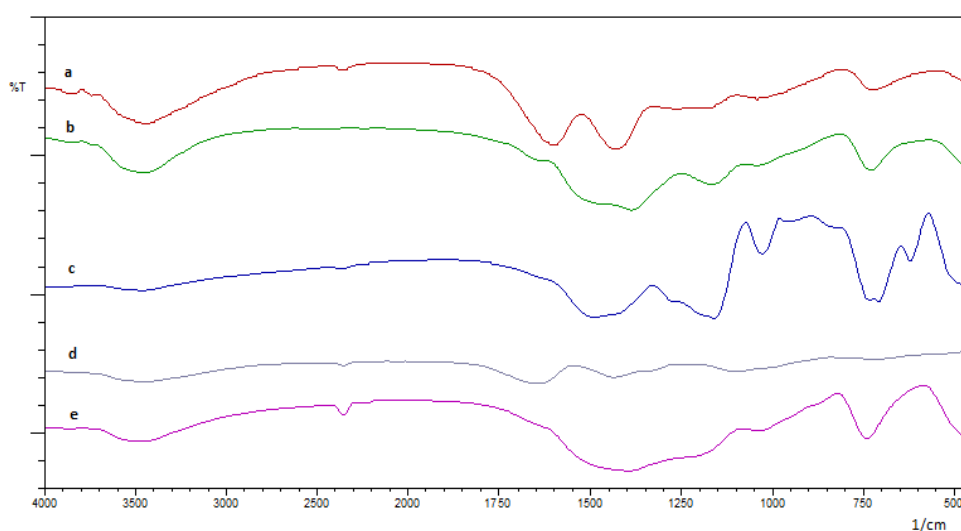
Figure 4.62. IR spectra of 0.005 mol Er doped Mg$_2$B$_2$O$_5$ at 400ºC 10min. using a) CA, b) U, c) Gly, d) TA, e) HMTA
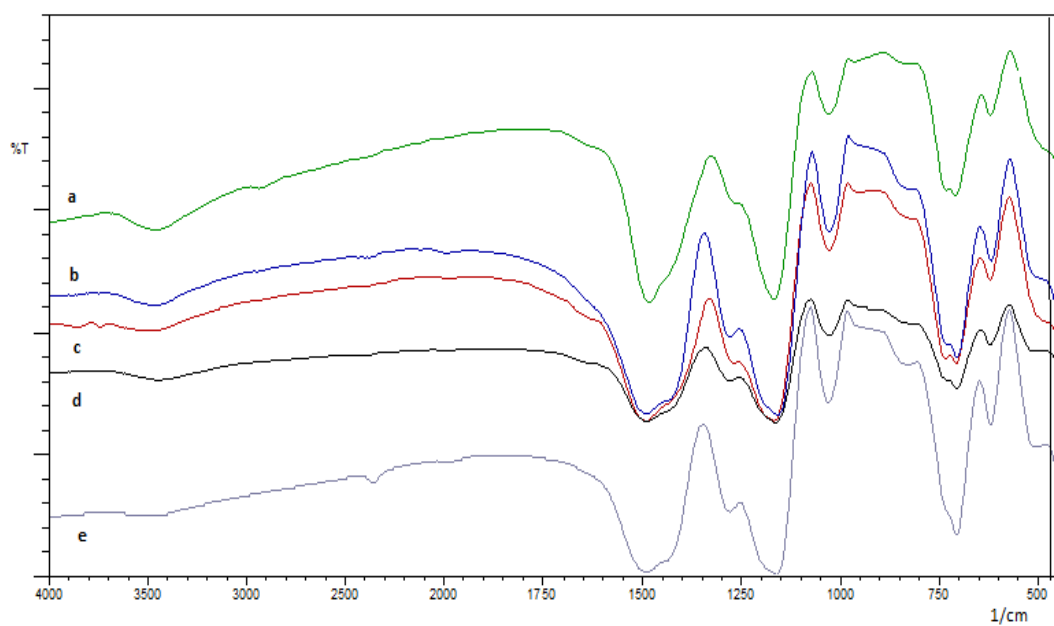
Figure 4.63. IR spectra of 0.005 mol Er doped $Mg_2B_2O_5$ at 700°C 1h. using
a) CA, b) U, c) Gly, d) TA, e) HMTA
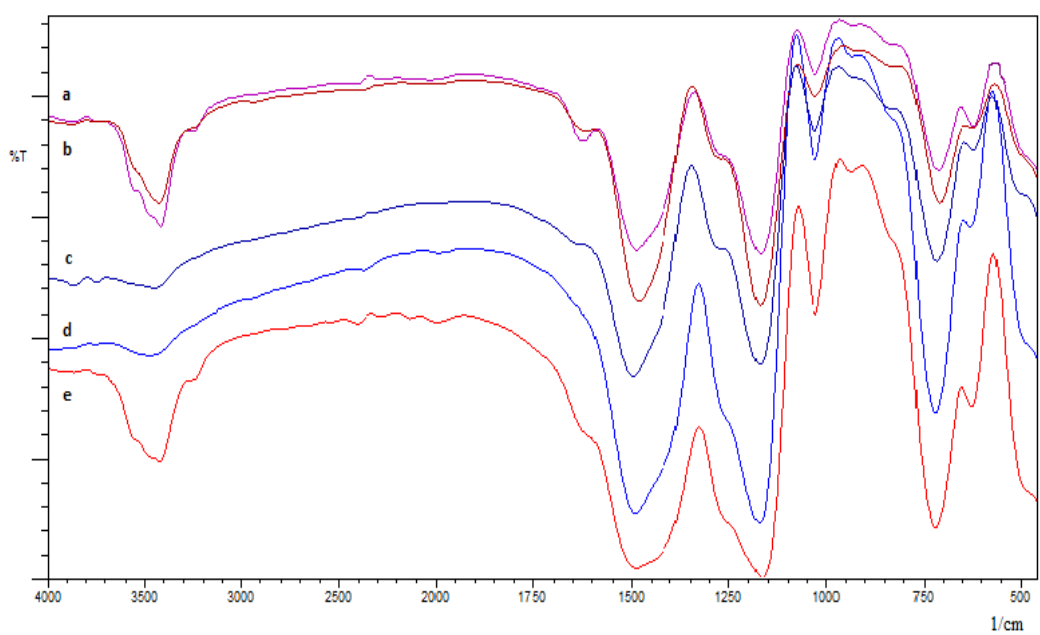
Figure 4.64. IR spectra of 0.005 mol Er doped $Mg_2B_2O_5$ at 800°C 1h. using
a) U, b) HMTA, c) CA, d) TA, e) Gly
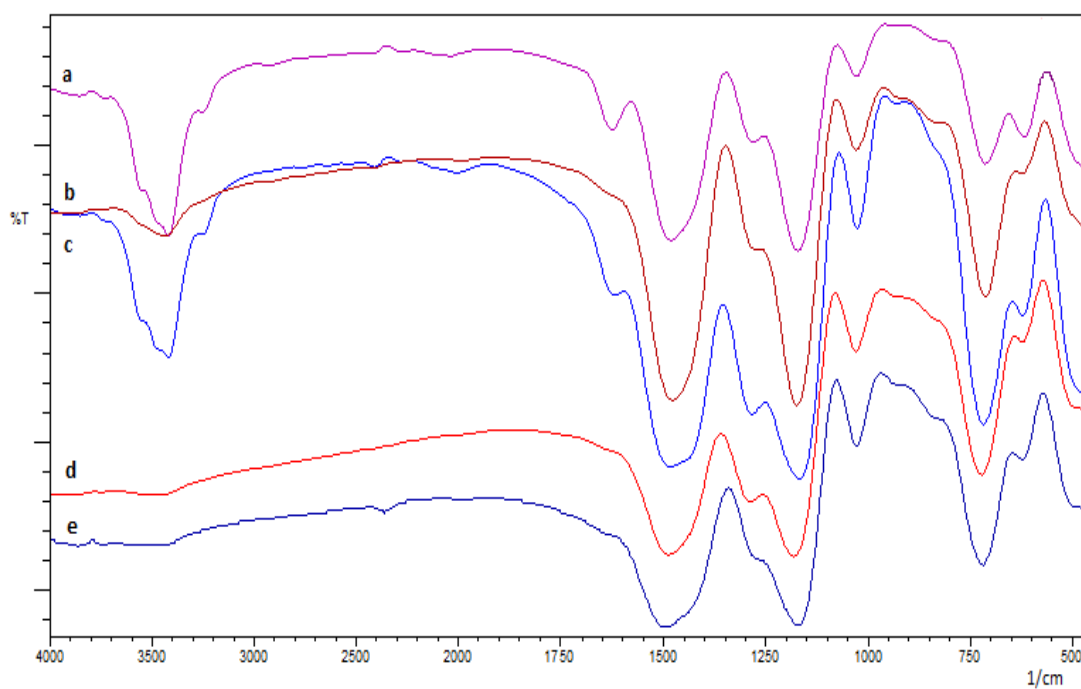
Figure 4.65. IR spectra of 0.005 mol Er doped $Mg_2B_2O_5$ at 900ºC 1h. using a) U, b) HMTA, c) Gly, d) CA, e) TA
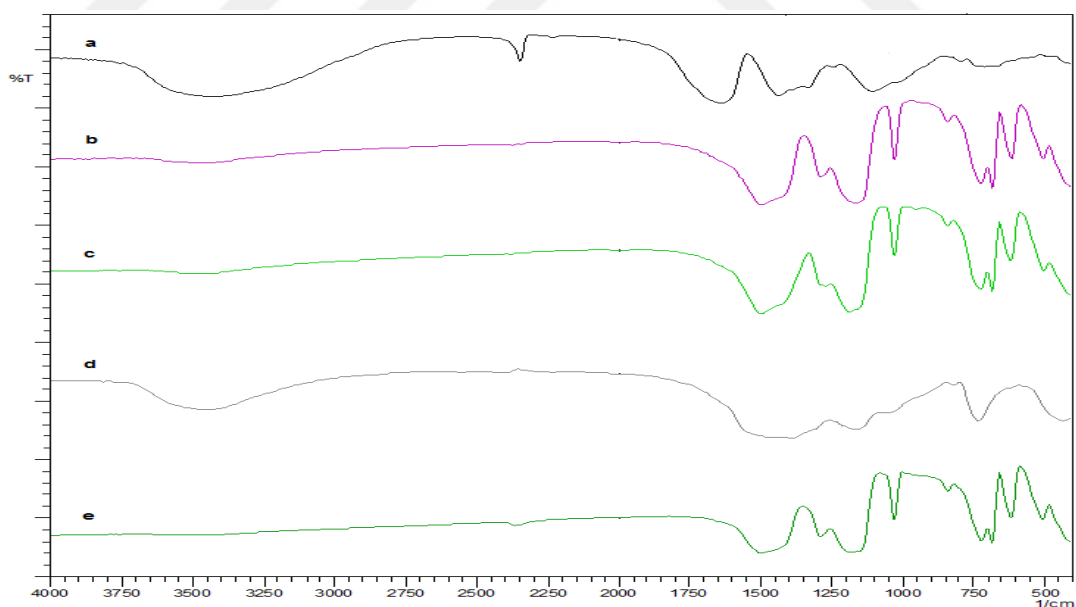
Figure 4.66. IR spectra of 0.010 mol Er doped $Mg_2B_2O_5$ at 400ºC 10min. using a) Gly, b) U, c) TA, d) CA, e) HMTA
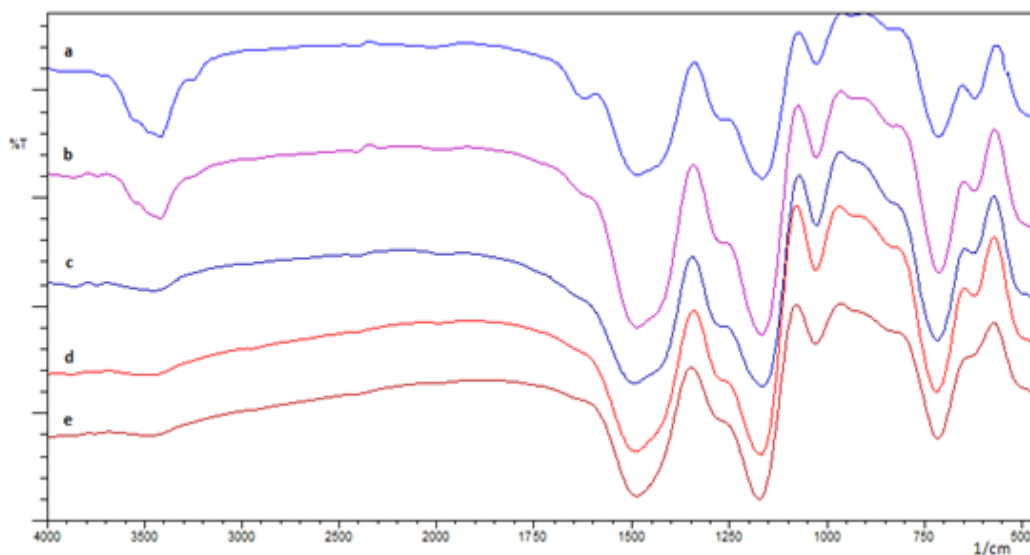
Figure 4.67. IR spectra of 0.010 mol Er doped $Mg_2B_2O_5$ at 800°C 1h. using
a) Gly, b) U, c) TA, d) CA, e) HMTA
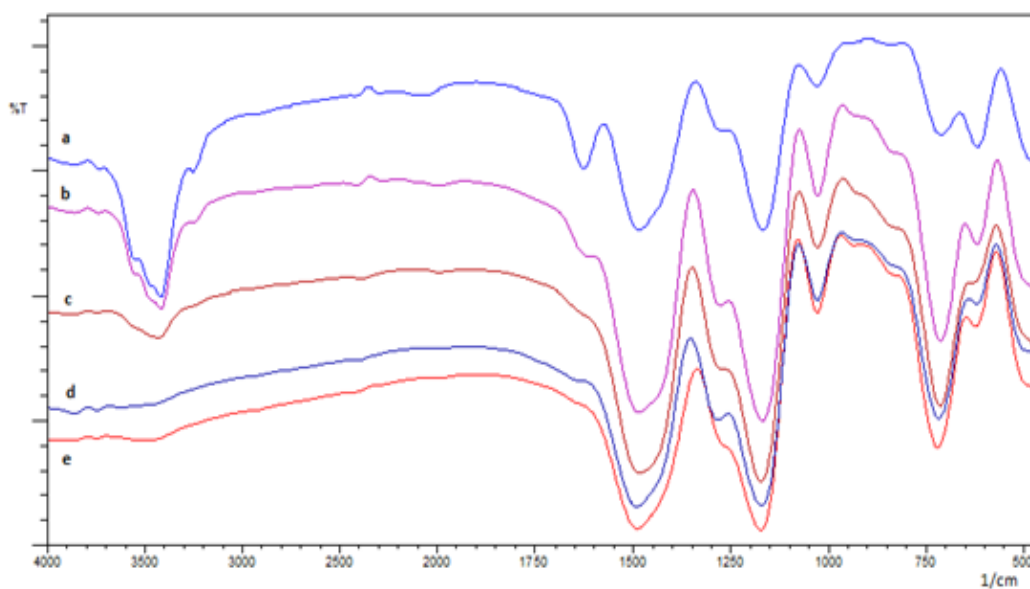
Figure 4.68. IR spectra of 0.010 mol Er doped $Mg_2B_2O_5$ at 900°C 1h. using
a) Gly, b) U, c) HMTA, d) TA, e) CA

4.4.3 Ultraviolet Visible Studies of Ho doped $Mg_2B_2O_5$

Optical properties of samples were determined with UV-VIS Spectroscopy. Absorbance and Reflectance of UV-VIS spectrum of $Mg_{(2-x)}Er_{(x)}B_2O_5$ (x = 0.005, 0.010, 0.020, 0.050 mol) samples at 700ºC 2h., 800ºC 1h. and 900ºC 1h with HMTA fuel were shown in below. When the doping amount moles of Er were increased, the absorbance of material was increased. On the other hand, when the doping amount moles of Er were increased, the reflectance of material was decreased at 700ºC and 800ºC. At 900ºC, the absorbance of materials was increased with decreasing doping amounts of Er. Otherwise, the reflectance of materials was increased with increasing doping amounts of Er.

In the consideration of 0.005 mol Er^{3+} doping with HMTA fuel, blue shift obtained with increasing temperature and wavelength. On the other hand, 0.010 mol Er^{3+}, 0.020 mol Er^{3+} and 0.050 mol Er^{3+} doping with HMTA fuel, red shift obtained with increasing temperature as 700ºC, 800ºC and 900ºC and with decreasing wavelength. 0.01 mol Er^{3+} doping with Urea fuel, red shift obtain with increasing temperature and decreasing wavelength. In reverse case, blue shift obtained with Urea fuel in 0.005, 0.020 and 0.050 mol concentrations with increasing temperature as 700ºC and 800ºC and decreasing wavelength.
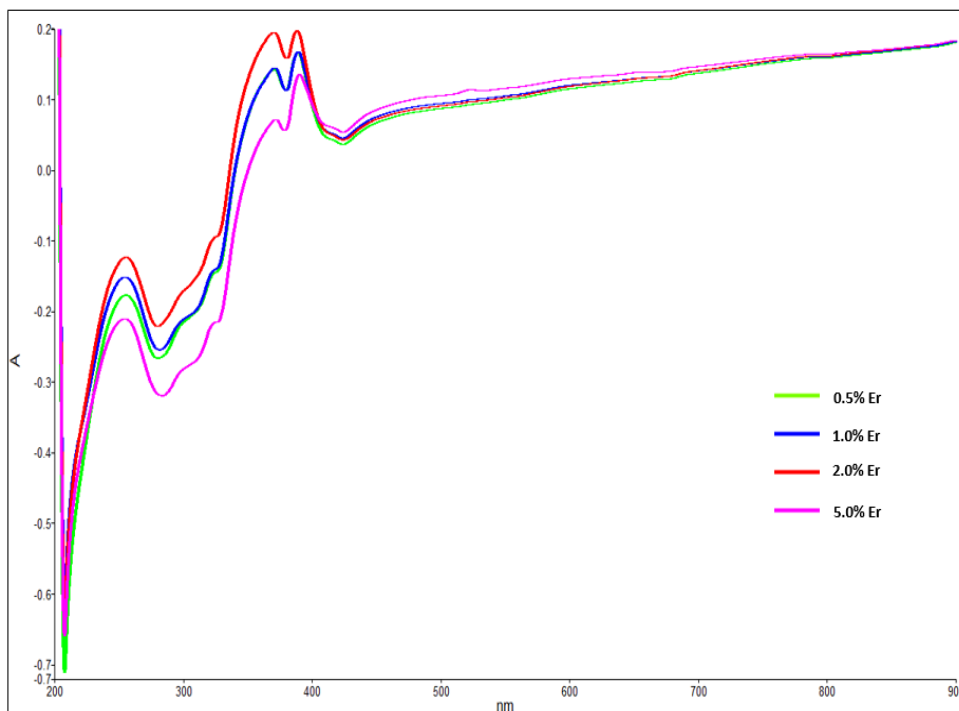
Figure 4.69. Absorbance UV-VIS Spectrum of 0.005(0.5%) mol, 0.010(1%) mol, 0.020(2%) mol and 0.5(5%) mol Er doped $Mg_2B_2O_5$ at 700^oC 2h. using HMTA fuel
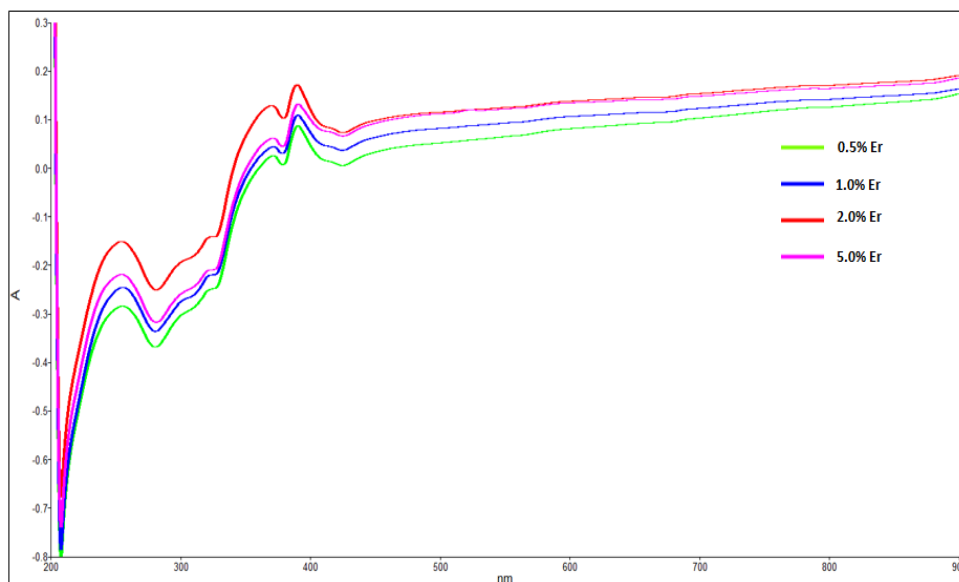
Figure 4.70. Absorbance UV-VIS Spectrum of 0.005(0.5%) mol, 0.010(1%) mol, 0.020(2%) mol and 0.5(5%) mol Er doped $Mg_2B_2O_5$ at 700^oC 2h. using Urea fuel
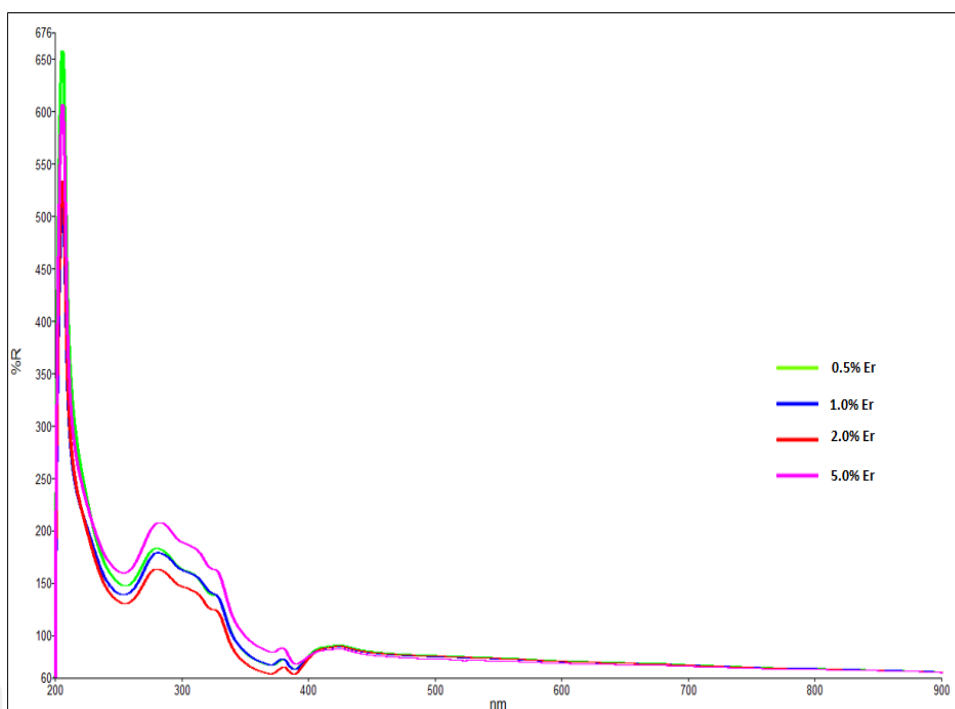
Figure 4.71. Reflectance UV-VIS Spectrum of 0.005(0.5%) mol, 0.010(1%) mol, 0.020(2%) mol and 0.5(5%) mol Er doped $Mg_2B_2O_5$ at 700ºC 2h. using HMTA fuel
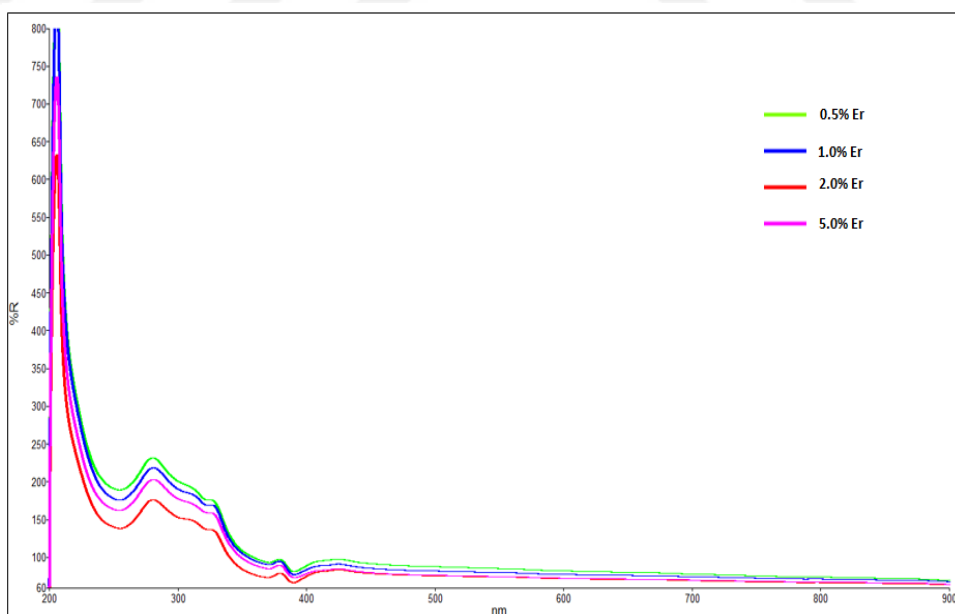
Figure 4.72. Reflectance UV-VIS Spectrum of 0.005(0.5%) mol, 0.010(1%) mol, 0.020(2%) mol and 0.5(5%) mol Er doped $Mg_2B_2O_5$ at 700ºC 2h. using Urea fuel

98
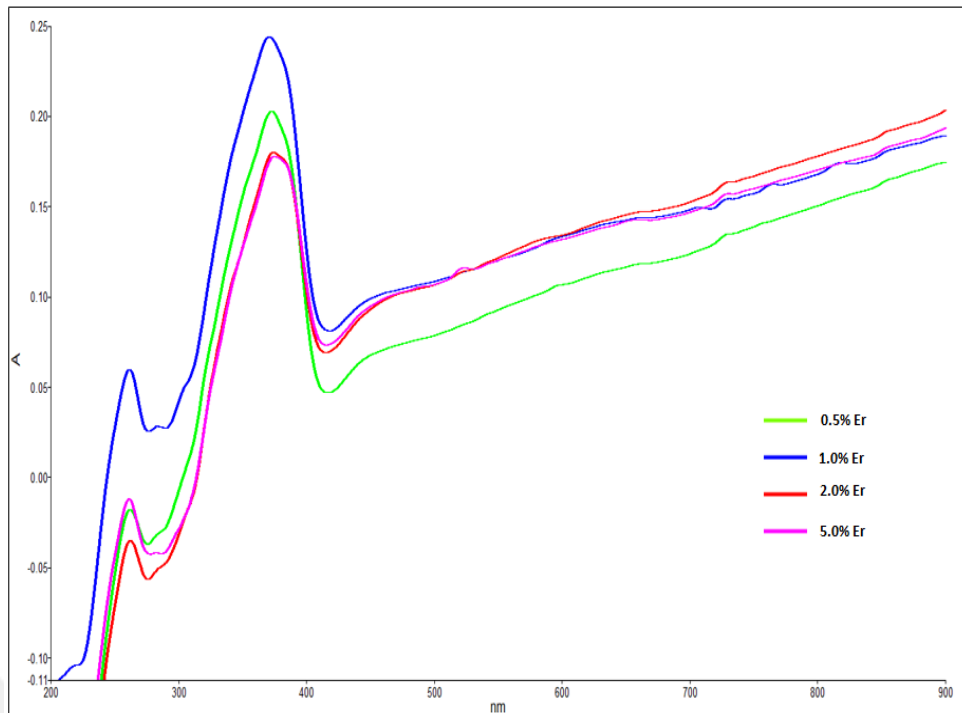
Figure 4.73. Absorbance UV-VIS Spectrum of 0.005(0.5%) mol, 0.010(1%) mol, 0.020(2%) mol and 0.5(5%) mol Er doped $Mg_2B_2O_5$ at 800ºC 1h. using HMTA fuel
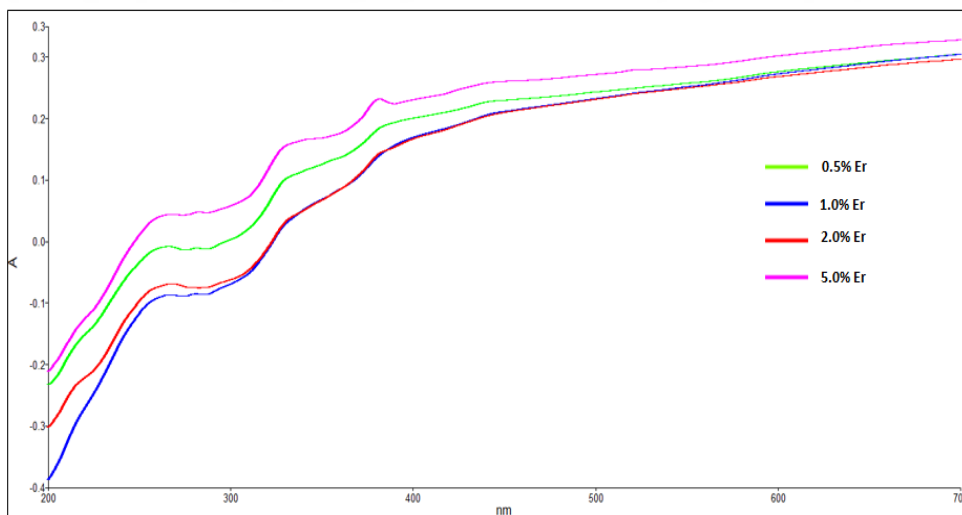
Figure 4.74. Absorbance UV-VIS Spectrum of 0.005(0.5%) mol, 0.010(1%) mol, 0.020(2%) mol and 0.5(5%) mol Er doped $Mg_2B_2O_5$ at 800ºC 1h. using Urea fuel
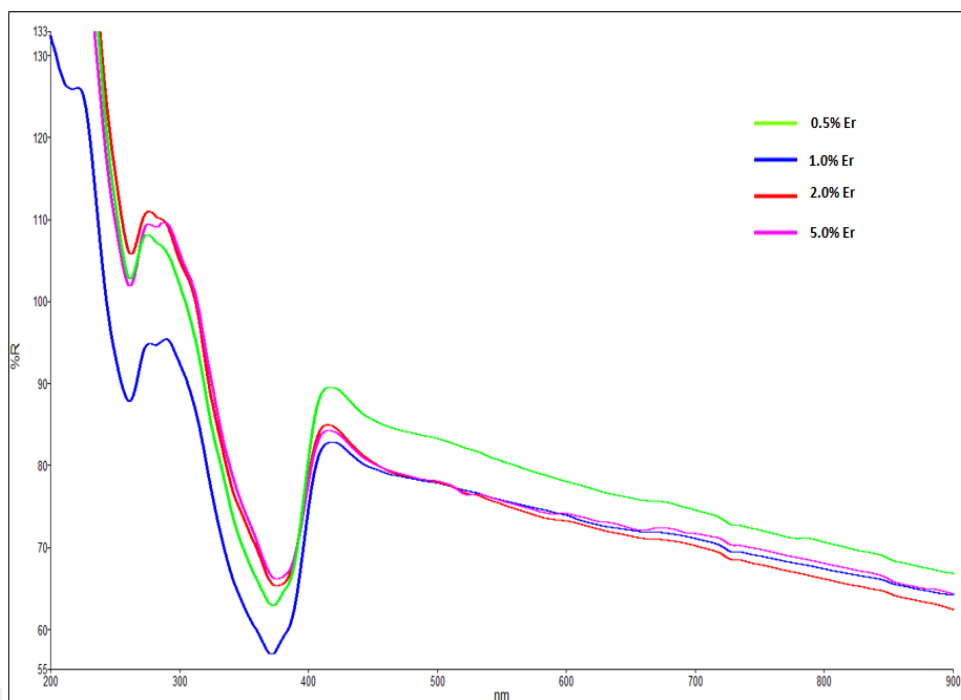
Figure 4.75. Reflectance UV-VIS Spectrum of 0.005(0.5%) mol, 0.010(1%) mol, 0.020(2%) mol and 0.5(5%) mol Er doped $Mg_2B_2O_5$ at 800°C 1h. using HMTA fuel
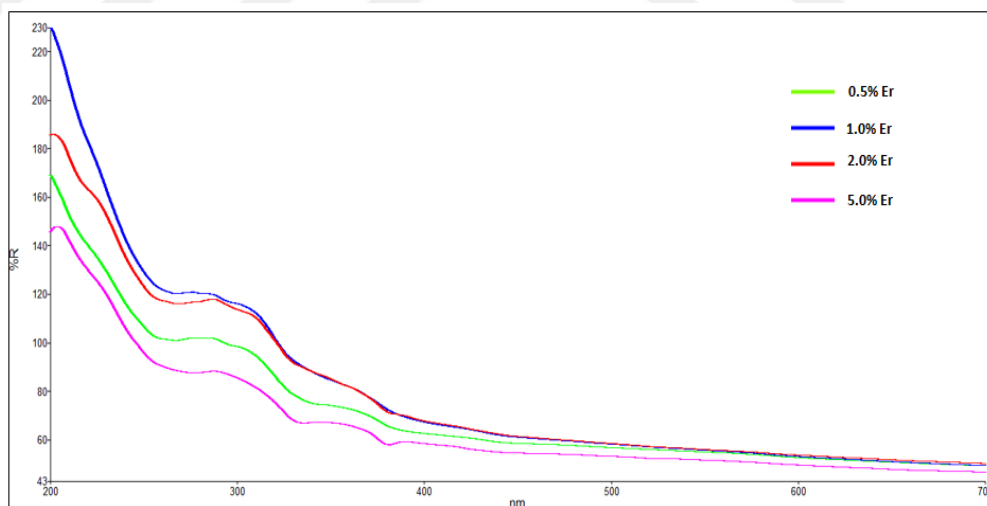
Figure 4.76. Reflectance UV-VIS Spectrum of 0.005(0.5%) mol, 0.010(1%) mol, 0.020(2%) mol and 0.5(5%) mol Er doped $Mg_2B_2O_5$ at 800°C 1h. using Urea fuel
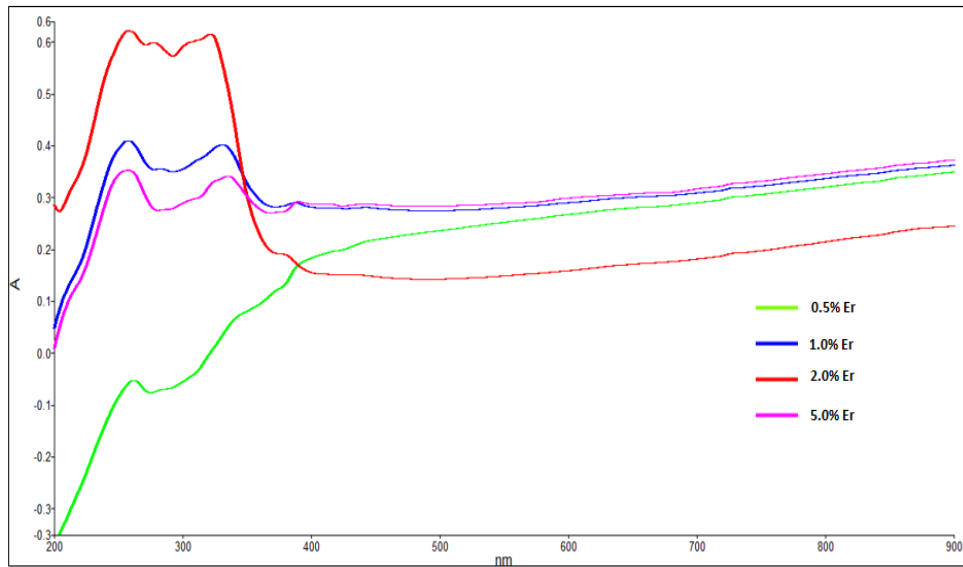
Figure 4.77. Absorbance UV-VIS Spectrum of 0.005(0.5%) mol, 0.010(1%) mol, 0.020(2%) mol and 0.5(5%) mol Er doped $Mg_2B_2O_5$ at 900°C 1h. using HMTA fuel
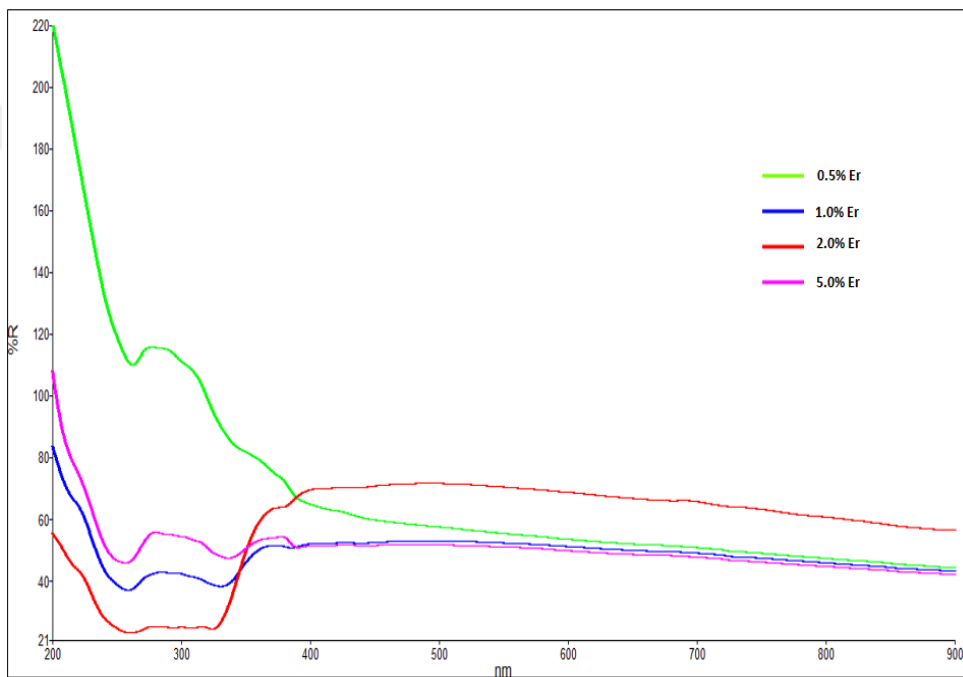
Figure 4.78. Reflectance UV-VIS Spectrum of 0.005(0.5%) mol, 0.010(1%) mol, 0.020(2%) mol and 0.5(5%) mol Er doped $Mg_2B_2O_5$ at 900°C 1h. using HMTA fuel

5. CONCLUSIONS

Dy^{3+}, Ho^{3+}, Er^{3+} doped $Mg_2B_2O_5$ nanoparticles were successfully synthesized with solution combustion synthesis method by using various fuels such as glycine, tartaric acid, citric acid, urea and HMTA. SCS method has many advantages such as saving of time and energy, simple experimental setup by comparison with other methods. During the preparation process, it was observed that the products with TA fuel has the highest yield whereas the products obtained by HMTA fuel has the lowest yield.

According to X-Ray Diffraction results of Dy^{3+}, Ho^{3+}, Er^{3+} doped $Mg_2B_2O_5$, all XRD peaks of doped compounds were matched with 15-0537 ICDD data card which belongs to triclinic $Mg_2B_2O_5$. The results exhibited that each fuel affected the crystallinity of doped $Mg_2B_2O_5$ products differently. After the combustion process at $400\,^{o}C$ 10min., Dy^{3+}, Ho^{3+}, Er^{3+} doped $Mg_2B_2O_5$ synthesized with HMTA fuel has highest crystallinity and lowest yield by considering all four concentrations (0.005, 0.010, 0.020, 0.050 mol). Consequently, HMTA and U are the most suitable fuels in this study because it produces $Mg_2B_2O_5$ with high crystallinity at higher temperature namely, $700\,^{o}C$.

According to Infrared Spectroscopy results of Dy^{3+}, Ho^{3+}, Er^{3+} doped $Mg_2B_2O_5$, the characteristic vibrational of $Mg_2B_2O_5$ were indicated by the existence of the strong bonds at 1450-1550 cm^{-1} and 600-750 cm^{-1}. The pyroborate group has strong and broad peaks between 1100 cm^{-1} and 1450 cm^{-1}. Also, the absorption peak at 1150–1200 cm^{-1} can be assigned to antisymmetric stretching vibrations of the BOB bonds. The spectra of synthetic triclinic $Mg_2B_2O_5$ exhibited a single band at 610 cm^{-1} and it observed that, as the heating process increased from $400^{o}C$ to $900^{o}C$, the absorption of the peak 600-750 cm^{-1} spectrum became sharper and proved the presence of $Mg_2B_2O_5$.

According to Ultraviolet Visible results of Dy^{3+}, Ho^{3+}, Er^{3+} doped $Mg_2B_2O_5$, showed the changed in wavelenght as either red shift or blue shift depends on the concentrations and temperatures that were applied. The products are red shift when the spectra move to longer wavelength and in reverse case it is called as blue shift. When the concentrations of Dy^{3+}, Ho^{3+}, Er^{3+} increased, the absorbance of prepared

products were increased. In consideration of Reflectance vs. Wavelenght graph, the reflections were obtained at the end of SCS process. It is known that, the ionic size of metals is related with absorption and reflectance which means Dy doped $Mg_2B_2O_5$ compounds show highest absorption and lowest reflection behaviour due to their order of ionic size, $Dy^{3+} > Ho^{3+} > Er^{3+}$. Observing the graphs of the products obtaned by HMTA fuel, it showed that the products with Dy^{3+} doped are blue shıfted at 700 °C, red shift at 800 °C and 900 °C as dopant concentration increases. Hence, the products with Er^{3+} are blue shift at 700 °C and 900 °C whereas the red shift is observed at 800°C with increasing the dopant concentrations. Furthermore, blue shift is not obtained in Ho^{3+} doped product since the wavelengths getting longer as concentrations of dopant increases at all heating temperatures. Additionally, observing the graphs of the products obtaned by Urea fuel, it showed that the products with Dy^{3+} doped are red shifted at 700°C and 800°C as dopant concentration increases. The products with Ho^{3+} and the products with Er^{3+} are blue shift at 700°C whereas the red shift is obtained at 800°C.

Consequently, the results showed that temperature, fuel, type of RE metal, concentration of RE metal had a significant effect on the properties of synthesized RE doped $Mg_2B_2O_5$ compounds such as crystallinity and purity. Also, the crystallite size calculations from Scherrer equation proved that all synthesized $Mg_2B_2O_5$ nanoparticles with solution combustion method technique are in nanoscale as 10-19 nm for five different fuels at 700°C as shown in Table 4.1, Table 4.2, Table 4.3, Table 4.4, Table 4.5, Table 4.6, Table 4.7, Table 4.8, Table 4.9, Table 4.10, Table 4.11, and Table 4.12. Additionally, the crystallite size of 0.010 mol Ho^{3+}, 0.020 mol Er^{3+} and 0.050 mol Er^{3+} doped $Mg_2B_2O_5$ compounds synthesized with TA were not calculated significantly because the products were obtained in amorphous phase. In conclusion, IR data and UV-VIS data also agreed to all the XRD patterns for doped $Mg_2B_2O_5$ compounds that synthesized in this thesis.

6. REFERENCES

Altuntaş Öztaş N and Erdoğan H (2009) "Synthesis and characterization of magnesium pyroborate by solution combustion and conventional ceramic methods: A comparative study" Zeitschrift für anorganische und allgemeine Chemie, 635(11): 1626-1632.

Barron VR, Ochoa FM, Vazquez CC and Bernal, R (2016) "Thermoluminescence of novel MgO–CeO2 obtained by a glycine-based solution combustion method" Applied Radiation and Isotopes, 117: 86-90.

Block S, Burley G, Perloff A and Mason Jr RD (1959) "Refinement of the crystal structure of triclinic magnesium pyroborate" J. Res. Nat. Bur. Stand, 62, 95:100.

Chen SH, Zhang DF and Sun G (2014) "In situ synthesis of porous ceramics with a framework structure of magnesium borate whiskers" Materials Letters, 121: 206-208.

Chick LA, Pederson LR, Maupin GD, Bates JL, Thomas LE and Exarhos GJ (1990) "Glycine-nitrate combustion synthesis of oxide ceramic powders" Materials Letters, 10(1-2): 6-12.

Deshpande K, Mukasyan A and Varma A (2004) "Direct synthesis of iron oxide nanopowders by the combustion approach: reaction mechanism and properties" Chemistry of materials, 16(24): 4896-4904.

Dosler U, Krzmanc MM and Suvorov D (2010) "The synthesis and microwave dielectric properties of Mg3B2O6 and Mg2B2O5 ceramics" Journal of the European Ceramic Society, 30(2): 413-418.

Dou L, Zhong J and Wang H (2010) "Preparation and characterization of magnesium borate for special glass" Physica Scripta, 2010(T139): 014010.

Ekambaram S, Patil KC and Maaza M (2005) "Synthesis of lamp phosphors: facile combustion approach" Journal of Alloys and Compounds, 393(1-2): 81-92.

Elssfah EM, Elsanousi A, Zhang J, Song HS and Tang C (2007) "Synthesis of magnesium borate nanorods" Materials Letters, 61(22), 4358:4361.

Fernandes JC, Sarrat FS, Guimaraes RB, Freitas RS, Continentino MA, Doriguetto AC and Dumas J (2003) "Structure and magnetism of MnMgB 2 O 5 and Mn 2 B 2 O 5" Physical Review B, 67(10): 104413.

Fibers optics for sale co, WHAT ARE RARE-EARTH DOPED FIBERS?, https://www.fiberoptics4sale.com/blogs/archive-posts/95044294-what-are-rare-earth-doped-fibers, 18.06.2019.

Gao Y, Meng F, Li X, Wen JZ and Li Z (2016) "Factors controlling nanosized Ni–Al 2 O 3 catalysts synthesized by solution combustion for slurry-phase CO methanation: the ratio of reducing valences to oxidizing valences in redox systems" Catalysis Science & Technology, 6(21): 7800-7811.

GAO, FAN JG, SUN HY, WANG ZM and PEI SH (2010) "The preparation and characterization of magnesium borate whiskers" [J]. Applied Chemical Industry, 10: 027.

Greenwood N (1998) Chemistry of The Elements, Second Edition, Butterworth Heinemann Pub., Great Britain.

Guo X, Wu H, Pan S, Yang Z, Yu H, Zhang B and Zhang F. (2014) "Synthesis, Crystal Structure, and Characterization of a Congruent Melting Compound Magnesium Strontium Diborate MgSrB2O5" Zeitschrift für anorganische und allgemeine Chemie, 640(8-9): 1805-1809.

Hegde V, Chauhan N, Viswanath CD, Kumar V, Mahato KK and Kamath SD (2019) "Photoemission and thermoluminescence characteristics of Dy3+-doped zinc sodium bismuth borate glasses" Solid State Sciences, 89: 130-138.

Hussain NS, Ali N, Dias AG, Lopes MA, Santos JD and Buddhudu S (2006) "Absorption and emission properties of Ho3+ doped lead–zinc–borate glasses" Thin Solid Films, 515(1): 318-325.

JIANG JW, WANG L, YANG Q and YANG DR (2006) "Synthesis of Magnesium Borate Nanorods by Sol-Gel Process" Journal of Inorganic Materials, 4: 012.

Kawano T, Morito H, Yamada, T, Onuma T, Chichibu SF and Yamane H. (2009) "Synthesis, crystal structure and characterization of iron pyroborate (Fe 2 B 2 O 5) single crystals" Journal of Solid State Chemistry, 182(8): 2004-2009.

Kelly TD, Petrosky JC, McClory JW, Adamiv VT, Burak YV, Padlyak BV and Dowben PA (2014) "Rare earth dopant (Nd, Gd, Dy, and Er) hybridization in lithium tetraborate." Frontiers in Physics, 2-31.

Kipcak AS, Yildirim, M, Aydin Yuksel S, Moroydor Derun E and Piskin S (2014) "The synthesis and physical properties of magnesium borate mineral of admontite synthesized from sodium borates" Advances in Materials Science and Engineering, 2014.

Kostka P, Kabalci I, Tay T, Gladkov P and Zavadil J (2017) "Investigation of Er doped zinc borate glasses by low-temperature photoluminescence" Journal of Luminescence, 192: 1104-1109.

Ma QL, Zhai BG and Huang YM (2015) "Effect of sol–gel combustion temperature on the luminescent properties of trivalent Dy doped SrAl2O4" Ceramics International, 41(4): 5830-5835.

Ma YQ and Liu ZH (2018) "Excellent adsorption performance for Congo red on hierarchical porous magnesium borate microsphere prepared by a template-free hydrothermal method" Journal of the Taiwan Institute of Chemical Engineers, 86: 92-100.

Maia LJQ, Fick J, Hernandes AC, Mastelaro and Ibanez A (2012) "Optical properties of amorphous, erbium-doped yttrium alumino-borate thin films" Optical Materials, 34(4): 665-670.

Moorthy LR, Jayasimhadri M, Saleem SA, and Murthy DVR (2007) "Optical properties of Er3+-doped alkali fluorophosphate glasses" Journal of non-crystalline solids, 353(13-15): 1392-1396.

Nana LI, Yihua HU, Haoyi WU, Li CHEN and Xiaojuan WANG (2012) "Investigation on luminescence properties of Ln3+ doped Sr3EuMgSi2O8 (Ln= Dy, Er, Ho)" Journal of Rare Earths, 30(11): 1079-1083.

Nemov SA, Jafarli KM, Aliyeva LN, Abdullayev NA, Kahramanov SS and Aliguliyeva KV (2017) "Effect of doping with rare-earth elements (Eu, Tb, Dy) on the conductivity of Bi2Te3 layered single crystals" Semiconductors, 51(7): 942-946.

Padlyak B V, Lisiecki R and Ryba-Romanowski W (2016) "Spectroscopy of the Er-doped lithium tetraborate glasses" Optical Materials, 54: 126-133.

Patil KC, Aruna ST and Mimani T (2002) "Combustion synthesis: an update" Current Opinion in Solid State and Materials Science, 6(6): 507-512.

Pawar PP, Munishwar SR and Gedam RS (2016) "Physical and optical properties of Dy3+/Pr3+ Co-doped lithium borate glasses for W-LED" Journal of Alloys and Compounds, 660: 347-355.

Qasrawi AF, Kayed TS, Mergen A, Gürü M "Synthesis and characterization of Mg2B2O5" Mater Res Bull. 2005; 40(4):583-589.

Rajagukguk J, Sinaga B and Kaewkhao J (2019) "Structural and spectroscopic properties of Er3+ doped sodium lithium borate glasses" Spectrochimica Acta Part A: Molecular and Biomolecular Spectroscopy, 223: 117342.

Rajaramakrishna R, Wongdeeying C, Yasaka P, Limkitjaroenporn P and Kaewkhao J (2019) "Spectral Analysis of Ho 3+ Doped Barium Zinc Boro-Tellurite Glasses for Yellow-Green Luminescent Applications" Glass Physics and Chemistry, 45(1): 29-35.

Rao KV, Babu S, Venkataiah G and Ratnakaram YC (2015) "Optical spectroscopy of Dy3+ doped borate glasses for luminescence applications" Journal of Molecular Structure, 1094: 274-280.

Ratnakaram Y C, Chakradhar R S, Ramesh K P, Rao J L and Ramakrishna J (2003) "Mixed alkali effect in borate glasses—optical absorption studies in Ho 3+ doped x (Na 2 O)·(30− x)(K 2 O)· 70 (B 2 O 3) glasses" Journal of materials science, 38(4): 833-841.

Ratnakaram YC, Chakradhar RS, Ramesh KP, Rao JL and Ramakrishna J (2003) "Mixed alkali effect in borate glasses—optical absorption studies in Ho 3+ doped x (Na 2 O)·(30− x)(K 2 O)· 70 (B 2 O 3) glasses" Journal of materials science, 38(4): 833-841.

Rayappan I A and Marimuthu K (2013) "Luminescence spectra and structure of Er3+ doped alkali borate and fluoroborate glasses" Journal of Physics and Chemistry of Solids, 74(11): 1570-1577.

Reddy AJ, Kokila MK, Nagabhushana H, Chakradhar RPS, Shivakumara C, Rao JL and Nagabhushana BM (2011) "Structural, optical and EPR studies on ZnO: Cu nanopowders prepared via low temperature solution combustion synthesis" Journal of Alloys and Compounds, 509(17): 5349-5355.

Righini GC and Ferrari M (2005) "Photoluminescence of rare-earth-doped glasses" Rivista Del Nuovo Cimento, 28(12): 1-53.

Saisudha MB and Ramakrishna J (1996) "Effect of host glass on the optical absorption properties of Nd 3+, Sm 3+, and Dy 3+ in lead borate glasses" Physical Review B, 53(10): 6186.

Sakane K, Kitamura T and Ogawa J (1988) "Formation of Fibrous Magnesium Pyroborate" Gypsum Lime, 7(216, 281-7): 281-287.

Sakane K, Kitamura T, Wada H and Suzue M (1992) "Effect of mixing state of raw materials in the preparation of Mg2B2O5 whiskers" Advanced Powder Technology, 3(1): 39-46.

Santiago M, Marcazzó J, Grasselli C, Lavat A, Molina P, Spano F and Caselli E (2011) "Thermo-and radioluminescence of undoped and Dy-doped strontium borates prepared by sol-gel method Radiation Measurements" 46(12): 1488-1491.

Sdiri N, Elhouichet H and Ferid M (2014) "Effects of substituting P2O5 for B2O3 on the thermal and optical properties of sodium borophosphate glasses doped with Er" Journal of Non-Crystalline Solids, 389: 38-45.

Sivasankari J, Sankar S, Selvakumar S, Vimaladevi L and Krithiga R (2014) "Synthesis, structural and optical properties of Er doped, Li doped and Er+ Li co-doped ZnO nanocrystallites by solution-combustion method" Materials Chemistry and Physics, 143(3): 1528-1535.

Swapna K, Mahamuda S, Venkateswarlu M, Rao AS, Jayasimhadri M, Shakya S and Prakash GV (2015) "Visible, up-conversion and NIR (~ 1.5 μm) luminescence studies of Er3+ doped zinc alumino bismuth borate glasses" Journal of Luminescence, 163: 55-63.

Termizi Ramli A, Hashim S, Alajerami YSM, Kasim A and Wan Hassan WMS (2012) "Optical properties of lithium magnesium borate glasses doped with Dy3+ and Sm3+ ions" Physica B: Condensed Matter, 407(13): 2398-2403.

Torres-Cortés CO , Hernández-Adame L , Baltazar-Raigosa A , Vega-Carrillo HR , Rodríguez-López JL and Pérez-Arrieta ML (2019) "Synthesis and thermoluminescent response to γ-rays and neutrons of MgB4O7: Dy and MgB4O7: Dy, Na" Applied Radiation and Isotopes, 147: 159-164.

Üçyıldız A and Girgin İ (2010) "Controlled synthesis, characterization and thermal properties of Mg2B2O5" Open Chemistry, 8(4): 758-765.

WANG LC, ZHANG Y, ZHANG YS, HUANG XP and WANG YQ (2009) "Preparation and Characterization of Magnesium Borate (Mg_2B_2O_5) Whisker" [J]. Chemical Industry and Engineering, 6: 003.

Watanabe T (1953) "Suanite, a new magnesium borate mineral from Hol Kol, Suan, North Korea" Mineralogical Journal, 1(1): 54-62_1.

Weber MJ (1967) "Selective Excitation and Decay of Er 3+ Fluorescence in La F 3. Physical Review" 156(2): 231.

Weir CE and Schroeder RA (1964) "Infrared spectra of the crystalline inorganic borates" Journal of Research of the National Bureau of Standards A, 68, 465:487.

Xiong Z, Xu, J, Zhao F, Zhang Y, Liu, J and Tang Q (2017) "Investigation on fluorescence and thermoluminescence of bismuth silicate crystal doped with Dy" Journal of Luminescence, 192: 85-88.

Xiu Z, Zhou G, Zou WG, Lü M, Gu F and Wang S (2005) "Luminescence properties of Eu3+ and Dy3+ doped β-BaB2O4 nanocrystals" .Optical Materials, 28(8–9): 988–991.

Xu B, Li T, Zhang Y, Zhang Z, Liu X and Zhao J (2008) "New synthetic route and characterization of magnesium borate nanorods" Crystal Growth and Design, 8(4): 1218-1222.

YAN PK, MA ZX, MA ZJ and WANG EL (2008) "Progress and application in magnesium borate whisker" [J]. Industrial Minerals & Processing, 9: 011.

Yanmin Y, Yanzhou L, Peiqing C, Maalej R and Seo H J (2015) "Thermal stability and spectroscopic properties of Ho3+ doped tellurite-borate glasses" Journal of Rare Earths, 33(9): 939-945.

Zaman F, Khan I, Khattak SA, Kaewkhao J, Shoaib M, Shah A and Rooh G (2019) "Investigation of luminescence and lasing properties of Dy3+-doped-borate glasses for white light generation" Solid State Sciences, 90: 68-75.

Zeng Y, Yang H, Fu W, Qiao L, Chang L, Chen J and Zou G (2008) "Synthesis of magnesium borate (Mg2B2O5) nanowires, growth mechanism and their lubricating properties" Materials Research Bulletin, 43(8-9): 2239-2247.

Zhu Y, Shen X, Zhou M, Su X, Li J, Yang G and Zhou Y (2019) "20 µm band emission enhancement and energy transfer in Ho3+/Yb3+/Er3+ tri-doped tellurite glasses" Journal of Luminescence, 210: 28-37.

7. CURRICULUM VITAE

Name SURNAME   **:** Ceren ŞAHİN

Place and Date of Birth **:** Üsküdar / 18.09.1993

Bachelor's Degree   **:** Abant İzzet Baysal University

e-mail   **:** cscerensahin@gmail.com

Address   **:** Kartal / İstanbul